

Survey of Period Variations of Superhumps in SU UMa-Type Dwarf Novae. VI: The Sixth Year (2013–2014)

Taichi KATO,^{1*} Pavol A. DUBOVSKY,² Igor KUDZEJ,² Franz-Josef HAMBSCHE,^{3,4,5} Ian MILLER,⁶
Tomohito OHSHIMA,¹ Chikako NAKATA,¹ Miho KAWABATA,⁷ Hirochika NISHINO,⁷ Kazunari MASUMOTO,⁷
Sahori MIZOGUCHI,^{8,7} Masayuki YAMANAKA,^{9,7} Katsura MATSUMOTO,⁷ Daisuke SAKAI,⁷ Daiki FUKUSHIMA,⁷
Minami MATSUURA,⁷ Genki BOUNO,⁷ Megumi TAKENAKA,⁷ Shinichi NAKAGAWA,⁷ Ryo NOGUCHI,⁷ Eriko IINO,⁷
Roger D. PICKARD,^{10,11} Yutaka MAEDA,¹² Arne HENDEN,¹³ Kiyoshi KASAI,¹⁴ Seiichiro KIYOTA,¹⁵
Hidehiko AKAZAWA,¹⁶ Kazuyoshi IMAMURA,¹⁶ Enrique de MIGUEL,^{17,18} Hiroyuki MAEHARA,¹⁹ Berto MONARD,^{20,21}
Elena P. PAVLENKO,²² Kirill ANTONYUK,²² Nikolaj PIT,²² Oksana I. ANTONYUK,²² Aleksei V. BAKLANOV,²²
Javier RUIZ,^{23,24,25} Michael RICHMOND,²⁶ Arto OKSANEN,²⁷ Caisey HARLINGTON,²⁸ Sergey Yu. SHUGAROV,^{29,30}
Drahomir CHOCHOL,³⁰ Gianluca MASI,³¹ Francesca NOCENTINI,³¹ Patrick SCHMEER,³² Greg BOLT,³³
Peter NELSON,³⁴ Joseph ULOWETZ,³⁵ Richard SABO,³⁶ William N. GOFF,³⁷ William STEIN,³⁸ Raúl MICHEL,³⁹
Shawn DVORAK,⁴⁰ Irina B. VOLOSHINA,²⁹ Vladimir Metlov,²⁹ Natalia KATYSHEVA,²⁹ Vitaly V. NEUSTROEV,⁴¹
George SJOBERG,^{42,13} Colin LITTLEFIELD,⁴³ Bartłomiej DEBSKI,⁴⁴ Paulina SOWICKA,⁴⁴ Marcin KLIMASZEWSKI,⁴⁴
Małgorzata CURYŁO,⁴⁴ Etienne MORELLE,⁴⁵ Ivan A. CURTIS,⁴⁶ Hidetoshi IWAMATSU,^{47,1} Neil D. BUTTERWORTH,⁴⁸
Maksim V. ANDREEV,^{49,50} Nikolai PARAKHIN,⁴⁹ Aleksandr SKLIYANOV,⁵¹ Kazuhiko SHIOKAWA,⁵² Rudolf NOVÁK,⁵³
Tat'yana R. IRSMAMBETOVA,²⁹ Hiroshi ITOH,⁵⁴ Yoshiharu ITO,⁵⁵ Kenji HIROSAWA,⁵⁶ Denis DENISENKO,⁵⁷
Christopher S. KOCHANÉK,⁵⁸ Benjamin SHAPPEE,⁵⁸ Krzysztof Z. STANEK,⁵⁸ José L. PRIETO,⁵⁹ Koh-ichi ITAGAKI,⁶⁰
Rod STUBBINGS,⁶¹ Jose RIPERO,⁶² Eddy MUYLLAERT,⁶³ Gary POYNER,⁶⁴

¹ Department of Astronomy, Kyoto University, Kyoto 606-8502

*tkato@kustastro.kyoto-u.ac.jp

² Vihorlat Observatory, Mierova 4, Humenne, Slovakia

³ Groupe Européen d'Observations Stellaires (GEOS), 23 Parc de Levesville, 28300 Bailleau l'Evêque, France

⁴ Bundesdeutsche Arbeitsgemeinschaft für Veränderliche Sterne (BAV), Munsterdamm 90, 12169 Berlin, Germany

⁵ Vereniging Voor Sterrenkunde (VVS), Oude Bleken 12, 2400 Mol, Belgium

⁶ Furzehill House, Ilston, Swansea, SA2 7LE, UK

⁷ Osaka Kyoiku University, 4-698-1 Asahigaoka, Osaka 582-8582

⁸ Sendai Astronomical Observatory, Nishikigaoka, Aoba-ku, Sendai 989-3123

⁹ Kwasan and Hida Observatories, Kyoto University, Yamashina, Kyoto 607-8471

¹⁰ The British Astronomical Association, Variable Star Section (BAA VSS), Burlington House, Piccadilly, London, W1J 0DU, UK

¹¹ 3 The Birches, Shobdon, Leominster, Herefordshire, HR6 9NG, UK

¹² Kaminishiyamamachi 12-14, Nagasaki, Nagasaki 850-0006

¹³ American Association of Variable Star Observers, 49 Bay State Rd., Cambridge, MA 02138, USA

¹⁴ Baselstrasse 133D, CH-4132 Muttenz, Switzerland

¹⁵ Variable Star Observers League in Japan (VSOLJ), 7-1 Kitahatsutomi, Kamagaya, Chiba 273-0126

¹⁶ Department of Biosphere-Geosphere System Science, Faculty of Informatics, Okayama University of Science, 1-1 Ridai-cho, Okayama, Okayama 700-0005

¹⁷ Departamento de Física Aplicada, Facultad de Ciencias Experimentales, Universidad de Huelva, 21071 Huelva, Spain

¹⁸ Center for Backyard Astrophysics, Observatorio del CIECEM, Parque Dunar, Matalascañas, 21760 Almonte, Huelva, Spain

¹⁹ Kiso Observatory, Institute of Astronomy, School of Science, The University of Tokyo 10762-30, Mitake, Kiso-machi, Kiso-gun, Nagano 397-0101

²⁰ Bronberg Observatory, Center for Backyard Astronomy Pretoria, PO Box 11426, Tiegerpoort 0056, South Africa

²¹ Kleinkaroo Observatory, Center for Backyard Astronomy Kleinkaroo, Sint Helena 1B, PO Box 281, Calitzdorp 6660, South Africa

²² Crimean Astrophysical Observatory, Kyiv Shevchenko National University, 98409, Nauchny, Crimea, Ukraine

²³ Observatorio de Cantabria, Ctra. de Rocamundo s/n, Valderredible, Cantabria, Spain

²⁴ Instituto de Física de Cantabria (CSIC-UC), Avenida Los Castros s/n, E-39005 Santander, Cantabria, Spain

²⁵ Agrupación Astronómica Cantabria, Apartado 573, 39080, Santander, Spain

²⁶ Physics Department, Rochester Institute of Technology, Rochester, New York 14623, USA

²⁷ Hankasalmi observatory, Jyväskylä Sirius ry, Vertaalantie 419, FI-40270 Palokka, Finland

²⁸ Searchlight Observatory Network, The Grange, Erpingham, Norfolk, NR11 7QX, UK

²⁹ Sternberg Astronomical Institute, Lomonosov Moscow University, Universitetsky Ave., 13, Moscow 119992, Russia

³⁰ Astronomical Institute of the Slovak Academy of Sciences, 05960, Tatranska Lomnica, the Slovak Republic

³¹ The Virtual Telescope Project, Via Madonna del Loco 47, 03023 Ceccano (FR), Italy

- ³² *Bischmisheim, Am Probstbaum 10, 66132 Saarbrücken, Germany*
- ³³ *Camberwarra Drive, Craigie, Western Australia 6025, Australia*
- ³⁴ *1105 Hazeldean Rd, Ellinbank 3820, Australia*
- ³⁵ *Center for Backyard Astrophysics Illinois, Northbrook Meadow Observatory, 855 Fair Ln, Northbrook, Illinois 60062, USA*
- ³⁶ *2336 Trailcrest Dr., Bozeman, Montana 59718, USA*
- ³⁷ *13508 Monitor Ln., Sutter Creek, California 95685, USA*
- ³⁸ *6025 Calle Paraiso, Las Cruces, New Mexico 88012, USA*
- ³⁹ *Instituto de Astronomía UNAM, Apartado Postal 877, 22800 Ensenada B.C., México*
- ⁴⁰ *Rolling Hills Observatory, 1643 Nightfall Drive, Clermont, Florida 34711, USA*
- ⁴¹ *Astronomy Division, Department of Physics, PO Box 3000, FIN-90014 University of Oulu, Finland*
- ⁴² *The George-Elma Observatory, 9 Contentment Crest, #182, Mayhill, New Mexico 88339, USA*
- ⁴³ *Department of Physics, University of Notre Dame, Notre Dame, Indiana 46556, USA*
- ⁴⁴ *Astronomical Observatory, Jagiellonian University, ul. Orła 171 30-244 Kraków, Poland*
- ⁴⁵ *9 rue Vasco de GAMA, 59553 Lauwin Planque, France*
- ⁴⁶ *2 Yandra Street, Vale Park, Adelaide, South Australia 5081, Australia*
- ⁴⁷ *St. Dominic Junior and Senior High School 2-2-14, Tsunogorou, Aoba Ward, Sendai, Miyagi 980-0874*
- ⁴⁸ *24 Payne Street, Mount Louisa, Queensland 4814, Australia*
- ⁴⁹ *Institute of Astronomy, Russian Academy of Sciences, 361605 Peak Terskol, Kabardino-Balkaria, Russia*
- ⁵⁰ *International Center for Astronomical, Medical and Ecological Research of NASU, Ukraine 27 Akademika Zabolotnoho Str. 03680 Kyiv, Ukraine*
- ⁵¹ *Kazan Federal University, Kremlevskaya str., 18, Kazan, 420008, Russia*
- ⁵² *Moriyama 810, Komoro, Nagano 384-0085*
- ⁵³ *Research Centre for Toxic Compounds in the Environment, Faculty of Science, Masaryk University, Kamenice 3, 625 00 Brno, Czech Republic*
- ⁵⁴ *VSOLJ, 1001-105 Nishiterakata, Hachioji, Tokyo 192-0153*
- ⁵⁵ *VSOLJ, Kamisugi 6-2-69, Aoba-ku, Sendai, Miyagi 980-0011*
- ⁵⁶ *216-4 Maeda, Inazawa-cho, Inazawa-shi, Aichi 492-8217*
- ⁵⁷ *Space Research Institute (IKI), Russian Academy of Sciences, Moscow, Russia*
- ⁵⁸ *Department of Astronomy, the Ohio State University, Columbia, OH 43210, USA*
- ⁵⁹ *Department of Astrophysical Sciences, Princeton University, NJ 08544, USA*
- ⁶⁰ *Itagaki Astronomical Observatory, Teppo-cho, Yamagata 990-2492*
- ⁶¹ *Tetoora Observatory, Tetoora Road, Victoria, Australia*
- ⁶² *President of CAA (Centro Astronomico de Avila) and Variable and SNe Group M1, Buenavista 7, Ciudad Sto. Domingo, 28110 Algete/Madrid, Spain*
- ⁶³ *Vereniging Voor Sterrenkunde (VVS), Moffelstraat 13 3370 Boutersem, Belgium*
- ⁶⁴ *BAA Variable Star Section, 67 Ellerton Road, Kingstanding, Birmingham B44 0QE, UK*

(Received 201 0; accepted 201 0)

Abstract

Continuing the project described by Kato et al. (2009), we collected times of superhump maxima for 56 SU UMa-type dwarf novae mainly observed during the 2013–2014 season and characterized these objects. We detected negative superhumps in VW Hyi and indicated that the low number of normal outbursts in some supercycle can be interpreted as a result of the disk tilt. This finding, combined with the Kepler observation of V1504 Cyg and V344 Lyr, suggests that the disk tilt is responsible for modulating the outburst pattern in SU UMa-type dwarf novae. We also studied the deeply eclipsing WZ Sge-type dwarf nova MASTER OT J005740.99+443101.5 and found evidence of a sharp eclipse during the phase of early superhumps. The profile can be reproduced by a combination of the eclipse of the axisymmetric disk and the uneclipsed light source of early superhumps. This finding confirms the lack of evince of a greatly enhanced hot spot during the early stage of WZ Sge-type outburst. We detected growing (stage A) superhumps in MN Dra and give a suggestion that some of SU UMa-type dwarf novae situated near the critical condition of tidal instability may show long-lasting stage A superhumps. The large negative period derivatives reported in such systems can be understood a result of the combination of stage A and B superhumps. The WZ Sge-type dwarf novae AL Com and ASASSN-13ck showed a long-lasting (plateau-type) rebrightening. In the early phase of the rebrightening, both objects showed a precursor-like outburst, suggesting that the long-lasting rebrightening is triggered by a precursor outburst.

Key words: accretion, accretion disks — stars: novae, cataclysmic variables — stars: dwarf novae

1. Introduction

Cataclysmic variables (CVs) are close binary systems transferring matter from a low-mass dwarf secondary to a white dwarf. The transferred matter forms an accretion disk. In dwarf novae (DNe), a class of CVs, thermal-viscous instability in the accretion disk causes outbursts. SU UMa-type dwarf novae, a subclass of DNe, show long outbursts (superoutburst) in addition to ordinary short outbursts, and semi-periodic modulations called superhumps are detected during the superoutbursts. The superhumps have periods a few percent longer than the orbital period. It is now widely believed that the 3:1 resonance in the accretion disk causes the eccentric deformation of the disk, resulting superhumps [tidal instability: Whitehurst (1988); Hirose, Osaki (1990); Lubow (1991)]. The superoutburst can be understood as a result of the increased tidal dissipation and removal of the angular momentum when the tidal instability works [thermal tidal instability (TTI) model: Osaki (1989); Osaki (1996)]. This process produces a relaxation oscillation in the total angular momentum of the disk, and the superoutbursts recur. The interval between the successive superoutbursts is called supercycle. [For general information of CVs, DNe, SU UMa-type dwarf novae and superhumps, see e.g. Warner (1995)].

In a series of papers Kato et al. (2009), Kato et al. (2010), Kato et al. (2012a) Kato et al. (2013a) and Kato et al. (2014), we systematically surveyed SU UMa-type dwarf novae particularly on period variations of superhumps. The change in the superhump period reflects the precession angular velocity of the eccentric (or flexing) disk, and is expected to be an excellent probe for studying the structure of the accretion disk during dwarf nova outbursts. In recent series of papers, we dealt with a various of topics related to SU UMa-type dwarf novae and superhumps: in Kato et al. (2012a), we also studied Kepler data and made a pilot study of variations of superhumps amplitudes motivated by Smak (2010). In Kato et al. (2013a), we systematically studied ER UMa-type dwarf novae (a class of SU UMa-type dwarf novae with very short supercycles, see e.g. Kato, Kunjaya 1995; Robertson et al. 1995; Kato et al. 1999) and helium dwarf novae (AM CVn-type objects). In Kato et al. (2014), we made a pilot study of the decline rate of the superoutburst motivated by Cannizzo et al. (2010) and studied negative superhumps (superhumps having periods shorter than the orbital period and are considered as a manifestation of a tilted disk, see e.g. Harvey et al. 1995; Patterson et al. 1997; Wood, Burke 2007) particularly in BK Lyn, which displays both states of a novalike variable (a thermally stable CV) and an ER UMa-type dwarf nova.

We continue this extended, comprehensive research of SU UMa-type dwarf novae and superhumps in general in this paper. Since most of the objects treated in this paper is little documented in the past, and since a compilation of historical descriptions of dwarf novae has not been issued for long since Glasby (1970), we intend these series of papers to be also a source of compiled information of

individual dwarf novae.

The present advances in understanding of the superhump periods and their variations started with the new interpretation of the Kepler observation (Osaki, Kato 2013a), who used the negative superhumps as a probe for the variation of the disk radius over the supercycle, and confirmed the radius variation predicted by the TTI model. Combined with Osaki, Kato (2013b), Osaki, Kato (2014), the TTI model is currently the only viable model to explain the SU UMa-type phenomenon.

In Kato et al. (2009), we demonstrated that most of the $O - C$ diagrams of superhumps in SU UMa-type dwarf novae can be expressed by three distinct stages: initial growing stage (stage A) with a long period and fully developed stage (stage B) with a systematically varying period and later stage C with a shorter, almost constant period. [see Kato et al. (2009) for the notation of stages A-B-C of superhumps]. The origin of these three stages of superhumps was a mystery when it was documented in Kato et al. (2009). After examination of the Kepler data, Osaki, Kato (2013b) proposed that the appearance of the pressure effect is responsible for the transition from stage A to stage B. In this interpretation, stage A reflects the state when the 3:1 resonance is confined to the resonance region. This interpretation allowed a new method to determine the mass ratio ($q = M_2/M_1$) only from superhump observations and the orbital period (Kato, Osaki 2013b). This method is particularly suitable for measuring mass ratios in WZ Sge-type dwarf novae (SU UMa-type dwarf novae with very long supercycles, and are considered to be the terminal stage of the CV evolution) and for discriminating hitherto very poorly known period bouncers (CVs which have passed the minimum orbital period in evolution: Kato et al. 2013b; Nakata et al. 2013b). Superhumps are now not only a powerful tool for diagnosing the accretion disk, but also a powerful tool for illuminating the CV evolution.

The material and methods of analysis are given in section 2, observations and analysis of individual objects including short discussions on individual objects are given in section 3, the general discussion is given in section 4 and the summary is given in section 5.

2. Observation and Analysis

The data were obtained under campaigns led by the VSNET Collaboration (Kato et al. 2004c). For some objects, we used the public data from the AAVSO International Database¹.

The majority of the data were acquired by time-resolved CCD photometry by using 30 cm-class telescopes located world-wide, whose observational details will be presented in future papers dealing with analysis and discussion on individual objects of interest. The list of outbursts and observers is summarized in table 1. The data analysis was performed just in the same way described in Kato et al. (2009) and Kato et al. (2014) and we mainly

¹ <<http://www.aavso.org/data-download>>.

used R software² for data analysis. In de-trending the data, we used both lower (1–5th order) polynomial fitting and locally-weighted polynomial regression (LOWESS: Cleveland 1979). The times of superhumps maxima were determined by the template fitting method as described in Kato et al. (2009). The times of all observations are expressed in Barycentric Julian Dates (BJD).

The abbreviations used in this paper are the same as in Kato et al. (2014): P_{orb} means the orbital period and $\varepsilon \equiv P_{\text{SH}}/P_{\text{orb}} - 1$ for the fractional superhump excess. Since Osaki, Kato (2013a), the alternative fractional superhump excess in the frequency unit $\varepsilon^* \equiv 1 - P_{\text{orb}}/P_{\text{SH}} - 1 = \varepsilon/(1 + \varepsilon)$ has been introduced because this fractional superhump excess can be directly compared to the precession rate. We therefore used ε^* in referring the precession rate.

We used phase dispersion minimization (PDM; Stellingwerf 1978) for period analysis and 1σ errors for the PDM analysis was estimated by the methods of Fernie (1989) and Kato et al. (2010). We also used least absolute shrinkage and selection operator (Lasso) method (Tibshirani 1996; Kato, Uemura 2012), which has been proven to yield very sharp signals. In this paper, we used the two-dimensional Lasso power spectra as introduced in the analysis of the Kepler data such as in Kato, Maehara (2013); Osaki, Kato (2013b); Kato, Osaki (2013a). These two-dimensional Lasso power spectra have been proven to be helpful in detecting negative superhumps (cf. Osaki, Kato 2013b) as well as superhumps with varying frequencies (cf. Kato, Maehara 2013). Although the application of two-dimensional Lasso power spectra to the Kepler data dealt with almost uniformly sampled data, we have demonstrated in Kato et al. (2014) and Ohshima et al. (2014) that two-dimensional Lasso power spectra are also effective in detecting multiple signals and their variations in non-uniformly sampled ground-based data.

The resultant P_{SH} , P_{dot} and other parameters are listed in table 2 in same format as in Kato et al. (2009). The definitions of parameters P_1, P_2, E_1, E_2 and P_{dot} are the same as in Kato et al. (2009). We also presented comparisons of $O - C$ diagrams between different superoutbursts since this has been one of the motivations of these surveys (cf. Uemura et al. 2005) and it has been demonstrated that a combination of $O - C$ diagrams between different superoutbursts can better describe the overall pattern of the period variation (Kato et al. 2009). In drawing combined $O - C$ diagrams, we usually used $E = 0$ for the start of the superoutburst, which usually refers to the first positive detection of the outburst. This epoch usually has an accuracy of ~ 1 d for well-observed objects, and if the outburst was not sufficiently observed, we mentioned how to estimated E in such an outburst. We also present representative $O - C$ diagrams and light curves especially for WZ Sge-type dwarf novae, which are not expected to undergo outbursts in the near future. In all figures, the binned magnitudes and $O - C$ values are accompanied by 1σ error bars, which are omitted when the error is smaller

than the plot mark.

We used the same terminology of superhumps summarized in Kato et al. (2012a). We especially call attention to the term “late superhumps”. We only used “traditional” late superhumps when an ~ 0.5 phase shift is confirmed [Vogt (1983); see also table 1 in Kato et al. (2012a) for various types of superhumps], since we suspect that many of the past claims of detections of “late superhumps” were likely stage C superhumps [cf. Kato et al. (2009); note that the Kepler observation of V585 Lyr also demonstrated this persistent stage C superhumps without a phase shift (Kato, Osaki 2013a)].

Early superhumps are double-wave humps seen during the early stages of WZ Sge-type dwarf novae, and have period close to the orbital periods (Kato et al. 1996; Kato 2002; Osaki, Meyer 2002). We used the period of early superhumps as approximate orbital period. The validity of this assumption is also reviewed in this paper.

As in Kato et al. (2009), we have used coordinate-based optical transient (OT) designations for some objects, such as Catalina Real-time Transient Survey (CRTS; Drake et al. 2009)³ transients and listed the original identifiers in table 1. When available, we preferably used the International Astronomical Union (IAU)-format names provided by the CRTS team in the public data release⁴

3. Individual Objects

3.1. FO Andromedae

FO And was discovered as a dwarf nova by Hoffmeister (1967). Meinunger (1984b) showed that the outbursts occur with intervals of 10–30 d, and there was already likely a superoutburst. Meinunger (1984a) reported the detection of three superoutbursts and the intervals between normal outbursts were 15–23 d. This object has been monitored by amateur observers since 1982, and both AAVSO and VSOLJ observers detected superoutbursts. Bruch (1989) obtained a spectrum in quiescence and detected Balmer and HeII emission lines. Szkody et al. (1989) reported time-resolved photometry in quiescence without detecting a significant period. According to Szkody et al. (1989), Grauer and Bond (1986) detected superhumps with a period of ~ 105 d, but this result was not published.

The first solid publication of the superhumps in this object was Kato (1995b), whose result was refined in Kato et al. (2009). Thorstensen et al. (1996) determined the orbital period by a radial-velocity study. Kato et al. (2012a) reported superhumps in the 2010 and 2011 superoutbursts.

The 2013 November–December superoutburst was detected on November 24 by J. Ripero (vsnet-alert 16647). Time-series observations started two nights later, and a total of three-night observation was obtained (vsnet-alert 16696). The times of superhump maxima are listed in

² The R Foundation for Statistical Computing;
<<http://cran.r-project.org/>>.

³ <<http://nessi.cacr.caltech.edu/catalina/>>. For the information of the individual Catalina CVs, see <<http://nessi.cacr.caltech.edu/catalina/AllCV.html>>.

⁴ <<http://nessi.cacr.caltech.edu/DataRelease/>>.

Table 1. List of Superoutbursts.

Subsection	Object	Year	Observers or references*	ID [†]
3.1	FO And	2013	Aka	
3.2	DH Aql	2000	Oud, Btw	
3.3	BB Ari	2013	GFB, OkC, HaC, Mhh	
3.4	UZ Boo	2013	KU, GFB, DPV, RIT, Rui, Mhh, AAVSO, RPc, Kai, CRI, IMi, Mdy, Iak, Ioh	
3.5	V342 Cam	2013	DPV	
3.6	V452 Cas	2013	IMi, RPc, DPV	
3.7	V359 Cen	2014	HaC	
3.9	YZ Cnc	2014	Aka, Mdy, HaC	
3.10	GZ Cnc	2014	Kis, Mdy, IMi, Kai, Aka	
3.11	AL Com	2013	OKU, NKa, KU, Irs, CRI, DKS, Kis, IMi, AAVSO	
3.12	V503 Cyg	2013	RPc	
3.13	IX Dra	2012	MEV, AAVSO, UJH	
3.14	MN Dra	2012	Ast, CRI	
		2013	CRI, Kai, Ter, KU	
3.15	CP Eri	2013	OkC, SWI	
3.16	V1239 Her	2013	RPc, IMi	
3.17	CT Hya	2014	Mdy	
3.18	VW Hyi	2012	HaC, CTA, Hen	
3.19	WX Hyi	1977	Bailey (1979a)	
		2014	HaC	

*Key to observers: Aka (H. Akazawa, OUS), Ast (Astrotel telescope, by A. Sklyanov), Btw (N. Butterworth), CRI (Crimean Astrophys. Obs.), CTA (I. Curtis), deM (E. de Miguel), DKS[‡](S. Dvorak), DPV (P. Dubovsky), GBo (G. Bolt), GFB[‡](W. Goff), HaC (F.-J. Hamsch, remote obs. in Chile), Han (Hankasalmi Obs., by A. Oksanen) Hsk (K. Hirose), Iha (Y. Ito), IMi[‡](I. Miller), Ioh (H. Itoh), Irs (T. Irsamambetova), Kai (K. Kasai), Kis (S. Kiyota), Krw (Krakow team), KU (Kyoto U., campus obs.), LCO (C. Littlefield), Mas (G. Masi team), Mdy (Y. Maeda), MEV[‡](E. Morelle), Mhh (H. Maehara), Mic (R. Michel-Murillo team), Nel[†](P. Nelson), Neu (V. Neustroev), NKa (N. Katysheva), Nov (R. Novák), OkC[‡](A. Oksanen, remote obs. in Chile), OKU (Osaya Kyoiku U.), Oud (Ouda station, Kyoto U.), RIT (M. Richmond), RPc[‡](R. Pickard), Rui (J. Ruiz), Shu (S. Shugarov), Siz (K. Shiokawa), SRI[‡](R. Sabo), SWI[‡](W. Stein), Ter (Terskol Obs.), UJH[‡](J. Ulowetz), Vol (I. Voloshina), AAVSO (AAVSO database)

[†]Original identifications, discoverers or data source.

[‡]Inclusive of observations from the AAVSO database.

table 3. A comparison of the $O - C$ diagrams (figure 1) suggests that the obtained global period is a mixture of different stages.

3.2. *DH Aquilae*

DH Aql was discovered as a Mira-type variable (=HV 3899) with a range of 12.5 to fainter than 16 in photographic range (Cannon 1925). This element was also used in Kholopov et al. (1985). Tsesevich (1969) recorded three outbursts and identified this object as a dwarf nova. The durations of outbursts were 3–4 d. Zhukov et al. (1972) also reported another outburst and confirmed the periodicity suggested by Tsesevich (1969). This object has been regularly monitored since 1980 [e.g Bateson (1982b); Bateson (1982a); also summarized in Mason, Howell (2003)].

Nogami, Kato (1995) detected superhumps during the 1994 September outburst and established the SU UMa-

Table 3. Superhump maxima of FO And (2013)

E	max*	error	$O - C$ [†]	N [‡]
0	56622.9587	0.0016	-0.0015	51
1	56623.0348	0.0006	0.0001	48
56	56627.1334	0.0019	0.0048	56
57	56627.2050	0.0018	0.0020	50
68	56628.0242	0.0030	0.0024	55
69	56628.0944	0.0017	-0.0018	56
70	56628.1647	0.0028	-0.0060	55

*BJD-2400000.

[†]Against max = 2456622.9602 + 0.074435 E .

[‡]Number of points used to determine the maximum.

Table 1. List of Superoutbursts (continued).

Subsection	Object	Year	Observers or references*	ID [†]
3.20	AY Lyr	2013	Aka	
3.21	AO Oct	2013	HaC	
3.22	DT Oct	2014	OkC	
3.23	V521 Peg	2013	KU, Mdy, Aka, DPV, RPc, IMi, Hsk, Mhh	
3.24	TY Psc	2013	Aka	
3.25	V893 Sco	2007	MLF, OKU	
		2008	GBo	
		2010	GBo, OKU	
		2013	HaC, MLF	
3.26	RZ Sge	2013	AAVSO, IMi, Rui	
3.27	AW Sge	2013	Vol, SRI	
3.28	V1265 Tau	2013	GFB, HaC, KU	
3.29	SU UMa	2013	OKU, DPV, Kis, Iha	
3.30	SS UMi	2013	DPV, Kai, Krw	
3.31	CU Vel	2013	HaC, Nel	
3.32	1RXS J231935	2013	DPV	
3.33	ASAS J224349	2013	Krw, HaC, Mdy, DPV, Shu, IMi, Rui, Mhh	ASAS J224349+0809.5
3.34	ASASSN-13cf	2013	LCO, IMi, RPc	
3.35	ASASSN-13cg	2013	LCO, CRI	
3.36	ASASSN-13ck	2013	deM, OkC, HaC, Mas, Han, DPV, UJH, IMi, RPc, AAVSO, Nel, Mdy, Mic, RIT	
3.37	ASASSN-13cv	2013	Kai	
3.38	ASASSN-13cz	2013	IMi	
3.39	ASASSN-13da	2013	HaC	
3.40	ASASSN-14ac	2014	OKU, Kis, Mdy, DPV, RPc, KU, RIT, Mic	
3.41	CSS J024354	2013	MLF	CSS131026:024354–160314
3.42	DDE 31	2014	Mdy	
3.43	MASTER J004527	2013	OKU, UJH, deM, AAVSO, IMi, Kai, SRI, RPc, DKS, DPV, Neu, RIT	MASTER OT J004527.52+503213.8

type classification. Bateson (1998) reported seven superoutbursts and the supercycle lengths of 259–450 d (361 d in average).

Kato et al. (2009) reported observations of superoutbursts in 2002, 2003 and 2008. We found the data of the unreported 2000 superoutburst (vsnet-alert 5163) and summarize the result here. The times of superhump maxima are listed in table 4. This superoutburst was observed in relatively early phase and stages B and C can be recognized. The resultant $O-C$ diagram agrees with the others well (figure 2).

3.3. *BB Arietis*

This object (=NSV 907) was suspected as a dwarf nova because this suspected variable is located close to an ROSAT X-ray source (Kato, vsnet-chat 3317). In 2004, two outbursts were detected P. Schmeer, confirming the dwarf nova-type nature. Superhumps were detected during the second outburst (Kato et al. 2009).

On 2013 August 3, ASAS-SN (Shappee et al. 2013) team detected this object in outburst (vsnet-alert 16111). Although the object once faded rapidly, it brightened five days later showing superhumps and the initial ASAS-SN detection turned out to be a precursor outburst (vsnet-alert 16169, 16170). The times of superhump maxima during the main superoutburst are listed in table 5. There was a stage B-C transition in the $O-C$ data. Although stage A superhumps were likely recorded between the precursor and the main superoutburst, we could not determine the period due to the insufficiency of observations. The present determination of superhump period confirmed the suggestion that we observed only stage C superhumps in 2004 (Kato et al. 2009) (figure 3).

3.4. *UZ Bootis*

UZ Boo is a renowned object selected for a small group of WZ Sge-type dwarf novae when this subclass was proposed (Bailey 1979b). Only a small number of outbursts

Table 1. List of Superoutbursts (continued).

Subsection	Object	Year	Observers or references*	ID [†]
3.44	MASTER J005740	2013	deM, NKa, Shu, Mas, SWI, UJH, AAVSO, KU, SRI, OKU, DPV, RPc	MASTER OT J005740.99+443101.5
3.45	MASTER J024847	2013	IMi	MASTER OT J024847.86+501239.7
3.46	MASTER J061335	2013	OKU, Ter, DPV, KU, Mas, Nov	MASTER OT J061335.30+395714.7
3.47	MASTER J073208	2013	Shu	MASTER OT J073208.11+064149.5
3.48	MASTER J095018	2013	HaC, OKU	MASTER OT J095018.04−063921.9
3.49	MASTER J141143	2014	DPV	MASTER OT J141143.46+262051.5
3.50	MASTER J162323	2013	Shu, IMi, Neu, Rui, DPV	MASTER OT J162323.48+782603.3
3.51	MASTER J234843	2013	OKU, Mas, DPV	MASTER OT J234843.23+250250.4
3.52	OT J013741	2014	deM, Kai	CSS140104:013741+220312
3.53	OT J210016	2013	MLF, deM, OKU, DKS	CSS130905:210016−024258
3.54	PNV J191501	2013	KU, deM, AAVSO, GBo, Vol, OkC, SWI, OKU, Mic, HaC, DPV, SRI, Mdy, MEV, RIT, Aka, Siz, GFB, RPc, Kis, IMi, Mhh, Nel, Ioh	PNV J19150199+0719471
3.55	SSS J094327	2013	Kis	SSS J094327.3−272038
		2014	GBo, Kis, HaC	
3.56	TCP J233822	2013	MLF, HaC, Nel	TCP J23382254−2049518

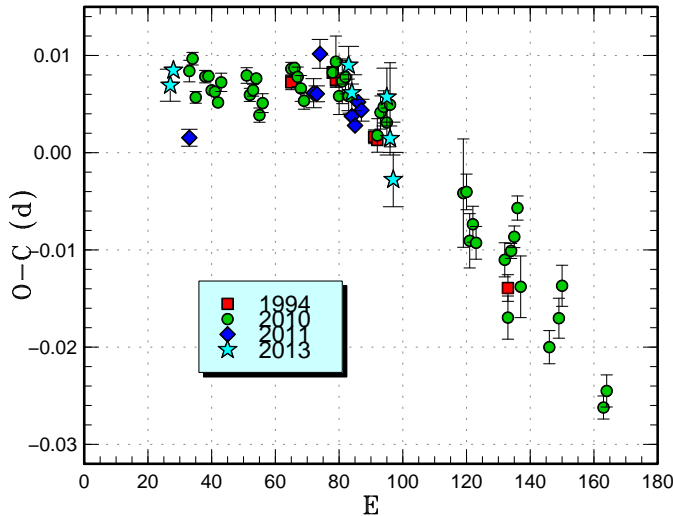


Fig. 1. Comparison of $O - C$ diagrams of FO And between different superoutbursts. A period of 0.07451 d was used to draw this figure. Approximate cycle counts (E) after the start of the superoutburst were used.

were recorded [1929 April, 1937 June, 1938 May, 1978 September (Richter 1986), 1994 August (Iida, York 1994), 2003 December (Kato et al. 2009)]. Although superhumps were first recorded During the 1994 superoutburst, the period was only marginally estimated to be 0.0619 d (Kato et al. 2001) due to the very unfavorable condition. During the 2003 superoutburst, the superhump period was established to be 0.06192(3) d (stage B, Kato et al. 2009) despite the unfavorable seasonal observing condition. The presence of multiple post-superoutburst

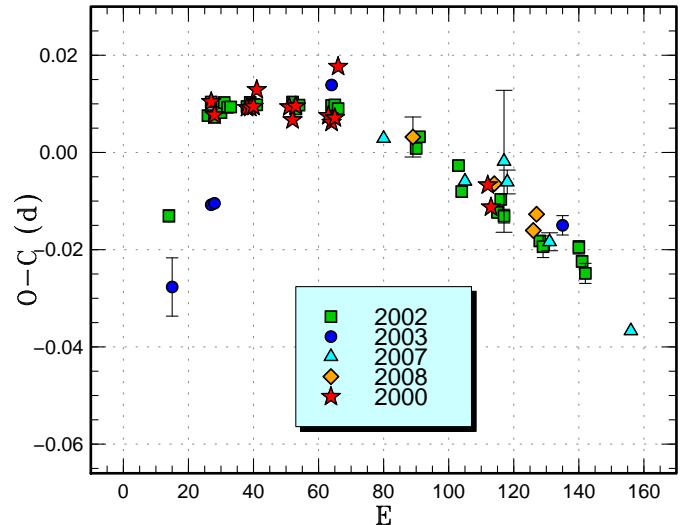


Fig. 2. Comparison of $O - C$ diagrams of DH Aql between different superoutbursts. A period of 0.08000 d was used to draw this figure. Approximate cycle counts (E) after the start of the outburst were used.

rebrightenings was suspected during the 1994 superoutburst (Kuulkers et al. 1996), although the detections of these rebrightenings were based on visual observations. It took additional two years before the phenomenon of multiple post-superoutburst rebrightenings was established in dwarf novae (EG Cnc: cf. Osaki et al. 1997, Patterson et al. 1998, Kato et al. 2004b). During the 2003 superoutburst, UZ Boo showed four post-superoutburst rebrightenings (Kato et al. 2009) and the close resemblance with EG Cnc was highlighted.

Table 2. Superhump Periods and Period Derivatives

Object	Year	P_1 (d)	err	E_1^*	P_{dot}^\dagger	err †	P_2 (d)	err	E_2^*	P_{orb} (d) ‡	Q §	
FO And	2013	0.074412	0.000070	1	70	–	–	–	–	0.07161	CGM	
DH Aql	2000	0.080005	0.000067	0	39	–	–	–	–	–	C	
BB Ari	2013	0.072544	0.000097	0	42	–	0.072135	0.000046	40	111	B	
UZ Boo	2013	0.062066	0.000029	15	85	5.1	5.1	–	–	–	B	
V342 Cam	2013	–	–	–	–	–	0.078067	0.000080	0	65	C	
V452 Cas	2013	0.088596	0.000068	0	92	–14.9	2.9	–	–	–	CG	
V359 Cen	2014	0.081064	0.000026	0	49	–6.3	4.2	0.080744	0.000052	60	86	B
FZ Cet	2014	0.058547	0.000062	0	43	–	–	–	–	–	C	
YZ Cnc	2014	0.090422	0.000069	0	41	–3.9	11.2	–	–	0.0868	CG	
GZ Cnc	2014	0.092699	0.000056	12	92	–2.5	4.8	–	–	0.08825	C	
AL Com	2013	0.057323	0.000022	87	210	4.9	1.9	–	–	0.056669	B	
IX Dra	2012	0.066955	0.000021	0	146	0.4	1.5	–	–	–	B	
MN Dra	2012	0.105299	0.000061	47	115	–	–	–	–	0.0998	C	
MN Dra	2013	0.105040	0.000066	26	66	–14.8	9.5	–	–	0.0998	C	
CP Eri	2013	0.019897	0.000003	0	111	3.1	0.9	–	–	0.019692	B	
CT Hya	2014	–	–	–	–	–	0.066178	0.000064	0	46	C	
VW Hyi	2012	0.076916	0.000014	11	90	2.9	1.3	0.076579	0.000019	87	159	A
WX Hyi	1977	0.077612	0.000113	0	14	–	–	0.077106	0.000091	26	40	C
WX Hyi	2014	0.077616	0.000037	0	52	–	–	0.077367	0.000072	52	103	C
AO Oct	2013	0.067326	0.000046	0	59	19.6	6.4	0.066776	0.000064	59	91	B
DT Oct	2014	–	–	–	–	–	–	0.074022	0.000113	54	81	C
V521 Peg	2013	0.061503	0.000032	0	67	13.8	5.8	0.061006	0.000029	67	199	B
TY Psc	2013	–	–	–	–	–	–	0.070381	0.000030	27	57	C

*Interval used for calculating the period (corresponding to E in section 3).

† Unit 10^{-5} .

‡ References: FO And (Thorstensen et al. 1996), V342 Cam (Shears et al. 2011b), YZ Cnc (Shafter, Hessman 1988), GZ Cnc (Tappert, Bianchini 2003), AL Com (this work), MN Dra (Pavlenko et al. 2010), CP Eri (Armstrong et al. 2012), VW Hyi (this work), WX Hyi (Schoembs, Vogt 1981), AO Oct (Woudt et al. 2004), V521 Peg (Rodríguez-Gil et al. 2005), TY Psc (Thorstensen et al. 1996), V893 Sco (this work), RZ Sge (Patterson et al. 2003), SU UMa (Thorstensen et al. 1986), SS UMi (Thorstensen et al. 1996), CU Vel (this work), ASASSN-13ck – TCP J233822 (this work)

§ Data quality and comments. A: excellent, B: partial coverage or slightly low quality, C: insufficient coverage or observations with large scatter, G: P_{dot} denotes global P_{dot} , M: observational gap in middle stage, 2: late-stage coverage, the listed period may refer to P_2 , E: P_{orb} refers to the period of early superhumps, P: P_{orb} refers to a shorter stable periodicity recorded in outburst.

The object was again detected in outburst on 2013 July 26 by C. Chiselbrook visually and confirmed by W. MacDonald II using a CCD. Since the object was not detected by the same observer on July 25, the outburst appeared to be a young one. Although this outburst was supposed to provide an opportunity to detect early superhumps, no meaningful coherent period was detected (vsnet-alert 16064, 16065, 16075) partly due to the high air mass and the short visibility in the evening. Only three days after the outburst detection, likely growing ordinary superhumps were detected (vsnet-alert 16080, 16087). The period of early superhumps, if there was any, was very short compared to other WZ Sge-type dwarf novae.

Since the comparison star was much redder than the variable and some observations were done at high air-masses, we corrected observations by using a second-order atmospheric extinction whose coefficients were experimen-

tally determined. The times of superhump maxima during the plateau phase are listed in table 6. The times of superhumps were not determined by the fitting method on July 29 (BJD 2456503). Although the amplitudes of superhumps grew during the initial three nights and they were likely stage A superhumps, the stages were not distinct on the $O - C$ diagram. This was probably due to the shortness of stage A itself and limited observation. We used $E \geq 15$ for determining the period in table 2 to avoid the inclusion of stage A superhumps. Using the data for BJD 2456503–2456506, we obtained a period of 0.06210(5) d with the PDM method. We regard it the likely period of stage A superhumps. The superhump period was almost constant during stage B and no clear transition to stage C was recorded.

After the rapid fading from the superoutburst, individual times of superhumps could not be measured due to the faintness. We could, however, detect signals with

Table 2. Superhump Periods and Period Derivatives (continued)

Object	Year	P_1	err	E_1	P_{dot}	err	P_2	err	E_2	P_{orb}	Q		
V893 Sco	2013	0.078675	0.000025	0	52	–	–	0.078288	0.000054	51	153	0.075961	B
RZ Sge	2013	0.070642	0.000026	0	58	11.5	4.2	–	–	–	–	0.06828	C
AW Sge	2013	–	–	–	–	–	–	0.074293	0.000025	62	90	–	C
V1265 Tau	2013	0.053428	0.000024	0	187	1.9	1.9	0.053086	0.000043	186	319	–	B
SU UMa	2013	–	–	–	–	–	–	0.078775	0.000131	0	51	0.07635	C
SS UMi	2013	–	–	–	–	–	–	0.069936	0.000095	0	59	0.06778	C
CU Vel	2013	–	–	–	–	–	–	0.080573	0.000043	0	63	0.078054	B
ASAS J224349	2013	0.069719	0.000048	0	55	25.2	7.5	0.069513	0.000015	87	149	–	B
ASASSN-13cf	2013	0.058407	0.000028	0	115	7.1	1.9	–	–	–	–	–	B
ASASSN-13cg	2013	0.060228	0.000037	0	63	24.4	6.9	–	–	–	–	–	C
ASASSN-13ck	2013	0.056186	0.000010	35	185	5.6	0.4	–	–	–	–	0.055348	AE
ASASSN-13cz	2013	0.079773	0.000058	0	13	–	–	–	–	–	–	–	C
ASASSN-13da	2013	0.071781	0.000037	56	140	6.5	4.1	0.071259	0.000309	154	182	–	C
ASASSN-14ac	2014	0.058550	0.000009	57	188	–1.7	1.2	–	–	–	–	–	B
CSS J024354	2013	0.062076	0.000042	0	129	–	–	–	–	–	–	–	CGM
MASTER J004527	2013	0.080365	0.000020	12	50	–3.8	4.8	0.080004	0.000012	50	144	–	A
MASTER J005740	2013	0.057067	0.000011	14	144	4.0	1.0	–	–	–	–	0.056190	B
MASTER J024847	2013	0.0644	0.0003	0	2	–	–	–	–	–	–	–	C
MASTER J061335	2013	0.056091	0.000021	61	269	5.1	0.6	0.055950	0.000072	268	321	–	B
MASTER J073208	2013	0.058836	0.000081	0	38	–	–	–	–	–	–	–	C
MASTER J162323	2013	0.088661	0.000020	35	192	3.9	0.9	–	–	–	–	–	B
MASTER J234843	2013	0.032007	0.000005	0	255	1.3	0.5	0.031977	0.000010	249	438	–	C
OT J210016	2013	0.058502	0.000020	17	160	2.3	1.5	–	–	–	–	0.05787	CE
PNV J191501	2013	0.058382	0.000010	58	297	5.2	0.2	0.058176	0.000033	292	366	0.05706	AE
SSS J094327	2014	0.070500	0.000010	14	60	5.6	2.3	0.070241	0.000048	57	88	–	C
TCP J233822	2013	0.057868	0.000014	39	206	2.7	1.1	–	–	–	–	0.057255	AE

Table 4. Superhump maxima of DH Aql (2000)

E	max*	error	$O - C^\dagger$	N^\ddagger
0	51759.1254	0.0005	–0.0030	101
1	51759.2027	0.0005	–0.0055	161
11	51760.0042	0.0002	–0.0019	171
12	51760.0842	0.0002	–0.0016	172
13	51760.1645	0.0003	–0.0012	122
14	51760.2479	0.0009	0.0025	49
24	51761.0444	0.0008	0.0011	174
25	51761.1217	0.0003	–0.0013	173
26	51761.2045	0.0011	0.0017	150
36	51762.0026	0.0002	0.0019	138
37	51762.0812	0.0003	0.0007	170
38	51762.1621	0.0004	0.0019	171
39	51762.2527	0.0011	0.0127	44
85	51765.9083	0.0011	–0.0017	54
86	51765.9838	0.0011	–0.0061	66

*BJD–2400000.

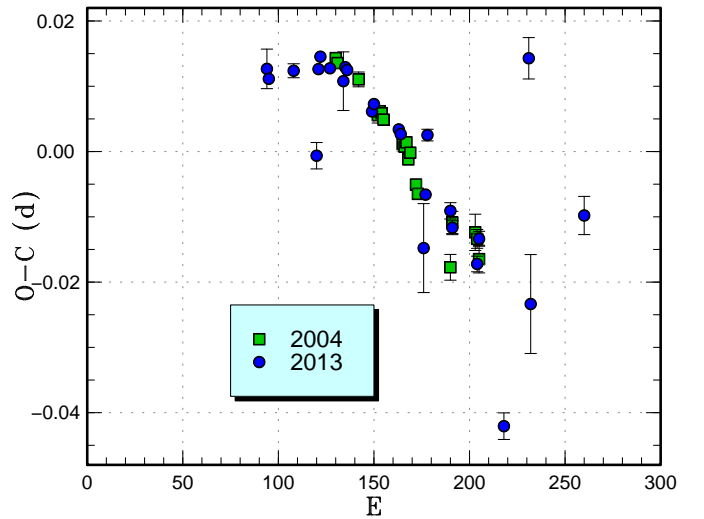
 † Against max = 2451759.1285 + 0.079783 E . ‡ Number of points used to determine the maximum.**Fig. 3.** Comparison of $O - C$ diagrams of BB Ari between different superoutbursts. A period of 0.07254 d was used to draw this figure. Approximate cycle counts (E) after the precursor outburst were used (2013). Since the start of the 2004 superoutburst was not well constrained, we shifted the $O - C$ diagram to best fit the 2013 one.

Table 5. Superhump maxima of BB Ari (2013)

E	max*	error	$O - C^\dagger$	N^\ddagger
0	56514.8763	0.0030	-0.0029	17
1	56514.9473	0.0009	-0.0042	24
14	56515.8916	0.0011	-0.0001	44
26	56516.7491	0.0020	-0.0104	25
27	56516.8349	0.0004	0.0031	71
28	56516.9093	0.0004	0.0053	99
33	56517.2702	0.0007	0.0046	69
40	56517.7760	0.0045	0.0042	24
41	56517.8507	0.0007	0.0066	58
42	56517.9228	0.0004	0.0064	74
55	56518.8595	0.0003	0.0029	110
56	56518.9332	0.0005	0.0043	35
69	56519.8723	0.0006	0.0033	52
70	56519.9441	0.0008	0.0029	25
82	56520.7971	0.0068	-0.0119	37
83	56520.8779	0.0004	-0.0035	121
84	56520.9595	0.0009	0.0059	8
96	56521.8184	0.0013	-0.0031	23
97	56521.8884	0.0011	-0.0054	27
110	56522.8258	0.0012	-0.0080	24
111	56522.9022	0.0011	-0.0040	47
124	56523.8165	0.0020	-0.0297	25
137	56524.8159	0.0032	0.0296	56
138	56524.8508	0.0076	-0.0079	67
166	56526.8955	0.0029	0.0120	48

*BJD-2400000.

†Against max = 2456514.8792 + 0.072315*E*.

‡Number of points used to determine the maximum.

the PDM method. During the interval BJD 2456511–2456515 (the “dip” after the fading), we obtained a period of 0.0610(1) d. During the interval BJD 2456515–2456522 (the initial two rebrightenings), we detected a period of 0.06182(4) d. During the interval BJD 2456522–2456532 (the last two rebrightenings), we detected a period of 0.06197(4) d. These periods suggest that superhumps persisted during the entire rebrightening phase.

The object underwent four post-superoutburst rebrightenings as in the 2003 superoutburst (figure 4). The object slightly brightened when superhump appeared. This phenomenon is common to what was observed in objects with multiple rebrightenings [EG Cnc (Patterson et al. 1998); EZ Lyn (Kato et al. 2012a); MASTER OT J211258.65+242145.4 and MASTER OT J203749.39+552210.3 (Nakata et al. 2013b); for a complete list, see Nakata et al. (2013b)]. It looks like this phenomenon is more apparent in systems with multiple rebrightenings.

The mean length of the supercycle has been updated 3170(110) d assuming that one superoutburst escaped detection around 1986.

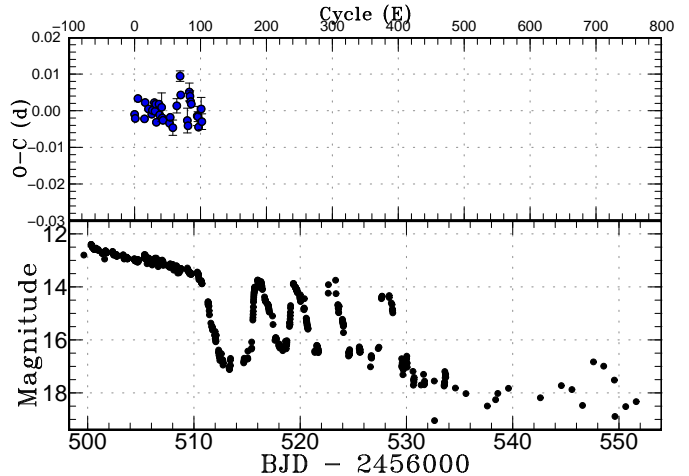


Fig. 4. $O - C$ diagram of superhumps in UZ Boo (2013). (Upper): $O - C$ diagram. A period of 0.062032 d was used to draw this figure. (Lower): Light curve. The observations were binned to 0.012 d.

3.5. *V342 Camelopardalis*

V342 Cam (=1RXS J042332+745300 =HS 0417+7445) was selected as a CV as an ROSAT X-ray source (Wu et al. 2001) and spectroscopic survey (Aungwerojwit et al. 2006). Kato et al. (2009) and Kato et al. (2010) reported observations of superhumps during the 2008 and 2010 superoutburst, respectively. Shears et al. (2011b) also presented analysis of the 2008 superoutburst and examined outburst behavior during the 2005–2010 interval. Shears et al. (2011b) photometrically obtained an orbital period of 0.07531(8) d.

On 2013 August 1, ASAS-SN detected an outburst (vsnet-alert 16096). The outburst was not young enough and only stage C superhumps were recorded (table 7). On the final night, the profile was double-humped. We showed the maxima on the smooth extension of stage C superhumps in the table. A comparison of $O - C$ diagrams of between different superoutbursts is shown in figure 5.

3.6. *V452 Cassiopeiae*

V452 Cas was discovered as a dwarf nova (=S 10453) with a range of 14–17.5 (photographic magnitudes) by Richter (1969). Bruch et al. (1987) also detected an outburst. Liu, Hu (2000) obtained a spectrum in quiescence and detected $H\alpha$ line in emission.

Although the object has been monitored visually by amateur observers since 1992, no secure outburst had been detected since 1999 October 8, when P. Schmeer detected an outburst of 16.2 mag (unfiltered CCD; vsnet-alert 3561). Schmeer suspected that past possible visual detections were likely the close companion star rather than true outbursts. The object further brightened to 15.52 mag on the next night. On 1999 November 9, P. Schmeer reported (private communication) a bright (around 15.0 mag) outburst and suspected it a superoutburst. This bright outburst was also confirmed visually at magnitude 14.7–14.9

Table 6. Superhump maxima of UZ Boo (2013)

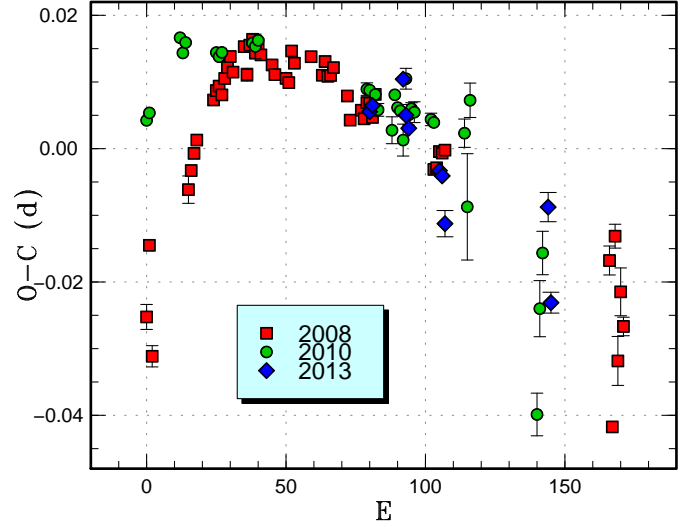
E	max*	error	$O - C^\dagger$	N^\ddagger
0	56504.4170	0.0005	-0.0007	136
1	56504.4762	0.0006	-0.0034	110
5	56504.7297	0.0003	0.0020	90
15	56505.3481	0.0002	0.0004	106
16	56505.4120	0.0004	0.0024	52
21	56505.7209	0.0003	0.0013	91
26	56506.0283	0.0005	-0.0013	266
27	56506.0914	0.0009	-0.0002	171
30	56506.2797	0.0004	0.0022	127
31	56506.3391	0.0006	-0.0004	125
32	56506.4039	0.0004	0.0024	222
33	56506.4631	0.0008	-0.0004	52
37	56506.7129	0.0004	0.0014	106
38	56506.7725	0.0006	-0.0010	58
41	56506.9606	0.0039	0.0011	117
42	56507.0198	0.0002	-0.0017	424
43	56507.0811	0.0003	-0.0024	445
53	56507.7009	0.0005	-0.0026	91
54	56507.7644	0.0006	-0.0011	62
58	56508.0069	0.0024	-0.0065	93
64	56508.3879	0.0019	0.0025	25
69	56508.7038	0.0015	0.0084	84
70	56508.7620	0.0011	0.0046	88
80	56509.3604	0.0015	-0.0169	28
81	56509.4368	0.0008	-0.0025	129
83	56509.5668	0.0021	0.0035	63
84	56509.6294	0.0015	0.0041	76
85	56509.6910	0.0009	0.0038	69
86	56509.7519	0.0009	0.0026	89
95	56510.3080	0.0035	0.0007	64
96	56510.3681	0.0008	-0.0011	132
97	56510.4276	0.0013	-0.0037	61
101	56510.6821	0.0032	0.0029	55
102	56510.7407	0.0021	-0.0005	67

*BJD-2400000.

 † Against max = 2456504.4177 + 0.0619954*E*. ‡ Number of points used to determine the maximum.**Table 7.** Superhump maxima of V342 Cam (2013)

E	max*	error	$O - C^\dagger$	N^\ddagger
0	56511.4451	0.0005	-0.0019	78
1	56511.5245	0.0005	-0.0006	72
12	56512.3914	0.0011	0.0076	70
13	56512.4645	0.0008	0.0025	78
14	56512.5410	0.0005	0.0010	70
25	56513.3975	0.0006	-0.0012	79
26	56513.4752	0.0006	-0.0016	73
27	56513.5465	0.0020	-0.0084	55
64	56516.4516	0.0022	0.0083	83
65	56516.5157	0.0016	-0.0057	83

*BJD-2400000.

 † Against max = 2456511.4471 + 0.078067*E*. ‡ Number of points used to determine the maximum.**Fig. 5.** Comparison of $O - C$ diagrams of V342 Cam between different superoutbursts. A period of 0.07845 d was used to draw this figure. Approximate cycle counts (E) after the start of the superoutburst were used. Since the start of the 2013 superoutburst was not well constrained, we shifted the $O - C$ diagram to best fit the others.

(vsnet-alert 3684). Schmeer suspected that this object is an SU UMa-type dwarf nova with (rather) frequent small-amplitude outbursts (vsnet-alert 3687). T. Vanmunster detected superhumps with a period of 0.0891 d (vsnet-alert 3698, 3707). Superhumps were also detected during the 2000 September outburst (vsnet-alert 5276).

Shears et al. (2009) systematically studied this object between 2005 and 2008, and obtained supercycle lengths of 146 ± 16 d. Shears et al. (2009) also reported superhumps during the 2007 September superoutburst. The long-period superhumps detected in the early stage were likely stage A superhumps. An analysis of the 1999 and 2008 superoutburst was reported in Kato et al. (2009).

I. Miller detected a superoutburst on 2013 November 19 and detected a superhump (vsnet-alert 16632). The times of superhump maxima are listed in table 8. On BJD 2456624, secondary maxima of superhumps became strong. In the table, we listed maxima which are in a smooth extension of earlier times of maxima. A comparison of $O - C$ diagram (figure 6) indicates that the evolution of superhumps during this superoutburst followed the trend previously recorded. The initial epoch likely detected the time near stage A-B transition. In table 2, a global P_{dot} including all stages is given.

The preceding superoutbursts occurred in 2013 January and June (BJD 2456305 and 2456445). The supercycles between these three superoutburst were 140 d and 171 d, suggesting that the supercycle significantly varies.

3.7. V359 Centauri

V359 Cen was originally discovered as a possible nova by A. Opolski [originally in Lwów Contr. 4 (Prager, Shapley 1941)]. The object was visible between 1930 April 20 and

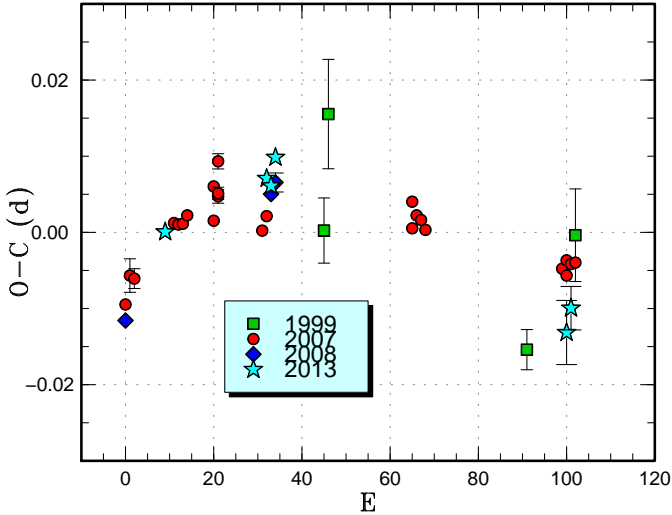


Fig. 6. Comparison of $O-C$ diagrams of V452 Cas between different superoutbursts. A period of 0.08880 d was used to draw this figure. Approximate cycle counts (E) after the start of the superoutburst were used.

Table 8. Superhump maxima of V452 Cas (2013)

E	max*	error	$O-C^\dagger$	N^\ddagger
0	56616.2975	0.0004	-0.0086	117
23	56618.3469	0.0007	0.0031	92
24	56618.4347	0.0005	0.0023	131
25	56618.5273	0.0010	0.0063	69
91	56624.3651	0.0042	-0.0033	41
92	56624.4570	0.0029	0.0001	38

*BJD-2400000.

† Against max = 2456616.3061 + 0.088596 E .

‡ Number of points used to determine the maximum.

27 and faded from 13.8 to 15.0 mag. Assuming a typical absolute maximum for a nova, a large distance of 160 kpc was inferred (McLaughlin 1945). McLaughlin (1945) already discussed the possibility of a dwarf nova. Duerbeck (1987) proposed a 21.0 mag quiescent counterpart. Munari, Zwitter (1998) tried to study the proposed quiescent counterpart spectroscopically, but the attempt failed due to the faintness. Gill, O’Brien (1998) could not find a nova shell in a deep image.

The second historical outburst was recorded by R. Stubbings on 1999 July 13. Woudt, Warner (2001) obtained time-resolved CCD photometry following the 1999 July outburst and detected a period of 0.0779 d. The object underwent further outbursts in 2000 May, 2001 April and 2002 June, and the object was recognized as an SU UMa-type dwarf nova. The detection of superhumps during the 1999 and 2002 superoutbursts was reported in Kato et al. (2002d).

The 2014 superoutburst was detected by R. Stubbings (cf. vsnet-alert 16941). Subsequent observations detected superhumps (vsnet-alert 16946, 16948, 16952). The times

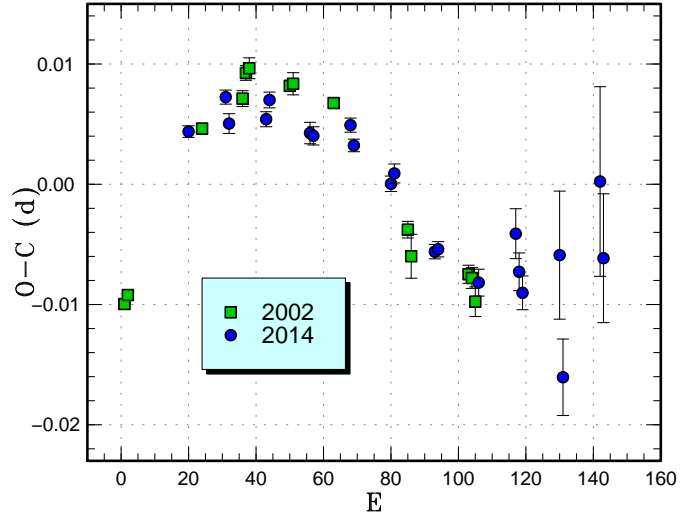


Fig. 7. Comparison of $O-C$ diagrams of V359 Cen between different superoutbursts. A period of 0.08110 d was used to draw this figure. Approximate cycle counts (E) after the start of the superoutburst were used. Since the start of the 2014 superoutburst was not well constrained, we shifted the $O-C$ diagram to best fit the 2002 one.

of superhump maxima are listed in table 9. The observation recorded the middle to later part of the superoutburst. The epochs for $E \geq 97$ correspond to the rapidly fading part of the superoutburst. The times of maxima and the identification of the superhumps was not secure due to the faintness of the object. The combined $O-C$ diagrams of the 2002 and 2014 superoutburst agree with each other (figure 7).

3.8. FZ Ceti

This object was discovered as a variable star of unknown type (=BV 1187, NSV 601) with a range of 12.2 to fainter than 14.4 in photographic magnitude (Avery, Sievers 1968). The object was also selected as a faint blue star (=PHL 3637)⁵ with a photographic magnitude of 18.7 and $U-V = -0.2$. The identification in Demartino et al. (1996) was incorrect. (Haro, Luyten 1962). S. Otero found in 2005 that this object is a dwarf nova based on ASAS-3 (Pojmański 2002) observations (vsnet-alert 8620). The ASAS-3 light curve immediately suggested that this object is an SU UMa-type dwarf nova showing superoutbursts (vsnet-alert 8621). The object was given the GCVS name FZ Cet in Kazarovets et al. (2008). Despite its brightness in outburst, the two superoutbursts occurred in unfavorable seasonal condition (2010 February and 2012 February) and superhumps had not been detected until 2014.

The 2014 outburst was detected by R. Stubbings on January 19 (vsnet-alert 16797). This outburst was in better seasonal condition than the preceding two superoutbursts, and subsequent observations detected superhumps

⁵ The name in the Downes CV catalog (Downes et al. 2001) is incorrect.

Table 9. Superhump maxima of V359 Cen (2014)

E	max*	error	$O - C^\dagger$	N^\ddagger
0	56712.8358	0.0005	-0.0034	17
11	56713.7308	0.0006	0.0009	19
12	56713.8097	0.0008	-0.0011	20
23	56714.7021	0.0006	0.0007	16
24	56714.7848	0.0007	0.0025	19
36	56715.7553	0.0009	0.0014	20
37	56715.8362	0.0008	0.0013	19
48	56716.7291	0.0006	0.0037	20
49	56716.8086	0.0005	0.0021	20
60	56717.6975	0.0006	0.0004	17
61	56717.7794	0.0008	0.0014	20
73	56718.7461	0.0006	-0.0034	20
74	56718.8274	0.0006	-0.0031	20
86	56719.7978	0.0011	-0.0042	20
97	56720.6940	0.0021	0.0013	19
98	56720.7719	0.0016	-0.0017	19
99	56720.8513	0.0014	-0.0033	19
110	56721.7465	0.0053	0.0013	20
111	56721.8175	0.0032	-0.0087	20
122	56722.7259	0.0079	0.0091	15
123	56722.8006	0.0054	0.0029	16

*BJD-2400000.

 \dagger Against max = 2456712.8393 + 0.080963 E . \ddagger Number of points used to determine the maximum.**Table 10.** Superhump maxima of FZ Cet (2014)

E	max*	error	$O - C^\dagger$	N^\ddagger
0	56678.0315	0.0002	0.0012	106
1	56678.0889	0.0003	0.0000	114
9	56678.5564	0.0006	-0.0008	17
17	56679.0233	0.0020	-0.0023	56
18	56679.0821	0.0003	-0.0020	107
19	56679.1463	0.0015	0.0036	33
43	56680.5482	0.0023	0.0004	12

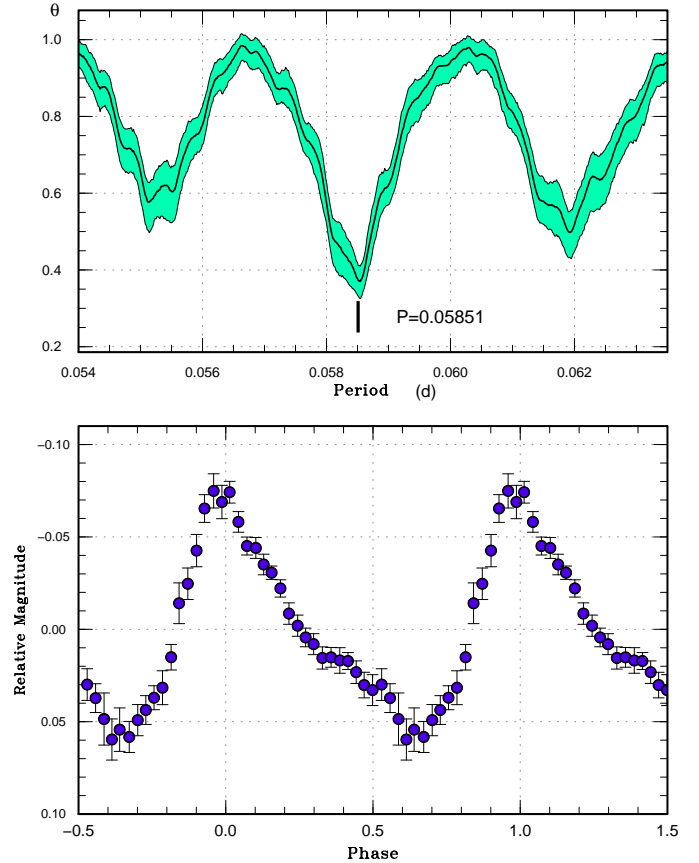
*BJD-2400000.

 \dagger Against max = 2456678.0303 + 0.058547 E . \ddagger Number of points used to determine the maximum.

(vsnet-alert 16803, 16808; figure 8). The times of superhump maxima are listed in table 10. The superoutburst lasted more than 11 d (vsnet-alert 16845).

3.9. YZ Cancri

YZ Cnc is a well-known active SU UMa-type dwarf nova (e.g. Szkody, Mattei 1984). Although Patterson (1979) detected superhumps, the identification of the period was incorrect (Kato et al. 2009). The 2007 and 2011 superoutbursts were reported in Kato et al. (2009). The 2014 superoutburst was reported in Kato et al. (2013a). We here reported another superoutburst in 2014 January. The times of superhump maxima during the main superoutburst are listed in table 11. Since we could not determine

**Fig. 8.** Superhumps in FZ Cet (2013). (Upper): PDM analysis. (Lower): Phase-averaged profile.

whether there was a jump in the phase (as in traditional late superhumps) after the fading from the main superoutburst, we listed the times of superhumps after the superoutburst separately (table 12). A comparison of the $O - C$ diagrams (figure 9) suggest that post-superoutburst superhumps in the 2014 superoutburst were indeed traditional late superhumps.

3.10. GZ Cancri

GZ Cnc is a variable star (=TmzV34) discovered by K. Takamizawa. The object turned out to be an active dwarf nova (Kato et al. 2001b; Kato et al. 2001b; Kato et al. 2002a). Tappert, Bianchini (2003) obtained the orbital period of 0.08825(28) d by radial-velocity observations. This period indicates that GZ Cnc is located in the period gap, and it became an interesting question whether GZ Cnc is an SU UMa-type dwarf nova. In 2010 March, a long outburst turned out to be a superoutburst (Kato et al. 2010). Another superoutburst was recorded in 2013 February (Kato et al. 2014).

The 2014 January superoutburst was detected by R. Stubbings (vsnet-alert 16758). The bright magnitude immediately suggested a superoutburst. The initial observation recorded a long superhump period (vsnet-alert 16782). The times of superhump maxima are listed in

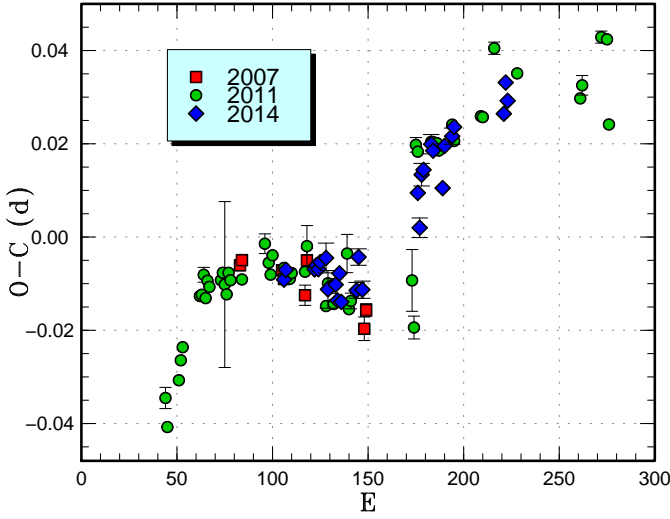


Fig. 9. Comparison of $O - C$ diagrams of YZ Cnc between different superoutbursts. A period of 0.09050 d was used to draw this figure. Approximate cycle counts (E) after the start of the superoutburst were used (in the case of YZ Cnc, this refers to the precursor outburst). Since the start of the 2014 superoutburst was not well constrained, we shifted the $O - C$ diagram to best fit the others.

Table 11. Superhump maxima of YZ Cnc (2014)

E	max*	error	$O - C^\dagger$	N^\ddagger
0	56678.6122	0.0016	-0.0023	23
1	56678.7048	0.0011	-0.0001	21
16	56680.0624	0.0006	0.0011	100
17	56680.1538	0.0007	0.0021	201
18	56680.2434	0.0005	0.0013	201
19	56680.3355	0.0013	0.0029	48
22	56680.6079	0.0032	0.0041	21
23	56680.6916	0.0040	-0.0026	20
27	56681.0546	0.0011	-0.0013	100
28	56681.1417	0.0011	-0.0046	101
29	56681.2380	0.0011	0.0013	99
30	56681.3224	0.0009	-0.0047	82
38	56682.0489	0.0017	-0.0016	55
39	56682.1466	0.0018	0.0056	48
41	56682.3205	0.0018	-0.0013	38

*BJD-2400000.

\dagger Against max = 2456678.6145 + 0.090422 E .

\ddagger Number of points used to determine the maximum.

Table 12. Superhump maxima of YZ Cnc (2014) (post-superoutburst)

E	max*	error	$O - C^\dagger$	N^\ddagger
0	56684.9658	0.0015	-0.0020	68
1	56685.0488	0.0021	-0.0098	65
2	56685.1507	0.0024	0.0011	66
3	56685.2422	0.0016	0.0017	68
7	56685.6098	0.0021	0.0056	24
8	56685.6989	0.0011	0.0038	22
13	56686.1433	0.0015	-0.0064	68
14	56686.2429	0.0007	0.0023	68
18	56686.6070	0.0017	0.0027	19
19	56686.6994	0.0011	0.0042	22
45	56689.0553	0.0010	-0.0038	66
46	56689.1525	0.0015	0.0025	68
47	56689.2391	0.0012	-0.0019	67

*BJD-2400000.

\dagger Against max = 2456684.9678 + 0.090918 E .

\ddagger Number of points used to determine the maximum.

Table 13. Superhump maxima of GZ Cnc (2014)

E	max*	error	$O - C^\dagger$	N^\ddagger
0	56663.1487	0.0015	-0.0142	60
1	56663.2486	0.0003	-0.0073	181
2	56663.3478	0.0003	-0.0010	181
12	56664.2934	0.0005	0.0149	69
53	56668.1021	0.0004	0.0118	127
54	56668.1945	0.0004	0.0112	162
55	56668.2812	0.0018	0.0050	64
75	56670.1309	0.0008	-0.0048	160
79	56670.5059	0.0005	-0.0017	102
80	56670.5937	0.0008	-0.0068	76
90	56671.5261	0.0005	-0.0042	96
91	56671.6229	0.0006	-0.0002	91
92	56671.7136	0.0006	-0.0026	89

*BJD-2400000.

\dagger Against max = 2456663.1629 + 0.092970 E .

\ddagger Number of points used to determine the maximum.

table 13. The maxima $E \leq 2$ correspond to stage A superhumps (see also figures 10; 11). A PDM analysis of this part of the data yielded a period of 0.0969(3) d (the period in vsnet-alert 16782 referred to $E \leq 12$). Due to the shortness of the run, the accuracy of this period of stage A superhumps is limited. This ε corresponds to $q=0.30(2)$ (Kato, Osaki 2013b; see subsection 4.2). Although this estimate is based on very limited observations, this observation seems to support that this object has a mass ratio near the borderline of the condition for the 3:1 resonance (q range 0.25–0.33 depending on simulations). The object is indeed likely a “borderline” SU UMA-type dwarf nova.

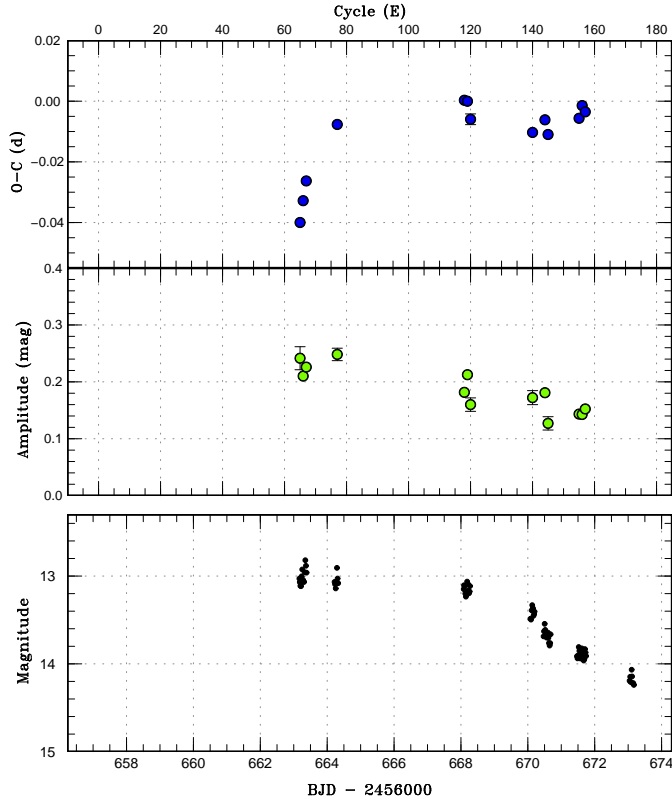


Fig. 10. $O - C$ diagram of superhumps in GZ Cnc (2014). (Upper): $O - C$ diagram. A period of 0.09270 d was used to draw this figure. Approximate cycle counts (E) after the start of the superoutburst were used. (Middle): Amplitudes of the superhumps. (Lower): Light curve. The observations were binned to 0.019 d.

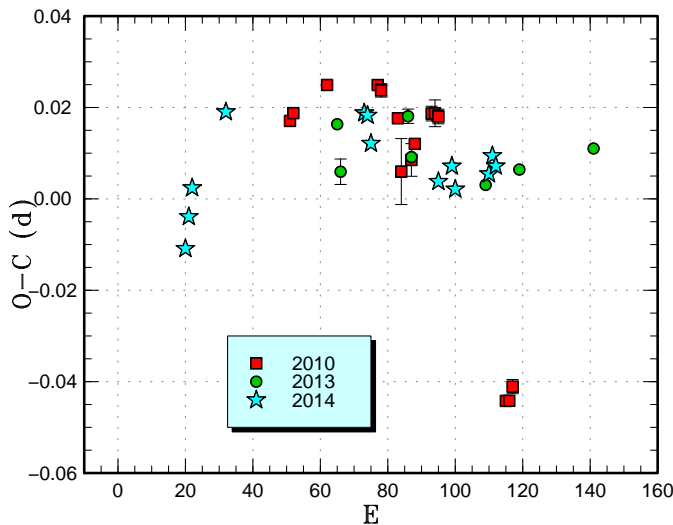


Fig. 11. Comparison of $O - C$ diagrams of GZ Cnc between different superoutbursts. A period of 0.09290 d was used to draw this figure. Approximate cycle counts (E) after the start of the superoutburst were used.

3.11. AL Comae Berenices

AL Com is one of the renowned high-amplitude dwarf novae since the discovery in 1962 by Rosino (Bertola 1964). Szkody (1987) showed a large amplitude variation with a period near 40 min and suggested that AL Com may belong to either DQ Her-type magnetic systems or AM CVn-type double degenerate systems. Further spectroscopic observation by Mukai et al. (1990) precluded the latter possibility. More extensive photometry by Abbott et al. (1992) showed two distinct periodicities of 41 min and 87–90 min; the latter was suggested to be the orbital period, and the former the rotation period of the white dwarf. From these periods, Abbott et al. (1992) concluded that AL Com bears the properties of both an enigmatic dwarf nova WZ Sge and a unique intermediate polar EX Hya. The 1995 superoutburst clarified that this object is a WZ Sge-type dwarf nova, and it shows double-wave modulations (now called early superhumps) during the early stage of the superoutburst (Kato et al. 1996). Based on the outburst light curve and the orbital parameters, AL Com was considered as a “twin” of WZ Sge. This superoutburst was particularly well documented (Patterson et al. 1996; Howell et al. 1996; Nogami et al. 1997).

Another superoutburst was recorded in 2001 (Ishioaka et al. 2002). A less observed superoutburst in 2007 indicated that the post-superoutburst rebrightenings are different between different superoutbursts (Uemura et al. 2008). There was an outburst in 2003 detected in SDSS, which was missed by visual observers.

The 2013 superoutburst was detected on December 6 by C. Gualdoni (cvnet-outburst 5738). Subsequent observations detected early superhumps (vsnet-alert 16695, 16712). The evolution of superhumps in the early stage was well observed (vsnet-alert 16718, 16724).

The period of early superhumps was determined to be 0.056660(8) d with the PDM method from observations before BJD 2456639.5. This value is in very good agreement with the 2001 measurement of early superhumps (figure 12; see subsection 4.4). The commonly accepted mechanism of early superhumps (cf. Osaki, Meyer 2002) suggests that the phases of early superhumps is constant between superoutburst (which is defined by the orientation of the observer against the binary orbit). Assuming that the phases of early superhumps are the same between the 1995, 2001 and 2013 superoutbursts, we can determine the orbital period. The refined orbital period of 0.056668589(9) d well expresses all the observations. An alias by one cycle is 0.056667180(9) d is not favored if we believe the identification of the period by Patterson et al. (1996).

The times of superhump maxima during the plateau phase of the superoutburst are listed in table 14. Stage A superhumps were better detected during the 2013 superoutburst than during the previous ones. The 2013 superoutburst showed a positive P_{dot} of $+4.9(19) \times 10^{-5}$. This value is larger than the 1995 and 2001 measurements. A comparison of the $O - C$ diagrams between different superoutbursts is presented in figure 14.

The times of superhump maxima after the rapid fading are listed in table 15. A PDM analysis of the combined data in this interval yielded a period of 0.057393(10) d. Although the overall $O - C$ diagram (figure 13) suggests the presence of a phase jump around the dip, the later times of superhump maxima appear to be on a smooth extension of stage B superhumps.

A comparison of light curves of different superoutbursts is shown in figure 15. All superoutbursts (except the poorly observed 2007 one) showed a dip and a plateau-type rebrightening. The second (rebrightening) plateau after the dip was almost flat for the 1995 superoutburst and was associated by an initial small dip in the 2013 one. The 2007 superoutburst was more structured, as reported in Uemura et al. (2008), but it is still unlike discrete rebrightenings such as EG Cnc (Patterson et al. 1998; Kato et al. 2004b). We consider that the 2007 superoutburst resembled the 2001 superoutburst of WZ Sge or with small brightenings with amplitudes less than 1 mag. Although the duration of the rebrightening plateau in the 2001 superoutburst appears longer than in other superoutbursts, this part of the observation was of low quality and it needs to be interpreted carefully. A variation in the rebrightening was also observed in EZ Lyn (Kato et al. 2012a) and suspected in WZ Sge (Patterson et al. 1981). Although there is subtle difference between the pattern of rebrightenings in the same object, the present comparison of the light curves in AL Com suggests that the pattern of rebrightening is in general reproducible.

The known outbursts of AL Com are listed in table 16. The supercycle appears to be 6–7 yr. Since the 2003 outburst escaped detection by visual observers, the true frequency of normal outburst may be higher than this table suggests.

3.12. V503 Cygni

This SU UMA-type dwarf nova is notable for its unusually short (89 d) supercycle and the occasional presence of negative superhumps (Harvey et al. 1995). Kato et al. (2002b) reported a dramatic variation in the number of normal outbursts, and this finding led to the discovery of the state with negative superhumps suppressing the number of normal outbursts (Ohshima et al. 2012; Zemko et al. 2013; Osaki, Kato 2013a; Osaki, Kato 2013b).

The superoutburst in 2013 August was observed only for two nights during in the final part. We obtained maxima of BJD 2456527.4717(11) ($N = 88$), 2456527.5580(27) ($N = 47$), 2456532.3896(20) ($N = 67$), 2456532.4696(13) ($N = 63$). Since the phases of the latter two maxima are ~ 0.5 phase different from the earlier ones, they may be traditional late superhumps.

3.13. IX Draconis

IX Dra was selected as an ultraviolet-excess object (=KUV 18126+6704) by Noguchi et al. (1980). Noguchi et al. (1982) detected its variability. Wegner, McMahan (1988) spectroscopically classified the object as a B subdwarf. Liu et al. (1999) classified the object as a dwarf nova by spectroscopy. Klose (1995) detected variability

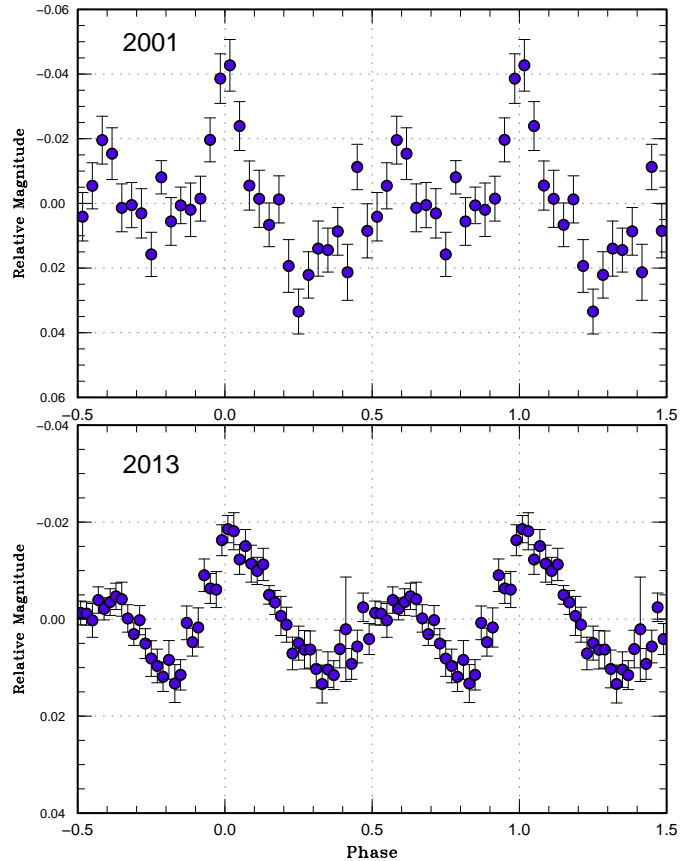


Fig. 12. Comparison of early superhumps in AL Com between 2001 and 2013.

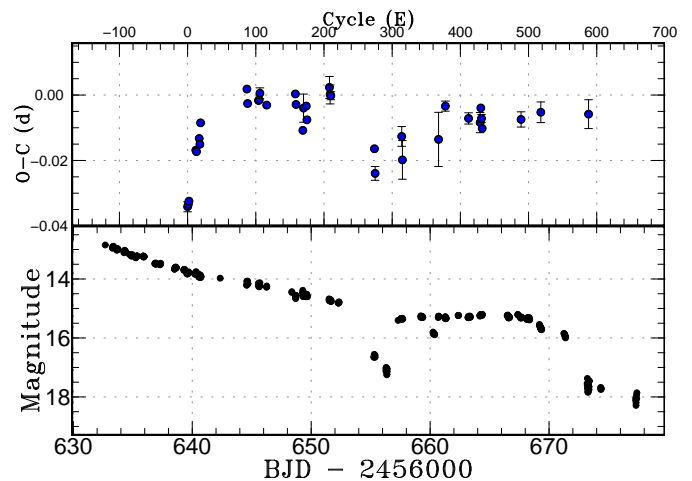


Fig. 13. $O - C$ diagram of superhumps in AL Com (2013). (Upper): $O - C$ diagram. A period of 0.05733 d was used to draw this figure. (Lower): Light curve. The observations were binned to 0.011 d.

Table 16. Outbursts of AL Com

Date*	Maximum [†]	Type	Reference
1892 April 26	14.3p	–	Bertola (1964)
1941 June 25	13.8p	–	Lucchetti, Usher (1972)
1961 November 17–December 20	13.8p	super	Rosino (1961); Bertola (1964)
1965 March 26–27	13.4p	super	Zwicky (1965); Bertola (1965)
1974 April 19–20	14.1v	normal?	AAVSO
1975 March 16–June 29	12.8v	super (two outbursts?)	AAVSO
1995 April 5–May 19	12.4V	super	Patterson et al. (1996); Nogami et al. (1997)
2001 May 18–June 9?	12.6v	super	Ishioka et al. (2002)
2003 January 28	15.5g	normal	SDSS
2007 November 6–24 [‡]	15.4V	super	Uemura et al. (2008)
2013 December 6–2014 January 15	12.7V	super	this work

*For modern data, the end date refers to the end of the (second) plateau phase.

[†]p: photographic, v: visual

[‡]Rebrightening part only.

Table 14. Superhump maxima of AL Com (2013)

E	max*	error	$O - C^{\dagger}$	N^{\ddagger}
0	56639.5761	0.0015	-0.0141	92
1	56639.6341	0.0010	-0.0135	93
2	56639.6924	0.0006	-0.0126	95
12	56640.2813	0.0004	0.0018	70
13	56640.3382	0.0003	0.0013	50
17	56640.5715	0.0005	0.0049	73
18	56640.6271	0.0006	0.0030	89
19	56640.6910	0.0004	0.0094	80
87	56644.5997	0.0004	0.0122	28
88	56644.6527	0.0008	0.0077	19
104	56645.5709	0.0003	0.0068	24
105	56645.6283	0.0005	0.0069	26
106	56645.6877	0.0016	0.0088	12
116	56646.2574	0.0006	0.0041	50
158	56648.6687	0.0006	0.0028	72
159	56648.7228	0.0006	-0.0005	67
169	56649.2882	0.0010	-0.0095	90
170	56649.3523	0.0043	-0.0028	77
174	56649.5823	0.0005	-0.0026	29
175	56649.6354	0.0007	-0.0070	28
208	56651.5372	0.0033	-0.0007	26
209	56651.5924	0.0029	-0.0030	52
210	56651.6493	0.0012	-0.0035	73

*BJD-2400000.

[†]Against max = 2456639.5902 + 0.057441 E .

[‡]Number of points used to determine the maximum.

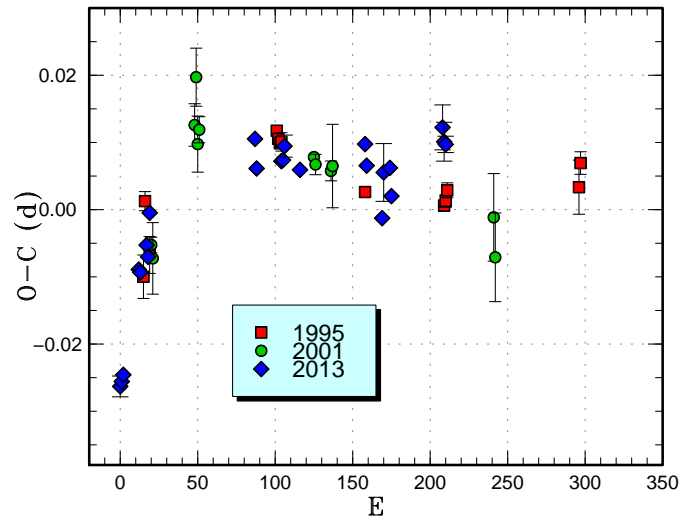


Fig. 14. Comparison of $O - C$ diagrams of AL Com between different superoutbursts. A period of 0.05732 d was used to draw this figure. Approximate cycle counts (E) after the emergence of superhump were used. Assuming that the stage A was best observed in 2013, the 1995 and 2001 $O - C$ diagrams were shifted within 20 cycles to best match the stage A-B transition in 2013.

of this object on photographic plates and obtained a period of ~ 45.7 d, although it was not strictly periodic. T. Vanmunster detected superhumps in 2000 (vsnet-alert 5368, 5369). Ishioka et al. (2001) studied this object and clarified that it is a new ER UMa-type dwarf nova with a supercycle of 53 d. Olech et al. (2004) studied the 2003 superoutburst and suggested a period of 0.06646(6) d, which they proposed to be the orbital period. This period led to a very small fractional superhump excess, from which Olech et al. (2004) suggested IX Dra to be a period bouncer. Otulakowska-Hypka et al. (2013) fur-

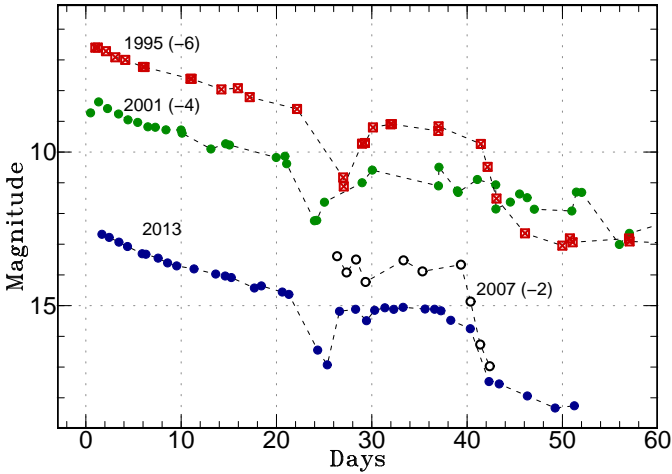


Fig. 15. Comparison of superoutbursts of AL Com. The data were binned to 1 d and shifted in magnitude. The dashed lines are added to aid recognizing the variation. The data for the 2007 superoutburst were from Uemura et al. (2008).

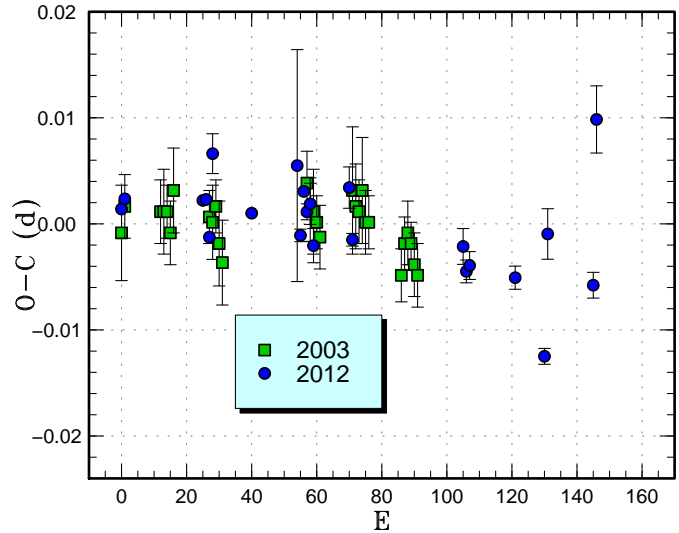


Fig. 16. Comparison of $O - C$ diagrams of IX Dra between different superoutbursts. A period of 0.06700 d was used to draw this figure. Approximate cycle counts (E) after the start of the observation were used. The starts of the superoutbursts were not well constrained.

Table 15. Superhump maxima of AL Com (2013) (post-superoutburst)

E	max*	error	$O - C^\dagger$	N^\ddagger
0	56655.3022	0.0011	0.0006	42
1	56655.3520	0.0021	-0.0070	39
40	56657.5992	0.0030	0.0023	65
41	56657.6493	0.0059	-0.0049	71
94	56660.6941	0.0083	-0.0014	28
104	56661.2776	0.0015	0.0083	59
138	56663.2230	0.0017	0.0028	16
155	56664.1963	0.0031	0.0007	55
156	56664.2582	0.0010	0.0051	60
157	56664.3123	0.0012	0.0018	60
158	56664.3666	0.0009	-0.0012	59
215	56667.6371	0.0023	-0.0014	58
244	56669.3019	0.0032	-0.0007	41
314	56673.3144	0.0044	-0.0048	30

*BJD-2400000.

† Against max = 2456655.3017 + 0.057381 E .

‡ Number of points used to determine the maximum.

ther studied this object and obtained a longer supercycle. Otulakowska-Hypka et al. (2013) discussed the secular increase of the supercycles in ER UMa-type dwarf novae. The identification of the orbital period, however, was less convincing as in Olech et al. (2004) and there is a possibility of another period which places IX Dra in a region of ordinary dwarf nova before the period minimum. Kato et al. (2013a) did not regard the orbital period by Otulakowska-Hypka et al. (2013) as the true one based on the high similarity of IX Dra to ER UMa.

We analyzed the superoutburst in 2012 July–August. The times of superhump maxima are listed in table 17. The resultant $O - C$ data indicate that the superhumps can be expressed by a single period without a strong period variation. A phase reversal as seen in ER UMa (Kato et al. 1996) was not apparent. Olech et al. (2004) also reported only small period variations. Although Kato et al. (2009) recognized stages B and C in the data of Olech et al. (2004), the present data did not show a strong sign of a stage transition (see also figure 16).

3.14. MN Draconis

This object is an SU UMa-type dwarf nova in the period gap (Antipin, Pavlenko 2002; Nogami et al. 2003). It is notable that this object showed negative superhump in quiescence (Pavlenko et al. 2010; Samsonov et al. 2010).

The 2012 July–August superoutburst was observed starting from the growing stage of superhumps. The times of superhump maxima are listed in table 18. Although the individual times of maxima were not well determined before $E \leq 10$, the $O - C$ diagram suggests that the interval $E \leq 39$ was stage A (figure 17). A PDM analysis of this segment yielded a period of 0.10993(9) d.

The 2013 November superoutburst (vsnet-alert 16611)

Table 17. Superhump maxima of IX Dra (2012)

E	max*	error	$O - C^\dagger$	N^\ddagger
0	56130.7403	0.0003	-0.0017	58
1	56130.8082	0.0003	-0.0007	56
25	56132.4161	0.0003	0.0002	126
26	56132.4832	0.0003	0.0003	144
27	56132.5466	0.0003	-0.0032	144
28	56132.6215	0.0019	0.0047	45
40	56133.4199	0.0005	-0.0003	75
54	56134.3624	0.0109	0.0048	24
55	56134.4228	0.0006	-0.0018	70
56	56134.4939	0.0005	0.0024	75
57	56134.5590	0.0008	0.0005	75
58	56134.6268	0.0019	0.0013	58
59	56134.6898	0.0016	-0.0026	44
70	56135.4323	0.0019	0.0034	75
71	56135.4944	0.0006	-0.0015	66
105	56137.7717	0.0017	-0.0006	66
106	56137.8364	0.0011	-0.0029	68
107	56137.9039	0.0013	-0.0023	68
121	56138.8408	0.0011	-0.0028	88
130	56139.4364	0.0008	-0.0098	70
131	56139.5149	0.0024	0.0017	75
145	56140.4481	0.0012	-0.0025	61
146	56140.5307	0.0032	0.0132	59

*BJD-2400000.

†Against max = 2456130.7420 + 0.066955 E .

‡Number of points used to determine the maximum.

was observed for eight nights. The times of superhump maxima are listed in table 19. A large period variation was detected. Up to $E = 18$, the amplitudes of the superhumps grew, and stage A superhumps were likely recorded (figure 18). Although we identified the following phase as stage B, the identification for $E = 95$ is uncertain due to the lower quality of the data. In table 2, we list a period derived for the interval $26 \leq E \leq 66$.

Assuming the orbital period of 0.0998(2) d (Pavlenko et al. 2010), the values of ε for stage A superhumps are 9.2(1)% for 2012 and 7.8(1)% for 2013, which correspond to $q=0.327(5)$ and $q=0.258(5)$. Since both observations were not ideal (the lack of well measured maxima for the 2012 observation and the lack of data for the early stage of the 2013 observation), we simply make an average of these values to obtain $q=0.029(5)$. A comparison of the $O - C$ diagrams between different superoutburst (figure 19) suggests that the large negative P_{dot} in the 2002b superoutburst reported in Nogami et al. (2003); Kato et al. (2009) reflected stage A-B transition.

3.15. CP Eridani

CP Eri was discovered as a faint blue variable showing an outburst (Luyten, Haro 1959). Szkody et al. (1989) obtained time-series photometry in quiescence and detected sporadic variations of 0.2–0.4 mag without clear periodicity. Howell et al. (1991) observed this object again

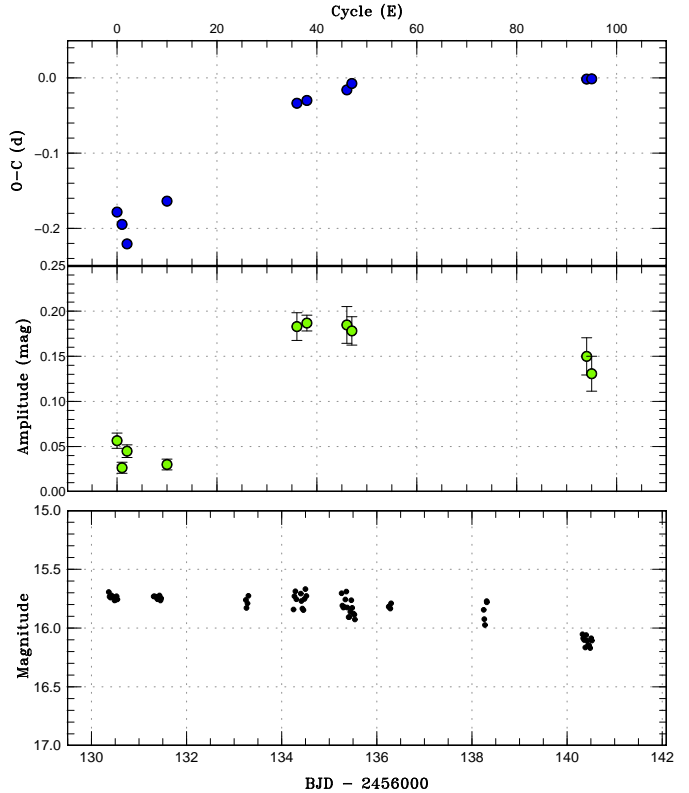


Fig. 17. $O - C$ diagram of superhumps in MN Dra (2012). (Upper): $O - C$ diagram. A period of 0.10504 d was used to draw this figure. Cycle counts (E) after the start of the observation were used. (Middle): Amplitudes of the superhumps. (Lower): Light curve. The observations were binned to 0.021 d.

Table 18. Superhump maxima of MN Dra (2012)

E	max*	error	$O - C^\dagger$	N^\ddagger
0	56130.3597	0.0048	-0.0239	42
1	56130.4483	0.0030	-0.0420	80
2	56130.5274	0.0017	-0.0696	56
10	56131.4246	0.0026	-0.0261	80
36	56134.2857	0.0011	0.0608	30
38	56134.4995	0.0006	0.0612	28
46	56135.3539	0.0015	0.0619	28
47	56135.4674	0.0012	0.0688	27
94	56140.4101	0.0017	-0.0035	27
95	56140.5155	0.0027	-0.0049	21
112	56142.3134	0.0042	-0.0209	32
113	56142.4136	0.0036	-0.0274	30
114	56142.5133	0.0045	-0.0344	28

*BJD-2400000.

†Against max = 2456130.3836 + 0.106703 E .

‡Number of points used to determine the maximum.

Table 19. Superhump maxima of MN Dra (2013)

E	max*	error	$O - C^\dagger$	N^\ddagger
0	56602.2479	0.0011	-0.0287	114
1	56602.3594	0.0010	-0.0231	116
9	56603.2248	0.0004	-0.0042	198
10	56603.3341	0.0014	-0.0007	90
18	56604.1967	0.0019	0.0154	13
26	56605.0438	0.0088	0.0159	99
27	56605.1550	0.0034	0.0213	166
28	56605.2595	0.0015	0.0200	20
46	56607.1492	0.0011	0.0051	64
47	56607.2544	0.0006	0.0044	106
48	56607.3611	0.0007	0.0053	131
57	56608.3064	0.0037	-0.0018	59
66	56609.2469	0.0012	-0.0136	95
95	56612.3137	0.0043	-0.0153	37

*BJD-2400000.

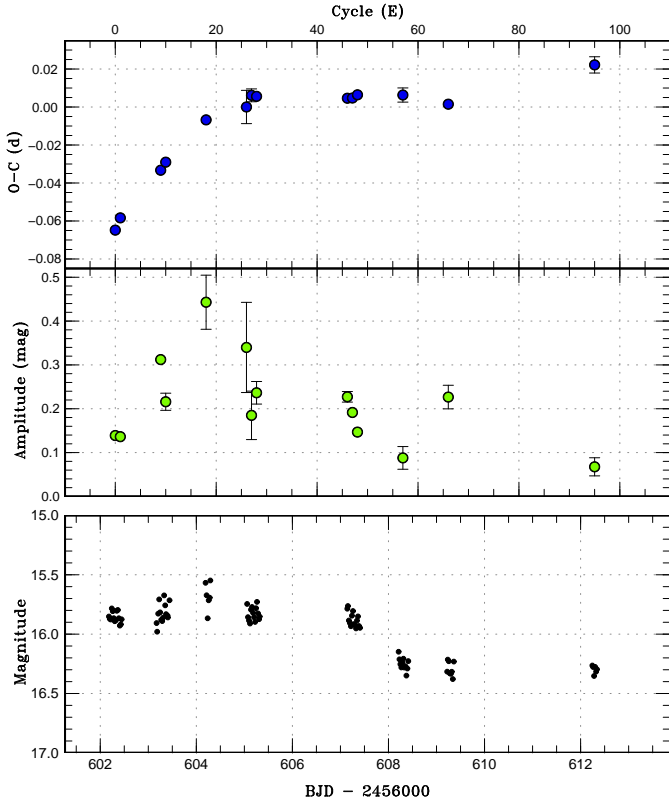
 † Against max = 2456602.2767 + 0.105815*E*. ‡ Number of points used to determine the maximum.

Fig. 18. $O - C$ diagram of superhumps in MN Dra (2013). (Upper): $O - C$ diagram. A period of 0.10504 d was used to draw this figure. Cycle counts (E) after the start of the observation were used. (Middle): Amplitudes of the superhumps. (Lower): Light curve. The observations were binned to 0.021 d.

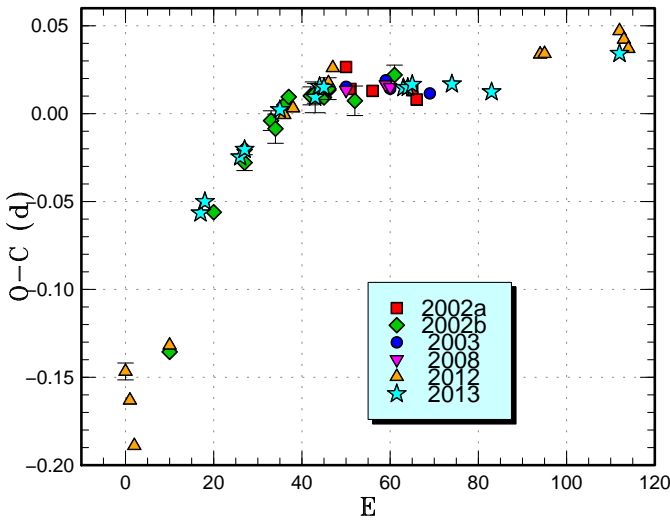


Fig. 19. Comparison of $O - C$ diagrams of MN Dra between different superoutbursts. A period of 0.1050 d was used to draw this figure. Approximate cycle counts (E) after the start of the outburst were used (2012). Since the start of the other superoutbursts was not well constrained, we shifted the $O - C$ diagram to best fit the 2012 one.

in quiescence and detected modulations with periods of 28.6–29.5 min. Due to its shortness, Howell et al. (1991) considered this period to be the spin period of the magnetic white dwarf. Abbott et al. (1992) obtained higher quality time-series photometry and identified a period of 1724(4) s (28.6 min). Furthermore, Abbott et al. (1992) obtained spectra both in high and low states, and clarified that this object lacks hydrogen lines. The helium lines were in emission in low state and in absorption in high state, and this behavior was very similar to that of CR Boo (Wood et al. 1987). Abbott et al. (1992) concluded that CP Eri is an interacting binary white dwarf (IBWD, or AM CVn-type star). Patterson et al. (1993), however, suggested that this photometric period is the superhump period since most of AM CVn-type stars show superhumps. Zwitter, Munari (1995) obtained a spectrum with a featureless blue continuum.

Although this object was discovered as an outbursting object, its outburst behavior was not clarified for a long time. Although J. Patterson (cba-info message on 1998 January 1) reported an outburst of 16.5 mag and 0.2 superhumps, the result was published only in Armstrong et al. (2012). Starting from 2003, B. Monard regularly monitored this object and detected several outbursts between 16.0 and 17.5 mag. More recently, CRTS data suggested a cycle length of ~ 100 d (Kato et al. 2012a). Ramsay et al. (2012) presented the result of long-term monitoring of AM CVn-type stars and detected three outbursts in CP Eri. The duration of the outbursts was 15 d and the outburst duty cycle was 27%. As judged from the duration, these outbursts were likely superoutbursts.

Armstrong et al. (2012), following the interpretation in Patterson et al. (1993), identified the orbital and superhump period from the 1998 data. According to this interpretation, the orbital modulation [1701.4(2) s] has doubly humped.

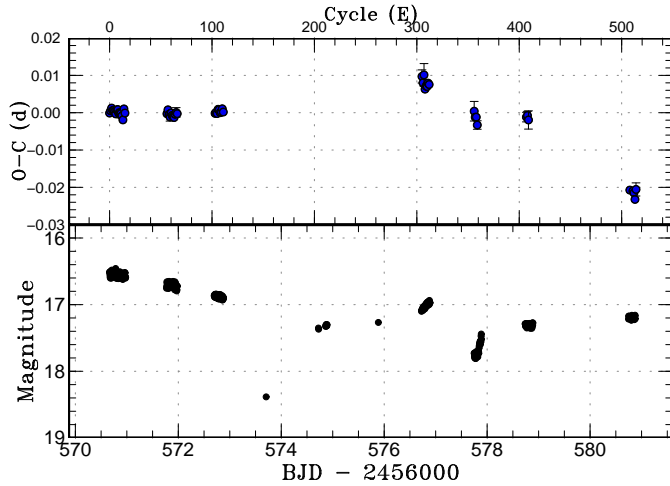


Fig. 20. $O - C$ diagram of superhumps in CP Eri (2013). (Upper): $O - C$ diagram. A period of 0.019897 d was used to draw this figure. (Lower): Light curve. The observations were binned to 0.004 d.

On 2013 October 3, ASAS-SN team detected an outburst of CP Eri (vsnet-alert 16501). Subsequent observations recorded superhumps (vsnet-alert 16510, 16515). This outbursting state near the peak was observed for three nights (the outburst lasted at least 5 d including the ASAS-SN detection) and followed by a dip (vsnet-alert 16526). After the dip, the superhump signal once became weaker, but became detectable again (vsnet-alert 16530, 16537). The later part of the outburst consisted of oscillations as reported in Armstrong et al. (2012).

The times of superhump maxima during the initial peak are listed in table 20. A positive P_{dot} of $+3.1(9) \times 10^{-5}$ was first time recorded in CP Eri. Superhumps after the dips had a shorter period [0.019752(4) d with the PDM method]. The times of maxima of these superhump are listed in table 21. The interpretation of these superhumps (whether they are superhumps as in the initial peak or “traditional” late superhumps) is not clear. It was, however, likely these superhumps were excited again after the dip phenomenon. The combined $O - C$ diagram (figure 20) may suggest that the phase of the superhumps was continuous if the superhump period continued to increase as in stage B of hydrogen-rich dwarf novae.

3.16. V1239 Herculis

This object is an eclipsing SU UMa-type dwarf nova in the period gap (Boyd et al. 2006; Littlefair et al. 2006). The 2005 and 2011 superoutbursts were reported in Boyd et al. (2006), Kato et al. (2009) and Kato et al. (2013a), respectively. On 2013 September 26, another outburst was reported (vsnet-alert 16462; also vsnet-alert 16464). Although this outburst was likely a superoutburst, only single-night observation covering an eclipse was reported. By using these observations, we refined an ephemeris of

$$\text{Min}(\text{BJD}) = 2453648.23651(1) + 0.1000822137(7)E(1)$$

Table 20. Superhump maxima of CP Eri (2013)

E	max*	error	$O - C^\dagger$	N^\ddagger
0	56570.6649	0.0008	-0.0001	14
1	56570.6854	0.0003	0.0005	19
2	56570.7060	0.0002	0.0012	19
3	56570.7253	0.0003	0.0006	19
4	56570.7452	0.0003	0.0006	19
5	56570.7649	0.0003	0.0004	19
6	56570.7841	0.0003	-0.0003	15
7	56570.8050	0.0003	0.0007	38
8	56570.8250	0.0003	0.0008	40
9	56570.8439	0.0006	-0.0002	24
10	56570.8640	0.0005	-0.0000	21
11	56570.8836	0.0012	-0.0002	21
12	56570.9029	0.0005	-0.0009	21
13	56570.9217	0.0006	-0.0019	21
14	56570.9446	0.0006	0.0010	20
15	56570.9634	0.0004	-0.0001	21
56	56571.7790	0.0006	-0.0003	15
57	56571.7999	0.0005	0.0008	15
58	56571.8186	0.0010	-0.0005	14
59	56571.8378	0.0011	-0.0012	15
60	56571.8587	0.0005	-0.0001	19
61	56571.8780	0.0004	-0.0008	32
62	56571.8975	0.0005	-0.0011	19
63	56571.9172	0.0004	-0.0013	14
64	56571.9380	0.0006	-0.0004	14
65	56571.9584	0.0013	0.0001	14
66	56571.9779	0.0008	-0.0003	11
103	56572.7142	0.0004	-0.0002	19
104	56572.7344	0.0004	0.0001	20
105	56572.7540	0.0005	-0.0002	20
106	56572.7750	0.0004	0.0009	18
107	56572.7948	0.0004	0.0008	20
108	56572.8139	0.0004	0.0000	19
109	56572.8340	0.0003	0.0002	20
110	56572.8547	0.0003	0.0011	19
111	56572.8737	0.0008	0.0002	17

*BJD-2400000.

† Against max = 2456570.6650 + 0.019897E.

‡ Number of points used to determine the maximum.

Table 21. Superhump maxima of CP Eri (2013) (after the dip)

E	max*	error	$O - C^\dagger$	N^\ddagger
0	56576.7433	0.0018	0.0013	19
1	56576.7615	0.0011	-0.0003	18
2	56576.7835	0.0030	0.0019	18
3	56576.7996	0.0006	-0.0017	20
4	56576.8203	0.0007	-0.0007	19
5	56576.8401	0.0006	-0.0007	19
6	56576.8609	0.0005	0.0003	20
7	56576.8804	0.0008	0.0001	19
51	56577.7487	0.0026	-0.0009	10
52	56577.7670	0.0010	-0.0024	16
53	56577.7869	0.0006	-0.0022	20
54	56577.8047	0.0011	-0.0042	20
102	56578.7619	0.0013	0.0047	17
103	56578.7822	0.0011	0.0052	19
104	56578.8009	0.0024	0.0042	19
203	56580.7519	0.0007	-0.0007	17
206	56580.8114	0.0009	-0.0006	19
207	56580.8308	0.0004	-0.0009	19
208	56580.8489	0.0007	-0.0025	19
209	56580.8715	0.0018	0.0003	19

*BJD-2400000.

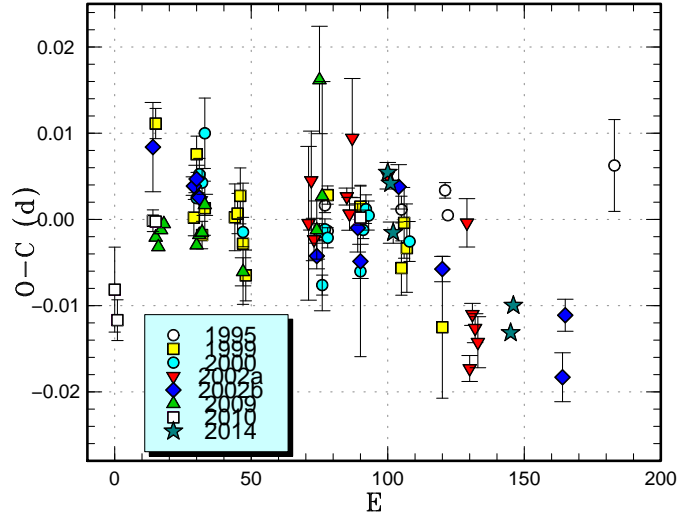
 † Against max = 2456576.7420 + 0.019757E. ‡ Number of points used to determine the maximum.

using the MCMC modeling introduced in Kato et al. (2013a). This ephemeris supersedes the one reported in Kato et al. (2013a) which was determined by the traditional minimum finding method.

3.17. CT Hydrae

CT Hya was discovered as a dwarf nova (=AN 114.1936) with a photographic range of 14.5 to fainter than 16.5 by Hoffmeister (1936). Hoffmeister (1936) recorded four outbursts between 1929 and 1934. The finding chart was published in Hoffmeister (1957). Vogt, Bateson (1982) presented a photographic chart and identified the quiescent counterpart. The first secure outburst since the discovery was reported on 1995 February 22 by CCD observations by M. Iida (VSOLJ). Iida observed the object on the subsequent night and detected variations compatible with superhumps. The same outburst was observed by Nogami et al. (1996), who reported the detection of superhumps. In Kato et al. (2009), superoutbursts in 1999, 2000, 2002 (two superoutbursts) and 2009 were reported. In Kato et al. (2010), another superoutburst in 2010 was reported.

The 2014 superoutburst was detected by CRTS (cf. vsnet-alert 16926) and observations on two nights were obtained. The times of superhump maxima are listed in table 22. The observation likely detected stage C superhumps (cf. figure 21).

**Fig. 21.** Comparison of $O - C$ diagrams of CT Hya between different superoutbursts. A period of 0.06650 d was used to draw this figure. Approximate cycle counts (E) after the maximum of the superoutburst were used. This figure is updated from the corresponding one in Kato et al. (2010), and includes the 1995 and 2014 observations. Since the start of the 2014 superoutburst was not well constrained, we shifted the $O - C$ diagram to best fit the others. The shift value for the 2002a superoutburst was corrected.**Table 22.** Superhump maxima of CT Hya (2014)

E	max*	error	$O - C^\dagger$	N^\ddagger
0	56708.1208	0.0004	0.0024	134
1	56708.1860	0.0004	0.0015	133
2	56708.2468	0.0012	-0.0039	123
45	56711.0947	0.0011	-0.0017	28
46	56711.1644	0.0007	0.0018	38

*BJD-2400000.

 † Against max = 2456708.1184 + 0.066178E. ‡ Number of points used to determine the maximum.

3.18. VW Hydri

We observed the 2012 November–December superoutburst of this famous SU UMa-type dwarf nova. By using the 2011–2012 data, we have determined the orbital period to be 0.0742705(1) d and the mean epoch of the maximum of BJD 2456116.7250(1) d. Combined with the ephemeris by Vogt (1974), we have obtained an updated ephemeris of

$$\text{Max(BJD)} = 2456116.7250(1) + 0.074271061(4)E. \quad (2)$$

The times of superhump maxima during the superoutburst plateau are listed in table 23. Although the evolution of superhumps was similar to the one in 2011 (Kato et al. 2013a), stage A superhumps were not well observed in the 2012 superoutburst. The precursor was not as apparent as in the 2011 superoutburst. During the rapid fading phase from the superoutburst, an ~ 0.5 phase jump

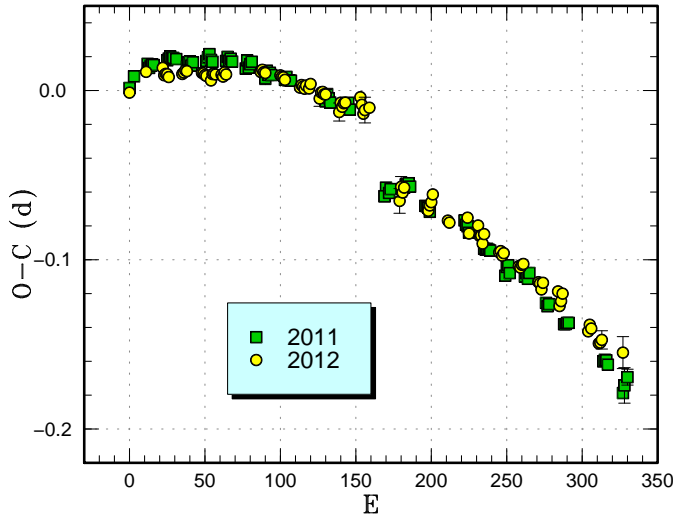


Fig. 22. Comparison of $O - C$ diagrams of VW Hyi between different superoutbursts. A period of 0.076914 d was used to draw this figure. Approximate cycle counts (E) after the maximum of the superoutburst were used.

was observed as in 2011. These superhumps can be interpreted as “traditional” late superhumps. The times of these post-superoutburst superhumps were determined after subtraction of the mean orbital profile (table 24).

A comparison of the $O - C$ diagrams between the 2011 (Kato et al. 2013a) and 2012 superoutbursts shows a slight difference in the curvature of the $O - C$ diagram during the superoutburst plateau. Although the times of post-superoutburst superhumps for the 2012 superoutburst were shown only before the next normal outburst, the signal remained detectable until ~ 40 d after the termination of the superoutburst by the PDM method. The resultant periods in 5-d intervals are listed in table 25.

The detection of negative superhumps in this object is discussed in subsection 4.8.

3.19. WX Hydri

WX Hyi was originally discovered as a variable star (=AN 9.1932) with a range of 10.7–14.2 (photographic scale at that time) by Luyten (1932). Hoffmeister (1949) classified the object as a Mira-type variable (also Kukarkin et al. 1969). Philip (1971) noted its blue color, rapid light variations and an emission-line spectrum on a low-dispersion objective-prism plate. Kukarkin (1971) suggested the variable to be either a dwarf nova or a symbiotic object, not a Mira as originally proposed. Fisher et al. (1971) communicated UBV and visual observations giving a range (visual and V) of 11.5–14.73. The blue color and variation was incompatible with the Mira-type classification. This object became recognized as a dwarf nova. Splittgerber (1971) also reported the detection of two outbursts.

Amateur observers (particularly RASNZ members) started visual observations since 1971 April. Bateson (1976) suggested the SU UMa-type classification based on

Table 23. Superhump maxima of VW Hyi (2012)

E	max*	error	$O - C^\dagger$	N^\ddagger
0	56254.8352	0.0012	-0.0172	14
11	56255.6936	0.0022	-0.0034	21
22	56256.5420	0.0019	0.0005	22
23	56256.6145	0.0007	-0.0037	31
24	56256.6923	0.0004	-0.0028	29
25	56256.7690	0.0004	-0.0028	31
26	56256.8442	0.0017	-0.0044	11
35	56257.5382	0.0005	-0.0013	29
36	56257.6160	0.0005	-0.0003	31
37	56257.6942	0.0005	0.0011	28
38	56257.7707	0.0004	0.0008	31
48	56258.5388	0.0006	0.0012	29
49	56258.6154	0.0006	0.0011	31
50	56258.6913	0.0006	0.0001	28
51	56258.7676	0.0004	-0.0003	31
54	56258.9958	0.0007	-0.0025	97
55	56259.0764	0.0003	0.0014	163
56	56259.1536	0.0003	0.0018	167
57	56259.2301	0.0003	0.0015	170
61	56259.5375	0.0013	0.0019	20
62	56259.6134	0.0009	0.0010	22
63	56259.6928	0.0007	0.0036	21
64	56259.7685	0.0009	0.0025	31
87	56261.5389	0.0010	0.0071	23
88	56261.6171	0.0009	0.0086	23
89	56261.6927	0.0010	0.0073	22
90	56261.7691	0.0008	0.0070	31
100	56262.5368	0.0011	0.0069	23
101	56262.6130	0.0010	0.0063	25
102	56262.6896	0.0008	0.0061	25
103	56262.7649	0.0007	0.0047	36
113	56263.5295	0.0014	0.0015	19

*BJD-2400000.

† Against max = 2456254.8524 + 0.076774 E .

‡ Number of points used to determine the maximum.

the presence of superoutbursts detected by visual observations. Walker et al. (1976) reported the detection of superhumps by photoelectric photometry. The reported period was 0.0783 d based on two-night observation. Walker et al. (1976) also reported a period of 0.0749 d, which was suggested to be the orbital period. Sanduleak (1976) reported a spectrum showing Balmer lines in emission, which is typical for a dwarf nova. Bailey (1979a) reported high-speed photometry both in superoutburst and in quiescence. Using observations on four consecutive nights in 1977 December, Bailey (1979a) derived a superhump period of 0.07737 d. This observation corresponded to the middle part of the superoutburst. In contrast to Walker et al. (1976), Bailey (1979a) could not detect orbital modulations in quiescence (also Bailey 1979, unpublished, see Schoembs, Vogt 1981). Schoembs, Vogt (1981) obtained high-time resolution spectroscopy and determined the orbital period to be 0.0748134(2) d. Pretorius et al.

Table 23. Superhump maxima of VW Hyi (2012) (continued)

E	max*	error	$O - C^\dagger$	N^\ddagger
114	56263.6079	0.0010	0.0032	25
115	56263.6839	0.0009	0.0024	24
116	56263.7595	0.0006	0.0012	37
117	56263.8383	0.0024	0.0033	14
119	56263.9904	0.0004	0.0018	127
120	56264.0700	0.0005	0.0047	145
126	56264.5229	0.0046	-0.0031	16
127	56264.6034	0.0010	0.0007	25
128	56264.6806	0.0010	0.0011	24
129	56264.7561	0.0008	-0.0002	38
130	56264.8330	0.0023	-0.0001	17
139	56265.5148	0.0053	-0.0093	15
140	56265.5973	0.0013	-0.0036	25
141	56265.6717	0.0009	-0.0059	25
142	56265.7507	0.0009	-0.0037	37
143	56265.8280	0.0025	-0.0031	22
153	56266.6003	0.0032	0.0013	25
154	56266.6727	0.0018	-0.0030	24
155	56266.7443	0.0015	-0.0081	37
156	56266.8234	0.0078	-0.0059	25
158	56266.9779	0.0100	-0.0049	68
159	56267.0557	0.0011	-0.0039	70

*BJD-2400000.

 † Against max = 2456254.8524 + 0.076774*E*. ‡ Number of points used to determine the maximum.

(2006) reported the detection of quasi-periodic oscillations (QPOs) in quiescence.

The identification of this object as a dwarf nova led to a suggestion that some of Mira-type variables could be misclassified SU UMa-type dwarf novae (Vogt 1980). DH Aql (Tsevevich 1969; Nogami, Kato 1995), SY Cap (Kato et al. 2009) and FQ Mon (vsnet-chat 3063, 3066; Kato et al. 2009) are indeed such objects. Despite that WX Hyi is a well-known SU UMa-type dwarf nova, the listed set of literature was probably the last published observation of superhumps before this paper.

Our 2014 January–February observation started after the detection of a bright outburst on January 27 by S. Hovell and R. Stubbings (the start of the outburst was on January 25). Observations on January 30 detected fully grown superhumps and the subsequent evolution was observed (vsnet-alert 16851, 16868, 16904). The times of superhump maxima are listed in table 26, which includes post-superoutburst observations.

A comparison of the $O - C$ diagrams (figure 23) suggests that the first two nights of Schoembs, Vogt (1981) recorded stage B superhumps and the last two nights stage C superhumps (since both superoutbursts started with a precursor, we used the maximum which was easier to define). The resultant period of stage B is in good agreement with the value by Walker et al. (1976), who reported an early part of the superoutburst. We listed the estimated periods in this interpretation in table 2.

Table 24. Superhump maxima of VW Hyi (2012) (post-superoutburst)

E	max*	error	$O - C^\dagger$	N^\ddagger
0	56268.5388	0.0073	-0.0124	17
1	56268.6241	0.0061	-0.0033	25
2	56268.6976	0.0011	-0.0061	30
3	56268.7775	0.0014	-0.0025	37
19	56269.9944	0.0009	-0.0054	113
20	56270.0744	0.0006	-0.0016	162
21	56270.1533	0.0006	0.0010	164
22	56270.2348	0.0009	0.0062	170
32	56270.9885	0.0004	-0.0025	115
33	56271.0642	0.0006	-0.0030	108
45	56271.9901	0.0006	0.0080	110
46	56272.0576	0.0004	-0.0007	128
52	56272.5238	0.0019	0.0080	15
53	56272.5946	0.0010	0.0026	25
54	56272.6717	0.0013	0.0034	26
55	56272.7439	0.0012	-0.0006	36
56	56272.8264	0.0011	0.0056	21
66	56273.5848	0.0007	0.0016	25
67	56273.6624	0.0007	0.0030	25
68	56273.7367	0.0006	0.0010	37
69	56273.8150	0.0008	0.0031	28
79	56274.5765	0.0016	0.0022	25
80	56274.6526	0.0018	0.0020	24
81	56274.7311	0.0009	0.0043	37
82	56274.8085	0.0015	0.0055	33
92	56275.5669	0.0018	0.0014	25
93	56275.6431	0.0020	0.0013	25
94	56275.7164	0.0010	-0.0015	38
95	56275.7973	0.0013	0.0031	36
105	56276.5613	0.0020	0.0047	15
106	56276.6296	0.0009	-0.0033	23
107	56276.7094	0.0009	0.0003	37

*BJD-2400000.

 † Against max = 2456268.5512 + 0.076242*E*. ‡ Number of points used to determine the maximum.**Table 24.** Superhump maxima of VW Hyi (2012) (post-superoutburst, continued)

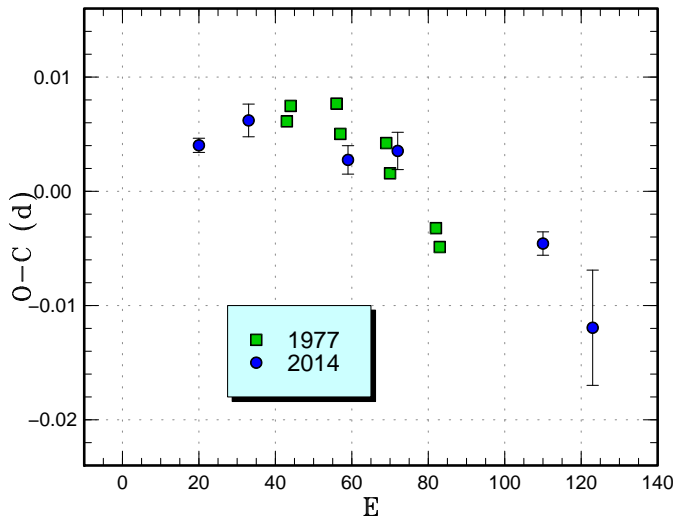
E	max*	error	$O - C^\dagger$	N^\ddagger
108	56276.7908	0.0011	0.0054	37
125	56278.0760	0.0006	-0.0055	163
126	56278.1569	0.0007	-0.0009	170
127	56278.2315	0.0008	-0.0025	164
132	56278.6073	0.0027	-0.0079	25
133	56278.6847	0.0024	-0.0068	22
134	56278.7632	0.0054	-0.0045	20
148	56279.8325	0.0094	-0.0026	22

*BJD-2400000.

 † Against max = 2456268.5512 + 0.076242*E*. ‡ Number of points used to determine the maximum.

Table 25. Post-superoutburst superhumps in VW Hyi (2012)

JD–2400000	Period (d)	Error (d)	Amplitude (mag)
56270–56275	0.07623	0.00001	0.33
56275–56280	0.07584	0.00004	0.36
56280–56285	0.07732	0.00011	0.08
56285–56290	0.07615	0.00014	0.13
56290–56295	0.07600	0.00005	0.15
56295–56300	0.07586	0.00005	0.07
56300–56305	–	–	–
56305–56310	0.07712	0.00013	0.08

**Fig. 23.** Comparison of $O - C$ diagrams of WX Hyi between different superoutbursts. A period of 0.07765 d was used to draw this figure. Approximate cycle counts (E) after the maximum of the superoutburst were used.**Table 26.** Superhump maxima of WX Hyi (2014)

E	max*	error	$O - C^\dagger$	N^\ddagger
0	56687.5605	0.0006	-0.0035	47
13	56688.5721	0.0014	0.0007	28
39	56690.5876	0.0012	0.0012	19
52	56691.5978	0.0016	0.0039	13
90	56694.5404	0.0010	0.0015	21
103	56695.5425	0.0050	-0.0039	21

*BJD–2400000.

 † Against max = 2456687.5640 + 0.077499 E . ‡ Number of points used to determine the maximum.**Table 27.** Superhump maxima of AY Lyr (2013)

E	max*	error	$O - C^\dagger$	N^\ddagger
0	56533.0467	0.0007	-0.0000	84
1	56533.1221	0.0005	-0.0007	79
2	56533.1996	0.0008	0.0008	55
14	56534.1116	0.0006	-0.0001	39

*BJD–2400000.

 † Against max = 2456533.0467 + 0.076064 E . ‡ Number of points used to determine the maximum.

3.20. AY Lyrae

Observations of this well-known SU UMa-type dwarf nova were performed only on two nights in 2013 August. The times of superhump maxima are listed in table 27.

3.21. AO Octantis

Due to the large outburst amplitude (7.5 mag) listed in Kholopov et al. (1985), this object had long been considered as a candidate WZ Sge-type dwarf nova (Downes 1990; Howell, Szkody 1990; O’Donoghue et al. 1991; Kato et al. 2001). Although Howell et al. (1991) observed this object in quiescence, no orbital modulation was detected. Mason, Howell (2003) obtained a spectrum in quiescence, which was typical for a dwarf nova with a low mass-transfer rate but was not so extreme as a WZ Sge-type dwarf nova. Patterson et al. (2003) observed the 2000 September outburst and obtained a superhump period of 0.06557(13) d. Woudt et al. (2004) obtained time-resolved photometry in quiescence and detected an orbital modulation with a period of 0.065345(15) d. The presence of the orbital modulation appears to be consistent with the relatively broad emission lines in Mason, Howell (2003).

The 2013 superoutburst of AO Oct was detected by R. Stubbings (vsnet-alert 16376). Subsequent observations detected superhumps (vsnet-alert 16388, 16396, 16411; figure 24). The times of superhump maxima are listed in table 28. The stages B and C were clearly present. The large P_{dot} of $+19(6) \times 10^{-5}$ for stage B superhumps is typical for this P_{orb} .

According to Woudt et al. (2004), the maximum magnitude of 13.5 in Kholopov et al. (1985) was probably a typographical error of 15.3 based on the discovery paper (von Gessner, Meinunger 1974). The object, however, has been detected as bright as 14.2 (visual magnitude) in outburst several times. The true range of variability can be regarded as 14.2–20.9, where the minimum magnitude is taken from Woudt et al. (2004). Considering the supercycle of ~ 300 d, this outburst amplitude is indeed slightly too large for this intermediate length of supercycle. Although TV Crv was reported to have similar parameters (cf. table 1 in Nogami et al. 1997), the maximum magnitude of TV Crv was probably an overestimate, since recent magnitudes of superoutbursts only reach 13.0. AO Oct apparently deserves a further study for its rather unusual outburst parameters.

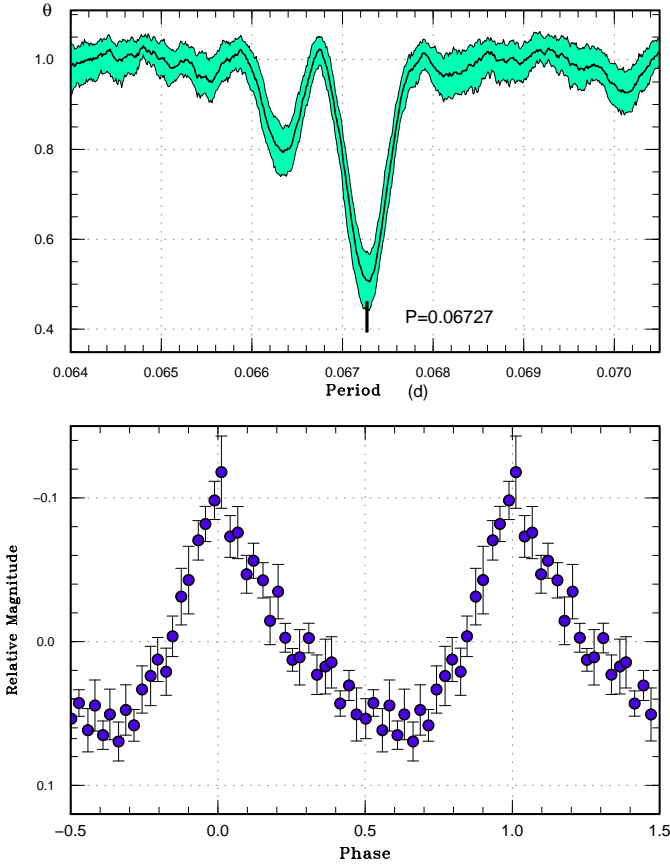


Fig. 24. Superhumps in AO Oct (2013). (Upper): PDM analysis. (Lower): Phase-averaged profile.

Table 28. Superhump maxima of AO Oct (2013)

E	max*	error	$O - C^\dagger$	N^\ddagger
0	56545.5712	0.0006	0.0003	29
1	56545.6371	0.0007	-0.0011	12
2	56545.7043	0.0021	-0.0011	9
3	56545.7744	0.0016	0.0017	8
14	56546.5113	0.0009	-0.0011	22
15	56546.5781	0.0011	-0.0015	28
16	56546.6466	0.0012	-0.0002	15
17	56546.7126	0.0009	-0.0015	15
29	56547.5202	0.0011	-0.0007	26
45	56548.5933	0.0066	-0.0035	10
46	56548.6664	0.0014	0.0024	13
59	56549.5480	0.0011	0.0099	27
75	56550.6161	0.0012	0.0022	25
76	56550.6872	0.0032	0.0061	12
89	56551.5518	0.0020	-0.0035	27
90	56551.6183	0.0052	-0.0043	12
91	56551.6855	0.0019	-0.0042	14

*BJD-2400000.

† Against max = 2456545.5710 + 0.067240 E .

‡ Number of points used to determine the maximum.

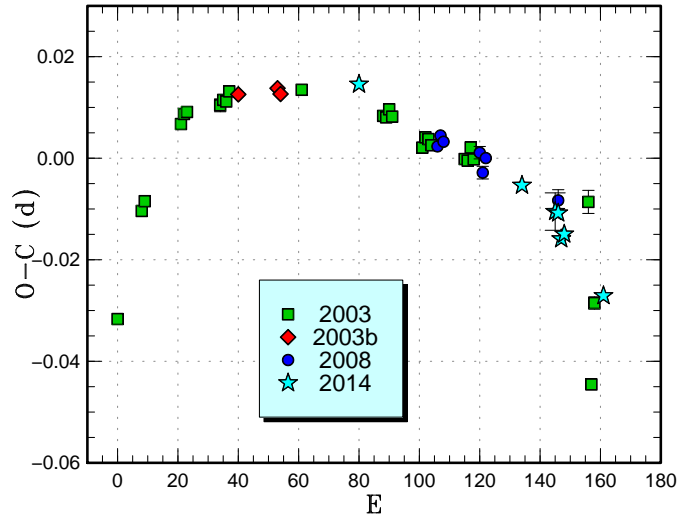


Fig. 25. Comparison of $O - C$ diagrams of DT Oct between different superoutbursts. A period of 0.07485 d was used to draw this figure. Approximate cycle counts (E) after the start of the superoutburst were used. Since the start of the 2014 superoutburst was not well constrained, we shifted the $O - C$ diagram to best fit the others.

3.22. DT Octantis

This object was discovered as a variable star (=BV 966) with a large amplitude (11.2 to fainter than 15.0 in photographic magnitudes) (Knigge, Bauernfeind 1967). Kato et al. (2002a) noticed the identification with a bright ROSAT source and suggested that the object is a cataclysmic variable. Kato et al. (2002a) detected multiple outbursts upon this suggestion. Although Kato et al. (2002a) initially suggested that these outbursts may be outbursts in an intermediate polar, Kato et al. (2004a) detected superhumps during the 2003 January outburst. DT Oct was thus recognized as an SU UMa-type dwarf nova. Kato et al. (2009) further studied another superoutburst in 2003 November and the superoutburst in 2008.

The 2014 superoutburst was detected by R. Stubbings (cf. vsnet-alert 16892) and the later part of the superoutburst was observed. The times of superhump maxima are listed in table 29. The data mostly recorded stage C superhumps (figure 25).

Using the near quiescent data in 2013 (by OkC, BJD 2456380–2456445), we have obtained a possible orbital signal of 0.072707(5) d with a mean amplitude of 0.16 mag. This period was adopted in table 2. The ε^* value for stage A superhumps [0.050(2)] in 2003 (Kato et al. 2009) corresponds to $q=0.147(7)$.

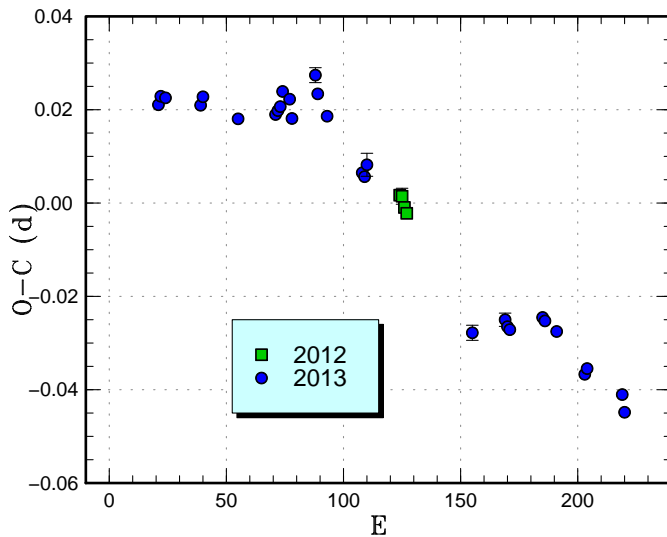
3.23. V521 Pegasi

This object (=HS 2219+1824) is a dwarf nova which was reported in Rodríguez-Gil et al. (2005). Although Rodríguez-Gil et al. (2005) reported the detection of superhumps and likely orbital modulation, subsequent superoutbursts occurred in poor seasonal condition, and it was only in 2012 when we succeeded in obtaining the su-

Table 29. Superhump maxima of DT Oct (2014)

E	max*	error	$O - C^\dagger$	N^\ddagger
0	56696.7567	0.0008	-0.0020	83
54	56700.7787	0.0006	0.0031	119
65	56701.5969	0.0037	0.0031	35
66	56701.6714	0.0007	0.0032	66
67	56701.7412	0.0006	-0.0014	80
68	56701.8170	0.0014	0.0000	63
81	56702.7779	0.0011	-0.0061	70

*BJD-2400000.

 \dagger Against max = 2456696.7587 + 0.074386 E . \ddagger Number of points used to determine the maximum.**Fig. 26.** Comparison of $O - C$ diagrams of V521 Peg between different superoutbursts. A period of 0.06150 d was used to draw this figure. Approximate cycle counts (E) after the start of the superoutburst were used.

perhump period (Kato et al. 2014).

The 2013 superoutburst was detected by the ASAS-SN team (vsnet-alert 16093). K. Wenzel also reported the outburst detection before the ASAS-SN detection. Subsequent observations detected superhumps (vsnet-alert 16121, 16129, 16134). After rapid fading from the superoutburst, the object continued to show superhumps (vsnet-alert 16146, 16149, 16166, 16186). The times of superhumps are listed in table 30, which includes post-superoutburst observations. Stages B and C were observed. During the phase of the rapid fading, the superhump profile became doubly humped. The maxima which are on the smooth extension of the rest of the data were selected in the table.

A comparison of the $O - C$ diagram clarified that the 2012 observation recorded stage C superhumps, rather stage B superhump identified in Kato et al. (2014).

Table 30. Superhump maxima of V521 Peg (2013)

E	max*	error	$O - C^\dagger$	N^\ddagger
0	56507.0874	0.0009	-0.0139	44
1	56507.1507	0.0006	-0.0118	66
3	56507.2734	0.0005	-0.0114	63
18	56508.1942	0.0007	-0.0074	70
19	56508.2575	0.0007	-0.0052	67
34	56509.1753	0.0006	-0.0043	40
50	56510.1601	0.0004	0.0026	91
51	56510.2223	0.0008	0.0037	86
52	56510.2848	0.0005	0.0050	96
53	56510.3497	0.0011	0.0088	41
56	56510.5325	0.0007	0.0082	66
57	56510.5899	0.0012	0.0045	28
67	56511.2146	0.0016	0.0179	63
68	56511.2718	0.0009	0.0140	62
72	56511.5129	0.0003	0.0106	47
87	56512.4234	0.0008	0.0042	52
88	56512.4840	0.0015	0.0037	159
89	56512.5469	0.0030	0.0055	211
134	56515.2792	0.0016	-0.0128	123
148	56516.1433	0.0014	-0.0044	113
149	56516.2033	0.0009	-0.0055	230
150	56516.2645	0.0012	-0.0054	226
164	56517.1278	0.0006	0.0021	80
165	56517.1885	0.0008	0.0017	128
170	56517.4937	0.0004	0.0013	54
182	56518.2226	0.0006	-0.0034	82
183	56518.2853	0.0006	-0.0018	125
198	56519.2022	0.0011	-0.0017	126
199	56519.2599	0.0012	-0.0051	120

*BJD-2400000.

 \dagger Against max = 2456507.1013 + 0.061124 E . \ddagger Number of points used to determine the maximum.

3.24. TY Piscium

Although the SU UMa-type nature of TY Psa had been long known, the information in the literature was very limited (Szkody, Feinswog 1988; Kunjaya et al. 2001). Kato et al. (2009) was the first to determine the superhump period precisely during the 2005 and 2008 superoutbursts. Thorstensen et al. (1996) determined the orbital period by a radial-velocity study.

The 2013 December superoutburst was detected by Kyoto and Kiso Wide-field Survey (KWS) (vsnet-alert 16682) and was observed for three nights. The times of superhump maxima are listed in table 31. The observation apparently detected stage B-C transition. This identification is confirmed by a comparison of the $O - C$ diagrams (figure 27. Also note that the figure in Kato et al. (2009) used the period of stage C superhumps, rather than that of stage B superhumps, making the impression of the figure different).

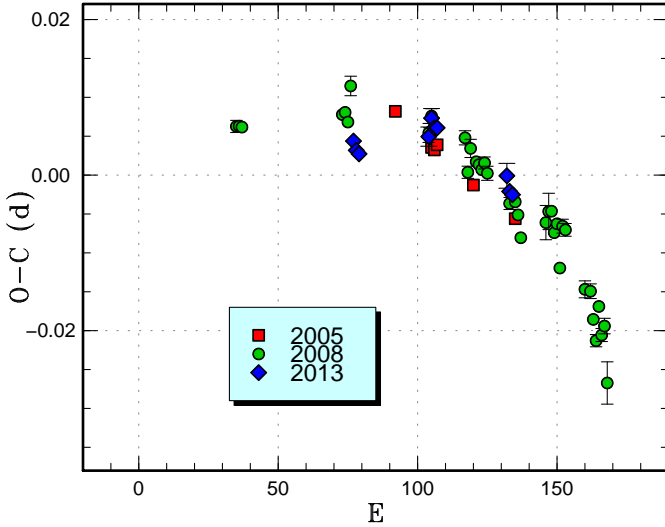


Fig. 27. Comparison of $O - C$ diagrams of TY Psc between different superoutbursts. A period of 0.07066 d was used to draw this figure. Approximate cycle counts (E) after the start of the superoutburst were used. Since the start of the 2013 superoutburst was not well constrained, we shifted the $O - C$ diagram to best fit the others.

Table 31. Superhump maxima of TY Psc (2013)

E	max*	error	$O - C^\dagger$	N^\ddagger
0	56635.0415	0.0006	-0.0012	91
1	56635.1110	0.0004	-0.0023	130
2	56635.1812	0.0005	-0.0027	109
27	56636.9499	0.0012	0.0018	25
28	56637.0230	0.0012	0.0043	46
29	56637.0924	0.0006	0.0031	63
30	56637.1630	0.0009	0.0032	47
55	56638.9234	0.0016	-0.0007	52
56	56638.9920	0.0008	-0.0026	52
57	56639.0622	0.0008	-0.0029	101

*BJD-2400000.

† Against max = 2456635.0428 + 0.070569 E .

‡ Number of points used to determine the maximum.

3.25. V893 Scorpii

V893 Sco was discovered as a variable star (=SVS 1772) by Satyvoldiev (1972). Since this object is located in the region of the Scorpius T1 association, Satyvoldiev (1982) classified this object as a rapid irregular variable of InSF type (object normally in faint states with occasional brightenings up to 3 mag) according to the classification scheme by Filin, Satyvoldiev (1975). This classification corresponded to “RWF”-type RW Aur-type in Tsesevich, Dragomiretskaia (1973). Around this time, the RW Aur-type or “In”-type (irregular, nebular, cf. Kholopov et al. 1985) referred to pre-main sequence variables. It is apparent that Satyvoldiev (1982) considered this variable as a pre-main sequence variable. In Kholopov et al. (1985), however, the object was reclassified as a dwarf nova probably based on the published light curve.

The finding chart in this discovery article was interchanged with that of a different star, and this bright dwarf nova remained virtually “lost” for a long time (cf. Downes et al. 1997). The presented light curves in Filin, Satyvoldiev (1975) and Satyvoldiev (1982), however, were so characteristic of a dwarf nova and at least two outbursts may be attributed to a superoutburst due to its long duration, this object attracted amateur astronomers (particularly VSOLJ members) since the late 1980s. Despite the high potentiality of being a bright SU UMa-type dwarf nova, all attempts (visually watching for the nominal position and photographic searches) to recover this variable had been unsuccessful.

In 1998, K. Haseda reported a detection of a transient object near the catalog position of V893 Sco, and this object was readily identified with an ROSAT X-ray source. A search for the plate collections at the time of observations of Satyvoldiev (1982) clarified that this outbursting object is indeed V893 Sco. This rediscovery was reported in Kato et al. (1998a).

Thorstensen (1999) confirmed spectroscopically that this object is indeed a dwarf nova and obtained an orbital period of 0.0760 d. This short orbital period strengthened the suggestion that this object belongs to the SU UMa-type dwarf novae. Thorstensen (1999) also measured a large proper motion, implying a nearby object.

Since 1998, this object has been regularly monitored by amateur observers, and outbursts reaching ~ 12 mag were recorded. During the observation in 1999, the group by K. Matsumoto clarified that this object is a grazing eclipsing dwarf nova below the period gap (vsnet-alert 3432, announced on 1999 September 2). Bruch et al. (2000) independently reached the same conclusion and submitted a paper on 1999 September 11. The result of the former research was published as Matsumoto et al. (2000).

Although Bruch et al. (2000) mentioned that V893 Sco cannot be an ER UMa-type dwarf nova, Mason et al. (2001) suggested that it is an ER UMa-type dwarf nova by demonstrating their new Doppler tomograms. Kato et al. (2002c) explained that this object cannot be an ER UMa-type dwarf nova.

Such a confusion apparently comes from the lack of a

definite superoutburst, despite that its existence has been expected for the short orbital period. Although there have been a number of possible detections of “slightly brighter” outbursts, none of them had been confirmed to be a genuine superoutburst until 2013.

On 2013 August 27, R. Stubbings reported a bright (11.6 mag) outburst (vsnet-alert 16276; figure 28). Subsequent observation of this outburst finally confirmed the presence of superhumps (vsnet-alert 16315; figure 29). We observed this superoutburst and report the result here.

Since the eclipse ephemeris by Bruch et al. (2000) does not fit modern observations (Mukai et al. 2009), we first refined the eclipse ephemeris. Since the white dwarf is partially eclipsed (Mukai et al. 2009), we used outburst observations in which the central part of the accretion disk is expected to be eclipsed, and the times of minima are expected to be close to the center of eclipse of the white dwarf. We used the combined set of the 2007 data (MLF and OKU data), 2008 data (GBo data), 2010 data (GBo and OKU data) and the present data. All observations other than the 2013 data were obtained during normal outbursts. We obtained an ephemeris of

$$\text{Min}(\text{BJD}) = 2454173.3030(4) + 0.0759614614(18)E \quad (3)$$

using the MCMC modeling Kato et al. (2013a). This orbital period is in good agreement with Mukai et al. (2009), suggesting that the original orbital period by Bruch et al. (2000) was systematically too long.

The times of superhump maxima after subtracting the mean orbital modulations were determined outside the eclipses (orbital phase 0.07–0.93) (table 32). Although some of superhumps were visible in the light curve, some of the times of maxima could not be determined because the superhump maxima coincided the eclipses. These superhumps were not included in table 32. We identified stages B and C and gave the measured periods in table 2.

As mentioned in Bruch et al. (2000), such a bright dwarf nova escaped detection of nova searches. This may have been the chance coincidence of superoutbursts occurring in unfavorable seasonal condition before modern CCD-based search became popular. In table 33, we list the possible superoutburst in modern observations. Except for the 2013 one, all suspected superoutburst occurred near the solar conjunction. It may be that the supercycle is close to one year, and all superoutbursts in the late 1990s and 2000s could not be observed due to the solar conjunction. The relatively small outburst amplitude is likely a result of the high system inclination. It was also likely that the magnitude scale in Satyvoldiev (1982) was ~ 1 mag brighter than the modern one.

3.26. RZ Sagittae

RZ Sge has long been known as a dwarf nova with a long cycle length (e.g. Petit 1956). Bond et al. (1982) reported the detection of superhumps during the 1981 October outburst. Retrospective examination of the past visual observation also clarified a number of superoutbursts in the 1970s (Bond et al. 1982). Kato (1996) and Semeniuk et al. (1997) reported observations of superhumps during the

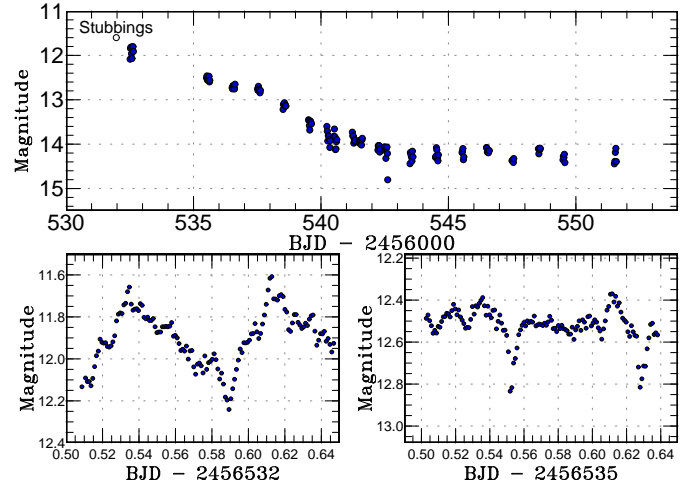


Fig. 28. Light curve of V893 Sco during the superoutburst (2013). (Upper): Overall light curve. (Lower panels): Examples of nightly observations. Both eclipses and superhumps were detected.

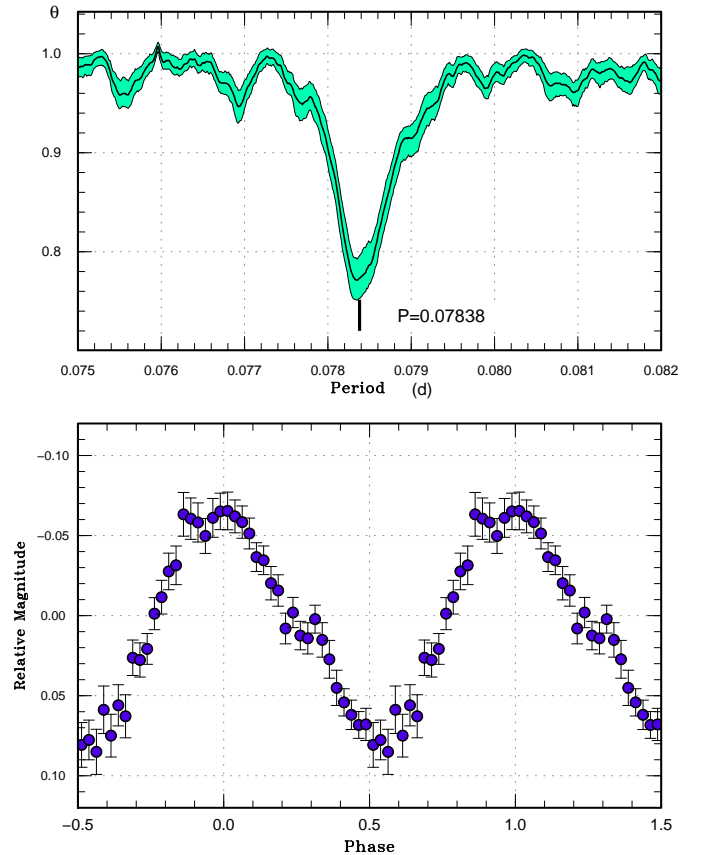


Fig. 29. Superhumps in V893 Sco after subtracting the orbital modulation (2013). (Upper): PDM analysis. (Lower): Phase-averaged profile.

Table 32. Superhump maxima of V893 Sco (2013)

E	max*	error	$O - C^\dagger$	phase‡	N^\S
0	56532.5397	0.0008	-0.0073	0.34	43
1	56532.6179	0.0010	-0.0075	0.37	45
38	56535.5283	0.0013	0.0032	0.68	42
39	56535.6098	0.0028	0.0063	0.76	36
51	56536.5526	0.0007	0.0087	0.17	36
52	56536.6294	0.0012	0.0071	0.18	15
89	56539.5270	0.0016	0.0050	0.32	40
99	56540.3015	0.0009	-0.0041	0.52	136
102	56540.5296	0.0005	-0.0111	0.52	41
128	56542.5793	0.0013	0.0009	0.51	47
140	56543.5208	0.0010	0.0020	0.90	36
141	56543.5975	0.0013	0.0003	0.91	35
153	56544.5343	0.0066	-0.0034	0.24	24

*BJD-2400000.

†Against max = 2456532.5471 + 0.078370*E*.

‡Orbital phase.

§Number of points used to determine the maximum.

Table 33. Possible superoutbursts of V893 Sco

JD	Date	maximum	duration (d)
2454883	2009 February 20	11.7	>8
2455975	2012 February 17	12.0	>4
2456532	2013 August 27	11.6	>8*

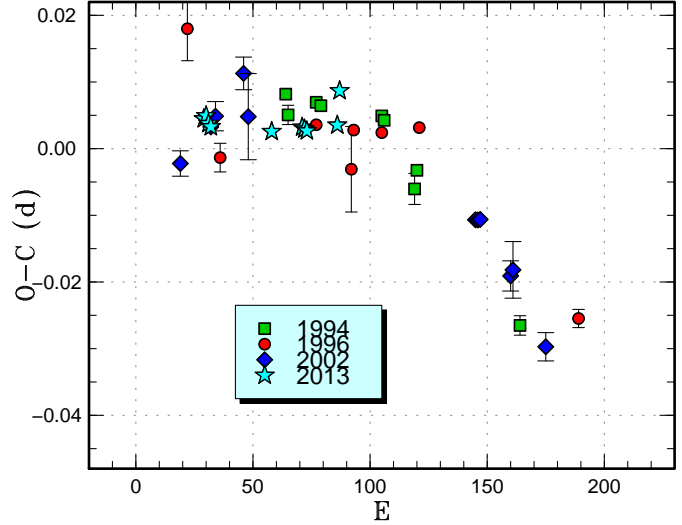
*Confirmed superoutburst.

1994 and 1996 superoutburst, respectively. Although both Kato (1996) and Semeniuk et al. (1997) resulted in global negative P_{dot} of about -10×10^{-5} , Kato et al. (2009) considered that this is a result of stage B-C transition and that P_{dot} for stage B can be positive. Patterson et al. (2003) also reported the 1996 superoutburst and detection of the photometric orbital period in 1999.

We observed the 2013 superoutburst, which was detected in relatively early phase (vsnet-alert 16326). The times of superhump maxima are listed in table 34. The present data suggest a positive P_{dot} (the data for $E = 58$ was better than $E = 57$, and the positive $O - C$ for $E = 58$ appears to be real). The $O - C$ values of present and past superoutbursts can be well expressed by the stage B and C (figure 30).

3.27. *AW Sagittae*

AW Sge was discovered as a dwarf nova by Wolf, Wolf (1906). The 2000 and 2006 superoutbursts were reported in Kato et al. (2009). Kato et al. (2014) further reported the best observed 2012 superoutburst. On 2013 October 6, R. Stubbings detected another likely superoutburst (vsnet-alert 16512). This outburst was independently detected several hours earlier by AAVSO observers. On the very night of this detection, no superhumps were detected. On the next night, a developing superhump

**Fig. 30.** Comparison of $O - C$ diagrams of RZ Sge between different superoutbursts. A period of 0.07063 d was used to draw this figure. Approximate cycle counts (E) after the start of the superoutburst were used.**Table 34.** Superhump maxima of RZ Sge (2013)

E	max*	error	$O - C^\dagger$	N^\ddagger
0	56539.3871	0.0002	0.0008	90
1	56539.4582	0.0002	0.0013	140
2	56539.5277	0.0002	0.0001	136
3	56539.5978	0.0013	-0.0004	51
29	56541.4335	0.0003	-0.0014	89
42	56542.3523	0.0003	-0.0010	90
43	56542.4227	0.0004	-0.0012	90
44	56542.4930	0.0002	-0.0015	77
57	56543.4121	0.0005	-0.0008	14
58	56543.4879	0.0006	0.0043	22

*BJD-2400000.

†Against max = 2456539.3863 + 0.070642*E*.

‡Number of points used to determine the maximum.

was detected. There was a 4-d gap after these observations. The times of superhump maxima are listed in table 35. The epoch $E = 0$ was given a cycle count assuming that this was a stage A superhump with a longer period. A comparison of the period for $E \leq 62$ indicated that they are stage C superhumps. This identification was confirmed by comparison of $O - C$ diagrams (figure 31). The negative detection of the outburst on October 3 could constrain the growth time of superhumps no larger than 3.5 d.

3.28. *V1265 Tauri*

V1265 Tau was originally detected as an optical transient (Skvarc, Palcic 2006). Shafter et al. (2007) studied this object and detected short-period [0.053394(7) d] superhumps, which has been the shortest known superhump

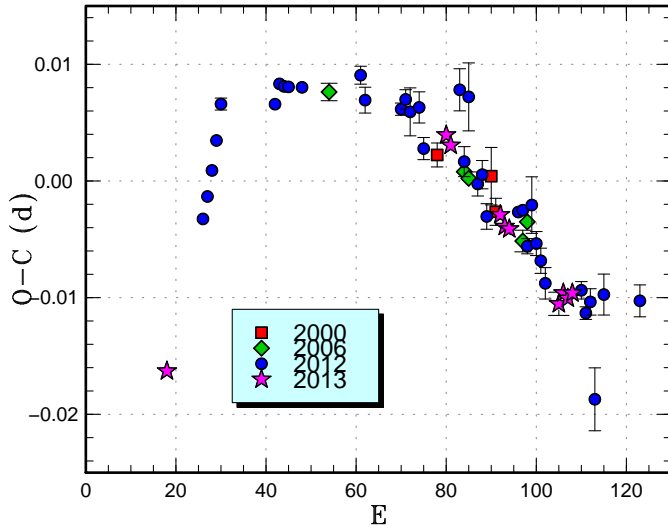


Fig. 31. Comparison of $O - C$ diagrams of AW Sge between different superoutbursts. A period of 0.07480 d was used to draw this figure. Approximate cycle counts (E) after the start of the superoutburst were used. Since the start of the superoutburst was best constrained in 2013, we shifted the $O - C$ diagrams to fit the 2013 one. This made a 18 cycle correction to the figure in Kato et al. (2014).

Table 35. Superhump maxima of AW Sge (2013)

E	max*	error	$O - C^\dagger$	N^\ddagger
0	56572.6575	0.0003	-0.0068	52
62	56577.3153	0.0004	0.0104	64
63	56577.3892	0.0005	0.0094	64
74	56578.2061	0.0003	0.0029	69
75	56578.2798	0.0004	0.0019	72
76	56578.3544	0.0005	0.0016	72
87	56579.1708	0.0010	-0.0054	45
88	56579.2465	0.0005	-0.0045	71
89	56579.3209	0.0006	-0.0050	69
90	56579.3961	0.0009	-0.0046	48

*BJD-2400000.

† Against max = 2456572.6642 + 0.074850 E .

‡ Number of points used to determine the maximum.

period in classical SU UMa-type dwarf novae.

On 2013 August 4, ASAS-SN team detect this object again in outburst (vsnet-alert 16120). The outburst was detected sufficiently early to follow the early evolution of the superhumps. On the first night of the observation, superhumps were already detected (vsnet-alert 16137). This observations has confirmed that V1265 Tau bears no characteristics of a WZ Sge-type dwarf nova, such as the existence of early superhumps, despite its very short superhump period.

The times of superhump maxima are listed in table 36. Due to the faintness (~ 16 mag) of the object, the errors in the times of superhump maxima were relatively large. We could determine the P_{dot} of $+1.9(1.9) \times 10^{-5}$ for stage B superhumps. This value is consistent with $P_{\text{dot}} = +2.1(0.8) \times 10^{-5}$ reported by Skvarc, Palcic (2006). This value of period derivative is small for an ordinary SU UMa-type dwarf nova with a short superhump period. After BJD 2456520, the object apparently showed a stage B-C transition. Since the measured times of superhump maxima during the late stage of the superoutburst were noisy, we determined the period with the PDM method to be 0.05309(4) d, which is adopted in table 2.

This unusual short-period system is unlike other systems with similar short superhump periods in that it neither exhibited WZ Sge-type characteristics nor a large positive P_{dot} as in a non-WZ Sge-type short-period system, V844 Her (Oizumi et al. 2007; Kato et al. 2009; Kato et al. 2013a). The evolution of superhumps was more similar to ER UMa-type dwarf novae such as RZ LMi (Olech et al. 2008; Kato et al. 2013a) although this object does not show frequent outbursts as in ER UMa-type dwarf novae. Further study is needed to clarify the unusual nature of this object.

3.29. *SU Ursae Majoris*

We observed this “prototype” of SU UMa-type dwarf novae (Udalski 1990) during the late stage of the 2013 November superoutburst. The times of superhump maxima (table 37) also includes first two nights of post-superoutburst state. The resultant period of stage C superhump is in agreement with previous observations (1989, 1999: Kato et al. 2009).

3.30. *SS Ursae Minoris*

SS UMi was originally discovered as the optical counterpart (dwarf nova) of the X-ray source E 1551+718 (Mason et al. 1982). This object was also selected as a CV by Palomer Green survey (Green et al. 1982). Andronov (1986) reported variations with a period of 127 min, which was considered to be the orbital period. Richter (1989) studied the behavior of this object and found that the mean cycle length is 30–48 d. Amateur astronomers also started observations of this object in 1987 and recorded frequent outbursts with cycle lengths as short as ~ 10 d.

Udalski (1990) observed this object and reported that the orbital period is much longer (likely 6.8 hr) in contrast to Andronov (1986). This contradiction between observations was resolved by the detection of superhumps with a

Table 36. Superhump maxima of V1265 Tau (2013)

E	max*	error	$O - C^\dagger$	N^\ddagger
0	56509.9538	0.0016	-0.0052	25
1	56510.0132	0.0024	0.0008	11
37	56511.9444	0.0045	0.0100	16
38	56511.9844	0.0004	-0.0034	37
56	56512.9464	0.0025	-0.0024	30
57	56512.9894	0.0025	-0.0128	24
94	56514.9731	0.0008	-0.0046	48
113	56515.9901	0.0012	-0.0019	32
131	56516.9515	0.0013	-0.0016	35
148	56517.8658	0.0031	0.0050	28
149	56517.9275	0.0015	0.0134	8
150	56517.9660	0.0065	-0.0015	49
167	56518.8748	0.0021	-0.0003	28
168	56518.9290	0.0049	0.0005	12
186	56519.8959	0.0028	0.0063	19
187	56519.9481	0.0019	0.0052	31
204	56520.8559	0.0014	0.0053	28
205	56520.9085	0.0056	0.0046	11
206	56520.9582	0.0007	0.0009	45
222	56521.8086	0.0038	-0.0030	14
223	56521.8692	0.0016	0.0042	25
260	56523.8356	0.0033	-0.0048	25
261	56523.8818	0.0013	-0.0120	23
278	56524.7991	0.0096	-0.0024	10
279	56524.8669	0.0023	0.0120	18
297	56525.8170	0.0104	0.0011	13
305	56526.2474	0.0089	0.0044	63
319	56526.9728	0.0041	-0.0177	35

*BJD-2400000.

 \dagger Against max = 2456509.9590 + 0.053390*E*. \ddagger Number of points used to determine the maximum.**Table 37.** Superhump maxima of SU UMa (2013)

E	max*	error	$O - C^\dagger$	N^\ddagger
0	56627.2982	0.0011	0.0051	127
1	56627.3712	0.0029	-0.0007	83
10	56628.0796	0.0013	-0.0013	45
11	56628.1626	0.0007	0.0030	198
12	56628.2401	0.0009	0.0017	85
13	56628.3141	0.0009	-0.0031	85
23	56629.1012	0.0010	-0.0037	13
24	56629.1703	0.0032	-0.0135	8
25	56629.2622	0.0014	-0.0003	86
26	56629.3573	0.0008	0.0160	111
27	56629.4194	0.0009	-0.0007	79
28	56629.4999	0.0007	0.0011	69
29	56629.5701	0.0016	-0.0075	50
38	56630.2856	0.0036	-0.0010	54
51	56631.3153	0.0009	0.0047	86

*BJD-2400000.

 \dagger Against max = 2456627.2931 + 0.078775*E*. \ddagger Number of points used to determine the maximum.**Table 38.** Superhump maxima of SS UMi (2013)

E	max*	error	$O - C^\dagger$	N^\ddagger
0	56540.3119	0.0010	0.0008	53
1	56540.3717	0.0012	-0.0092	77
2	56540.4451	0.0012	-0.0058	78
3	56540.5170	0.0008	-0.0038	77
29	56542.3524	0.0010	0.0132	73
30	56542.4149	0.0008	0.0058	33
31	56542.4847	0.0005	0.0056	77
32	56542.5575	0.0006	0.0085	70
33	56542.6244	0.0012	0.0054	41
43	56543.3123	0.0008	-0.0060	33
44	56543.3922	0.0015	0.0039	37
57	56544.2931	0.0008	-0.0043	38
58	56544.3588	0.0021	-0.0085	35
59	56544.4318	0.0030	-0.0055	22

*BJD-2400000.

 \dagger Against max = 2456540.3111 + 0.069936*E*. \ddagger Number of points used to determine the maximum.

period of 101 min (Chen et al. 1991): neither Andronov (1986) nor Udalski (1990) turned out to be correct. Kato et al. (1998b) also reported observations of superhumps.

This object started receiving attention because of its high frequency of outbursts. Kato et al. (2000) clarified that the supercycle of this object is 84.7 d, the shortest known supercycle in ordinary SU UMa-type dwarf novae [note that this object was not classified as an ER UMa-type dwarf nova in this reference; see also Kato et al. (2001a) for the similar case of BF Ara]. Olech et al. (2006) reported that the supercycle lengthened to 197 d in 2004. Olech et al. (2006) also reported development of superhumps. Kato et al. (2013a) also studied the 2012 superoutburst. The supercycle as short as 84.7 d has never been convincingly recorded in the recent decade.

We observed the final part of the superoutburst in 2003 August–September (the early part of this superoutburst was likely missed). The times of superhump maxima are listed in table 38. The times for $E \geq 29$ were obtained after the rapid fading from the superoutburst. Although these epochs of maxima could be expressed without a phase jump from those for $E \leq 3$, the identification of the phase was not complete due to the gap in the observation.

3.31. CU Velorum

Although CU Vel is a well-known SU UMa-type dwarf nova, only limited amount of information has been published (Vogt 1980; Mennickent, Diaz 1996). We reported observations of the 2002 superoutburst in Kato et al. (2009).

The 2013 superoutburst was detected on November 25 (vsnet-alert 16648), but the actual start of the superoutburst must have been several days earlier as later shown in the comparison of the $O - C$ diagrams. The 2013 observation, however, well recorded the post-superoutburst state.

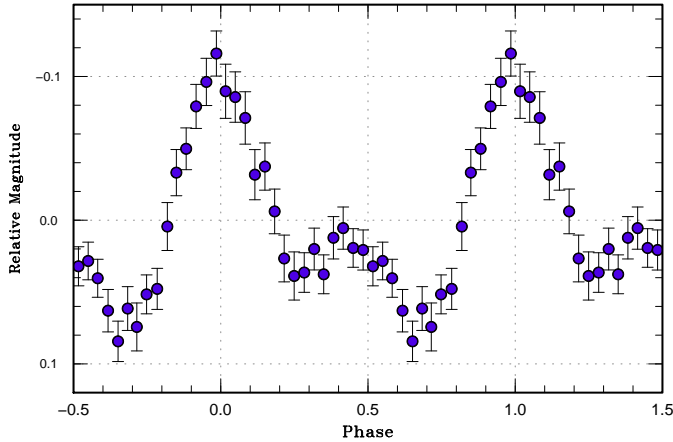


Fig. 32. Orbital variation of CU Vel in quiescence.

The times of superhump maxima during the plateau phase are listed in table 39. These superhumps are likely stage C superhumps since they were observed during the late stage of the superoutburst. A comparison of the $O-C$ diagrams supports this identification (figure 33).

Since orbital modulations are clearly seen in the light curve, we refined the orbital period by using observations around quiescence. The 2013–2014 data after the 2013 November superoutburst yielded a period of 0.078043(5) d. The 2013 January data (Nel and HaC) yielded a period of 0.07805(4) d. Using the combined data set, we selected a period of 0.0780541(3) d. The resultant profile (figure 32) showed two maxima of different amplitudes. This feature of double maxima is to some extent similar to WZ Sge-type dwarf nova in quiescence (e.g. Patterson et al. 1998; Araujo-Betancor et al. 2005). CU Vel may bear intermediate characteristics between ordinary SU UMa-type dwarf novae and WZ Sge-type dwarf novae.

We subtracted the mean orbital light curve from the post-superoutburst light curve. A PDM analysis yielded a strong signal at 0.079906(4) d. The times of these post-superoutburst superhumps are listed in table 40. The $O-C$ diagram (figure 34) indicates that the superhump phase was continuous before and after the rapid fading from the superoutburst. There was a decrease in period after $E = 110$ (after the rapid fading) and the period was almost constant at least until $E = 400$. Both the signals of superhumps and orbital period are clearly seen in the Lasso power spectrum (figure 35). The post-superoutburst superhumps survived at least 30 d after the fading.

3.32. 1RXS J231935.0+364705

This object (hereafter 1RXS J231935) was selected as a variable star (=DDE 8, likely a dwarf nova) during the course of identification of the ROSAT sources (Denisenko, Sokolovsky 2011). There was a well-observed superoutburst in 2011 (Kato et al. 2013a). D. Denisenko detected a new outburst on 2013 September 27 (vsnet-alert 16460).

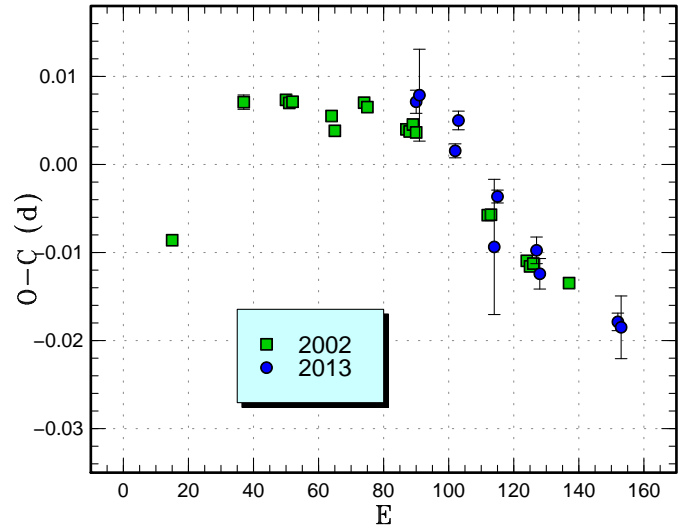


Fig. 33. Comparison of $O-C$ diagrams of CU Vel between different superoutbursts. A period of 0.08100 d was used to draw this figure. Approximate cycle counts (E) after the start of the superoutburst were used. Since the start of the 2013 superoutburst was not well constrained, we shifted the $O-C$ diagram to best fit the 2002 one.

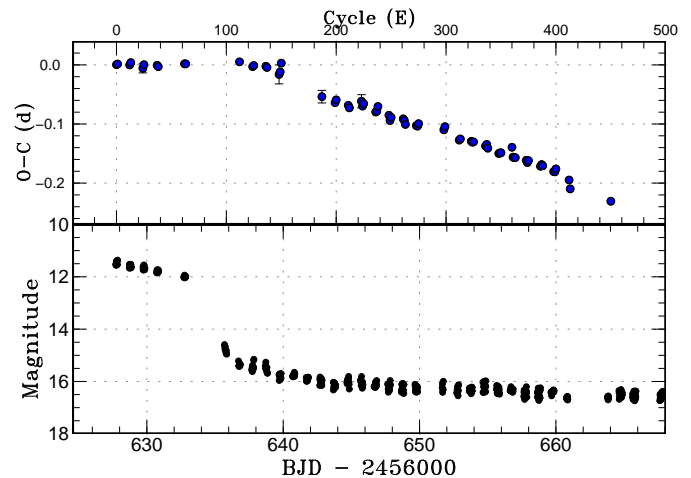


Fig. 34. $O-C$ diagram of superhumps in CU Vel (2013). (Upper): $O-C$ diagram. A period of 0.080573 d was used to draw this figure. (Lower): Light curve. The observations were binned to 0.016 d.

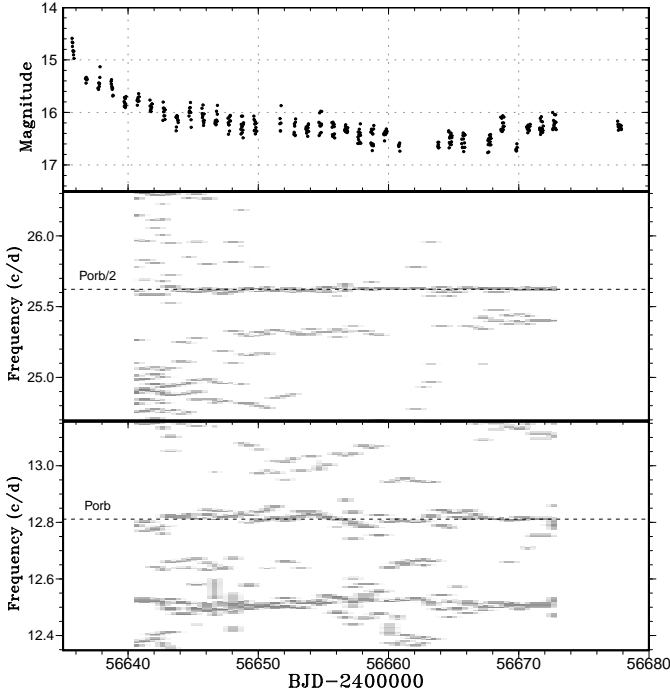


Fig. 35. Two-dimensional Lasso period analysis of CU Vel in the post-superoutburst stage (2013). The superoutburst plateau was excluded from the analysis because it did not yield a meaningful spectrum due to the shortness of the observation. (Upper:) Light curve. The data were binned to 0.01 d. (Middle:) First harmonics of the superhump and orbital signals. (Lower:) Fundamental of the superhump and the orbital signal. The orbital signal was present both in the fundamental and the first harmonic. The signal of (positive) superhumps with increasing frequency was recorded during the post-superoutburst stage. No indication of negative superhump was present. $\log \lambda = -8.5$ was used. The width of the sliding window and the time step used are 10 d and 0.4 d, respectively.

Table 39. Superhump maxima of CU Vel (2013)

E	max*	error	$O - C^\dagger$	N^\ddagger
0	56627.7714	0.0013	0.0004	17
1	56627.8531	0.0052	0.0016	8
12	56628.7378	0.0008	-0.0001	16
13	56628.8223	0.0011	0.0038	17
24	56629.6989	0.0077	-0.0059	6
25	56629.7856	0.0007	0.0003	17
37	56630.7515	0.0015	-0.0007	17
38	56630.8298	0.0017	-0.0029	15
62	56632.7684	0.0010	0.0019	17
63	56632.8488	0.0036	0.0017	10

*BJD-2400000.

† Against max = 2456627.7710 + 0.080573E.

‡ Number of points used to determine the maximum.

Table 40. Superhump maxima of CU Vel in (2013) (post-superoutburst)

E	max*	error	$O - C^\dagger$	N^\ddagger
0	56636.8003	0.0026	-0.0013	17
12	56637.7592	0.0021	-0.0014	15
13	56637.8416	0.0023	0.0010	10
24	56638.7266	0.0037	0.0070	16
25	56638.8052	0.0027	0.0057	16
36	56639.6797	0.0160	0.0011	8
37	56639.7645	0.0063	0.0060	15
38	56639.8600	0.0028	0.0215	7
75	56642.7844	0.0106	-0.0109	15
87	56643.7411	0.0017	-0.0133	8
88	56643.8264	0.0048	-0.0079	11
99	56644.7034	0.0057	-0.0099	13
100	56644.7798	0.0033	-0.0134	15
111	56645.6772	0.0112	0.0049	10
112	56645.7496	0.0016	-0.0026	14
113	56645.8343	0.0017	0.0021	15
124	56646.7064	0.0039	-0.0048	14
125	56646.7885	0.0016	-0.0027	17
126	56646.8770	0.0049	0.0059	6
136	56647.6679	0.0028	-0.0023	9
137	56647.7395	0.0043	-0.0106	13
138	56647.8254	0.0021	-0.0047	20
149	56648.7093	0.0032	0.0002	14
150	56648.7870	0.0016	-0.0020	17
151	56648.8610	0.0024	-0.0080	12
161	56649.6647	0.0022	-0.0034	9
162	56649.7443	0.0012	-0.0037	13
163	56649.8291	0.0018	0.0012	20
186	56651.6719	0.0027	0.0059	9
187	56651.7578	0.0048	0.0118	6
200	56652.7825	0.0016	-0.0024	19
201	56652.8650	0.0036	0.0003	11

*BJD-2400000.

† Against max = 2456636.8016 + 0.079916E.

‡ Number of points used to determine the maximum.

This outburst turned out to be a superoutburst. Only single superhump maximum of BJD 2456565.5851(18) ($N = 19$) was obtained during the observation on two nights.

3.33. ASAS J224349+0809.5

This dwarf nova (hereafter ASAS J224349) was selected by P. Wils (cf. Shears et al. 2011a). There was one well-recorded outburst (superoutburst) in the ASAS data in 2005 October–November. The outburst in 2009 October was well observed, and superhumps were detected (Kato et al. 2010; Shears et al. 2011a). Although there was another superoutburst in 2011 June, the outburst was observed only for two nights (Kato et al. 2013a).

On 2013 August 14, ASAS-SN team detected another outburst (vsnet-alert 16197). This outburst turned out to be a superoutburst, and stages B and C were well recorded (table 41). This superoutburst was followed by one post-

Table 40. Superhump maxima of CU Vel in (2013) (post-superoutburst, continued)

E	max*	error	$O - C^\dagger$	N^\ddagger
211	56653.6668	0.0017	0.0028	12
212	56653.7459	0.0023	0.0020	14
213	56653.8269	0.0013	0.0031	19
224	56654.7062	0.0020	0.0034	9
225	56654.7896	0.0018	0.0068	19
226	56654.8637	0.0027	0.0010	11
236	56655.6604	0.0012	-0.0014	12
237	56655.7420	0.0020	0.0003	14
238	56655.8228	0.0014	0.0011	20
248	56656.6379	0.0061	0.0171	11
249	56656.7018	0.0013	0.0011	19
250	56656.7815	0.0019	0.0009	19
251	56656.8621	0.0031	0.0015	16
261	56657.6633	0.0038	0.0036	13
262	56657.7400	0.0034	0.0004	16
263	56657.8239	0.0028	0.0044	22
274	56658.7006	0.0016	0.0020	15
275	56658.7841	0.0025	0.0055	20
276	56658.8626	0.0027	0.0042	18
286	56659.6585	0.0026	0.0008	18
287	56659.7386	0.0030	0.0011	18
288	56659.8242	0.0031	0.0067	22
300	56660.7723	0.0020	-0.0042	32
301	56660.8379	0.0023	-0.0185	34
338	56663.7981	0.0028	-0.0152	25

*BJD-2400000.

†Against max = 2456636.8016 + 0.079916*E*.

‡Number of points used to determine the maximum.

superoutburst rebrightening 4 d later than the rapid fading from the plateau phase (figure 36). This interval was rather short for an ordinary SU UMa-type dwarf nova. As in the 2009 superoutburst, a definitely positive P_{dot} was recorded during stage B. The $O - C$ diagrams in the two superoutbursts was very similar (figure 37). Although the coincidence in cycle counts between two superoutbursts was by chance, the 2013 superoutburst was confirmed to be detected sufficiently early (vsnet-alert 16207, within 3 d of the start of the outburst).

3.34. ASASSN-13cf

This object was discovered by ASAS-SN survey on 2013 August 24 (vsnet-alert 16261). The coordinates are $21^{\text{h}}55^{\text{m}}12^{\text{s}}.76$, $+27^{\circ}41'18''.9$. One previous outburst was detected in the CRTS data and another outburst was recorded Palomar quick-V plate (D. Denisenko, vsnet-alert 16263). Subsequent observations detected superhumps (vsnet-alert 16284, 16308; figure 38). The times of superhump maxima are listed in table 42. A positive P_{dot} of $+7.1(1.9) \times 10^{-5}$, characteristic to this short superhump period, was obtained.

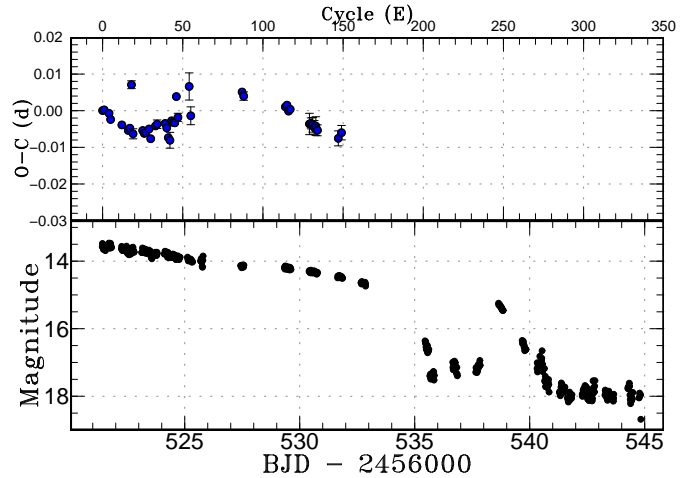
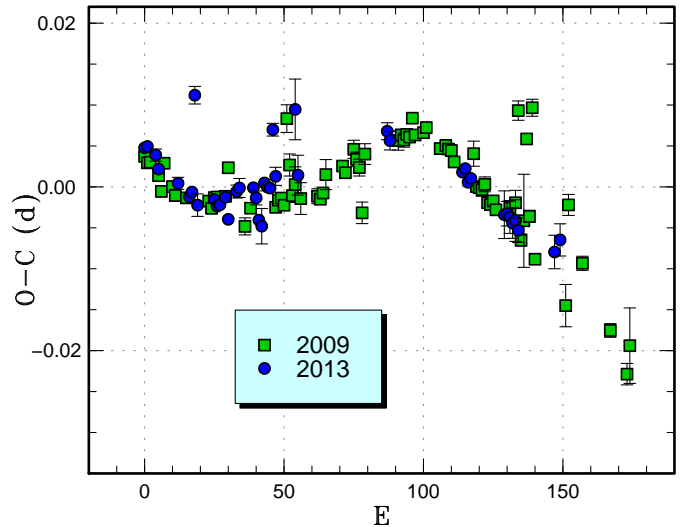
**Fig. 36.** $O - C$ diagram of superhumps in ASAS J2243 (2013). (Upper): $O - C$ diagram. A period of 0.069715 d was used to draw this figure. (Lower): Light curve. The observations were binned to 0.014 d.**Fig. 37.** Comparison of $O - C$ diagrams of ASAS J2243 between different superoutbursts. A period of 0.06975 d was used to draw this figure. Approximate cycle counts (E) after the start of the superoutburst were used. The coincidence in cycle counts between two superoutbursts was by chance.

Table 41. Superhump maxima of ASAS J224349 (2013).

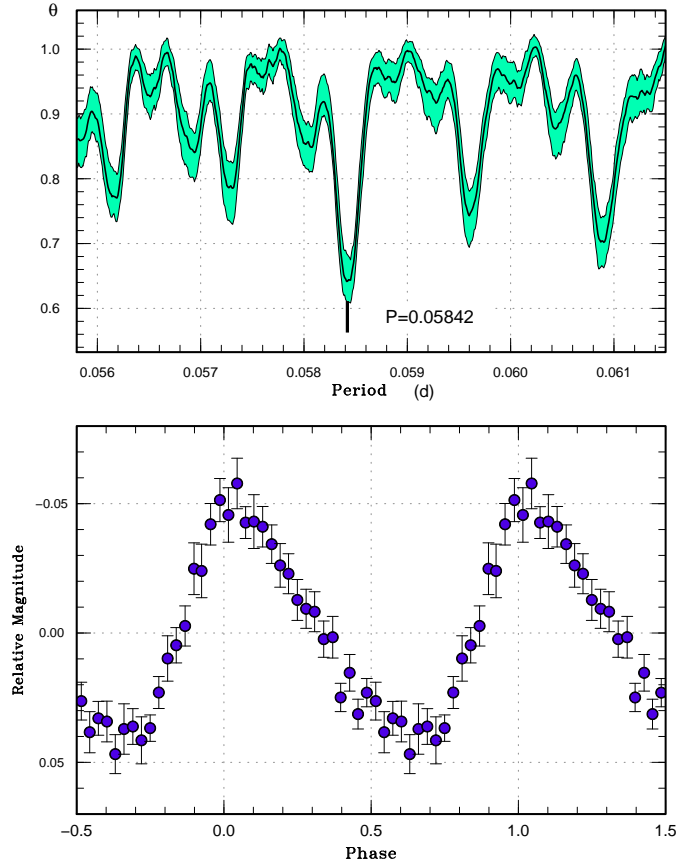
E	max*	error	$O - C^\dagger$	N^\ddagger
0	56521.4291	0.0002	0.0027	116
1	56521.4990	0.0003	0.0028	146
4	56521.7072	0.0007	0.0019	19
5	56521.7753	0.0006	0.0002	24
12	56522.2618	0.0007	-0.0013	45
16	56522.5392	0.0004	-0.0028	123
17	56522.6095	0.0003	-0.0022	142
18	56522.6911	0.0011	0.0097	40
19	56522.7474	0.0014	-0.0037	20
25	56523.1666	0.0006	-0.0028	57
26	56523.2355	0.0004	-0.0036	65
27	56523.3054	0.0003	-0.0034	134
29	56523.4459	0.0003	-0.0024	130
30	56523.5129	0.0006	-0.0050	143
33	56523.7255	0.0008	-0.0016	22
34	56523.7957	0.0012	-0.0011	17
39	56524.1445	0.0003	-0.0009	125
40	56524.2130	0.0009	-0.0021	66
41	56524.2801	0.0006	-0.0048	68
42	56524.3491	0.0022	-0.0055	86
43	56524.4241	0.0005	-0.0002	143
44	56524.4934	0.0004	-0.0006	139
45	56524.5630	0.0004	-0.0007	142
46	56524.6398	0.0008	0.0065	29
47	56524.7039	0.0011	0.0008	33
54	56525.2003	0.0037	0.0092	61
55	56525.2620	0.0024	0.0012	22
87	56527.4994	0.0010	0.0077	49
88	56527.5680	0.0011	0.0066	39
114	56529.3777	0.0004	0.0036	136
115	56529.4478	0.0004	0.0041	158
116	56529.5159	0.0005	0.0025	154
117	56529.5861	0.0006	0.0030	138

*BJD-2400000.

 † Against max = 2456521.4265 + 0.069715*E*. ‡ Number of points used to determine the maximum.**Table 41.** Superhump maxima of ASAS J224349 (2013) (continued).

E	max*	error	$O - C^\dagger$	N^\ddagger
129	56530.4187	0.0029	-0.0010	53
130	56530.4886	0.0015	-0.0009	58
131	56530.5579	0.0020	-0.0013	66
132	56530.6269	0.0019	-0.0020	43
133	56530.6970	0.0025	-0.0016	17
134	56530.7656	0.0015	-0.0028	17
147	56531.6697	0.0020	-0.0050	23
149	56531.8106	0.0020	-0.0034	25

*BJD-2400000.

 † Against max = 2456521.4265 + 0.069715*E*. ‡ Number of points used to determine the maximum.**Fig. 38.** Superhumps in ASASSN-13cf (2013). (Upper): PDM analysis. (Lower): Phase-averaged profile.**Table 42.** Superhump maxima of ASASSN-13cf (2013)

E	max*	error	$O - C^\dagger$	N^\ddagger
0	56529.7208	0.0008	0.0007	101
1	56529.7839	0.0013	0.0054	61
2	56529.8388	0.0007	0.0018	96
29	56531.4116	0.0028	-0.0026	27
48	56532.5201	0.0004	-0.0040	100
49	56532.5772	0.0007	-0.0053	65
98	56535.4447	0.0012	-0.0002	52
114	56536.3780	0.0020	-0.0016	40
115	56536.4419	0.0015	0.0039	43
149	56538.4257	0.0015	0.0015	63
150	56538.4828	0.0011	0.0002	64

*BJD-2400000.

 † Against max = 2456529.7201 + 0.058416*E*. ‡ Number of points used to determine the maximum.

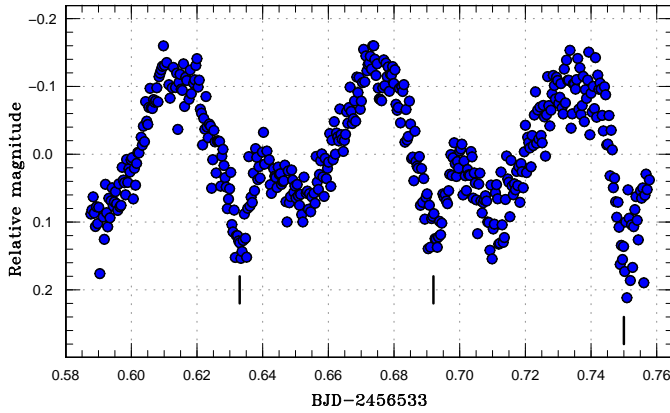


Fig. 39. Superhumps and possible eclipses in ASASSN-13cg on 2013 August 29. The vertical ticks represent possible shallow eclipses.

Table 43. Superhump maxima of ASASSN-13cg (2013)

E	max*	error	$O - C^\dagger$	N^\ddagger
0	56533.6131	0.0003	0.0013	132
1	56533.6735	0.0004	0.0015	138
2	56533.7326	0.0005	0.0003	140
12	56534.3338	0.0008	-0.0008	23
13	56534.3939	0.0013	-0.0009	23
46	56536.3759	0.0020	-0.0064	21
61	56537.2850	0.0021	-0.0007	22
62	56537.3490	0.0012	0.0031	23
63	56537.4088	0.0030	0.0026	23

*BJD-2400000.

† Against max = 2456533.6118 + 0.060228 E .

‡ Number of points used to determine the maximum.

3.35. ASASSN-13cg

This object was discovered by ASAS-SN survey on 2013 August 27. The coordinates are $20^{\text{h}}52^{\text{m}}52^{\text{s}}.74$, $-02^{\circ}39'53''.0$. This object attracted attention because it has a very blue ($u - g = -0.2$) SDSS color (vsnet-alert 16280). It also has an X-ray counterpart of 1RXS J205252.1-023952. Time-resolved photometry detected superhumps and possible shallow eclipses (vsnet-alert 16302; figures 39, 40). These eclipse-like fadings were not recorded on later nights and we could not determine its period. The reality of the eclipses requires future observations. The times of superhump maxima are listed in table 43, which clearly shows a positive P_{dot} .

3.36. ASASSN-13ck

This object was discovered by ASAS-SN survey on 2013 August 29 (vsnet-alert 16303). The coordinates are $00^{\text{h}}11^{\text{m}}33^{\text{s}}.71$, $+04^{\circ}51'23''.0$. The object had a blue SDSS counterpart ($g = 20.8$) and its outburst amplitude immediately suggested a WZ Sge-type dwarf nova.

Subsequent observations recorded early superhumps (vsnet-alert 16307, 16309, 16313, 16314, 16332, 16368; fig-

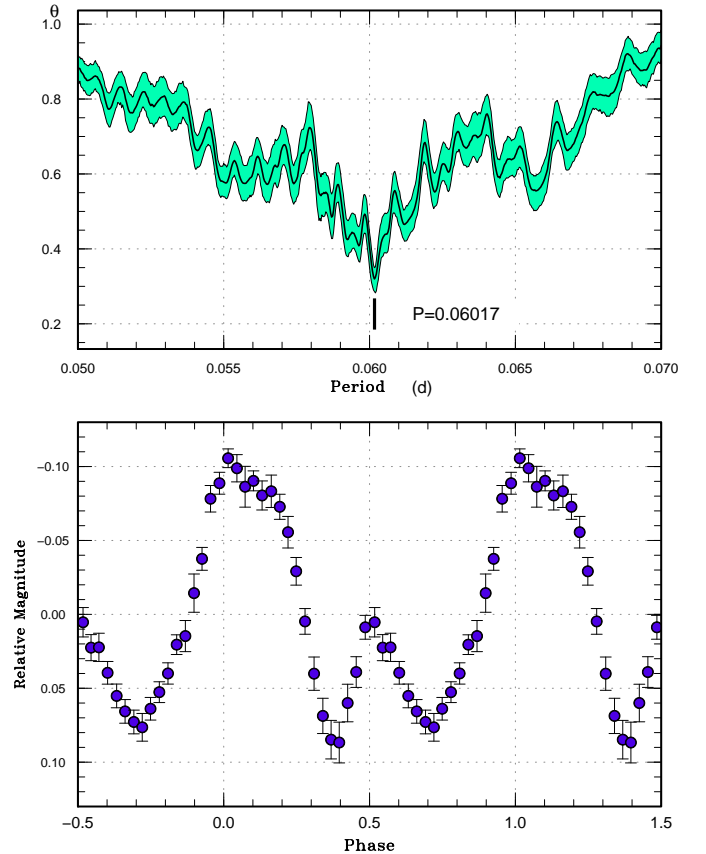


Fig. 40. Superhumps in ASASSN-13cg (2013). (Upper): PDM analysis. (Lower): Phase-averaged profile. The dip around phase 0.4 is a result of eclipse-like feature recorded on the first night.

ure 41). Ten days after the outburst detection, ordinary superhumps grew (vsnet-alert 16370, 16374, 16375, 16385; figure 42). As judged from the evolution of superhumps, the outburst of this object was detected sufficiently early.

The times of superhump maxima during the superoutburst plateau are listed in table 44. Clear stages A and B can be recognized as in many WZ Sge-type dwarf novae (figure 43). The last point ($E = 202$) was obtained during the fading branch of the superoutburst, and its large positive $O - C$ probably reflects the decrease of the pressure effect (cf. Nakata et al. 2013b). This maximum was not used to determine P_{dot} for stage B. As in many WZ Sge-type dwarf novae, this object did not show a marked transition to stage C superhumps.

Five days after the rapid fading, the object showed a short rebrightening (September 23, BJD 2456558.5). The object showed another rebrightening (September 26, BJD 2456561.7), which served as a precursor outburst to the second plateau phase. This second plateau phase lasted for 6 d (figure 43). During the second plateau phase, superhumps were also present. The mean superhump period during this phase was 0.056172(14) d, indicating that the precession rate was smaller than in the main superoutburst. This smaller precession rate can be interpreted as

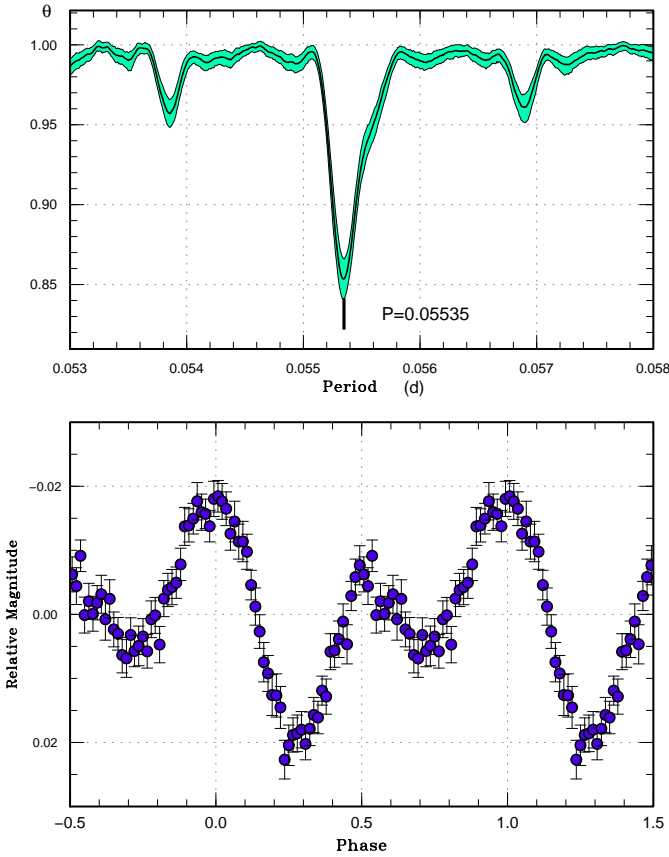


Fig. 41. Early superhumps in ASASSN-13ck (2013). (Upper): PDM analysis. (Lower): Phase-averaged profile.

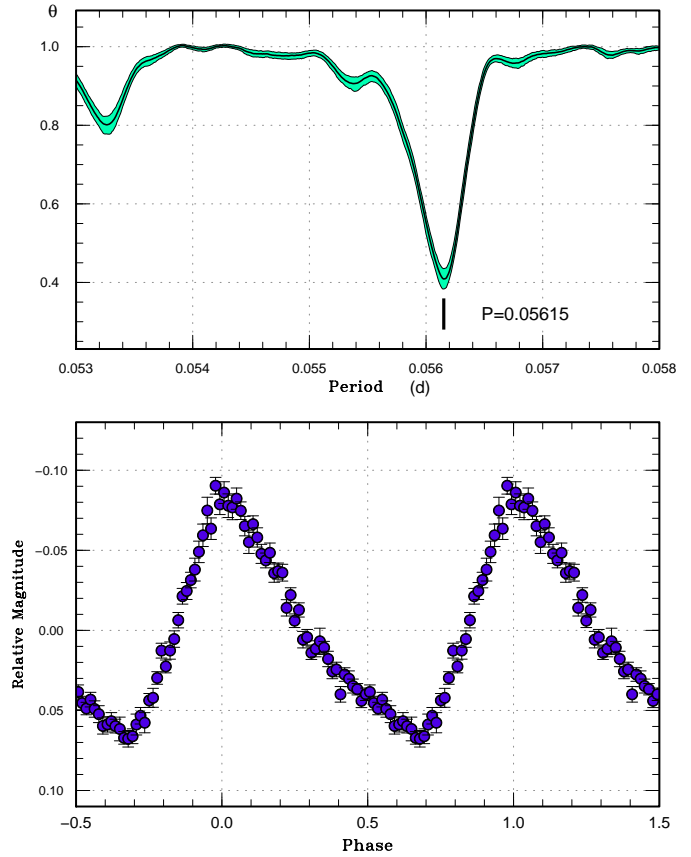


Fig. 42. Ordinary superhumps in ASASSN-13ck (2013). (Upper): PDM analysis. (Lower): Phase-averaged profile.

a result of a smaller disk radius.

The pattern of rebrightening was like a “hybrid” type between long-lasting plateau type (type A rebrightening in Kato et al. 2009) and distinct repetitive rebrightenings (type B rebrightening in Kato et al. 2009). There appears to be a smooth transition between these types of rebrightenings. The presence of a precursor outburst in the second plateau is also intriguing. Such a precursor was also recorded in AL Com in 1995 (cf. Nogami et al. 1997; also subsection 3.11). It is likely that a normal outburst triggered the second plateau phase (second superoutburst) as in ordinary SU UMa-type dwarf novae (Osaki 1989).

A two-dimensional Lasso analysis is presented in figure 44. The orbital signal was only present during the stage of early superhumps. The signal of (positive) superhumps showed a decrease in frequency (increase in period) during the superoutburst plateau. The superhumps appeared with slightly higher frequencies during the rebrightening plateau.

3.37. ASASSN-13cv

This object was discovered by ASAS-SN survey on 2013 September 5 (vsnet-alert 16303). The coordinates are $22^{\text{h}}10^{\text{m}}25^{\text{s}}.24$, $+30^{\circ}46'06''.9$. Although the quiescent counterpart was not listed in the photometric cat-

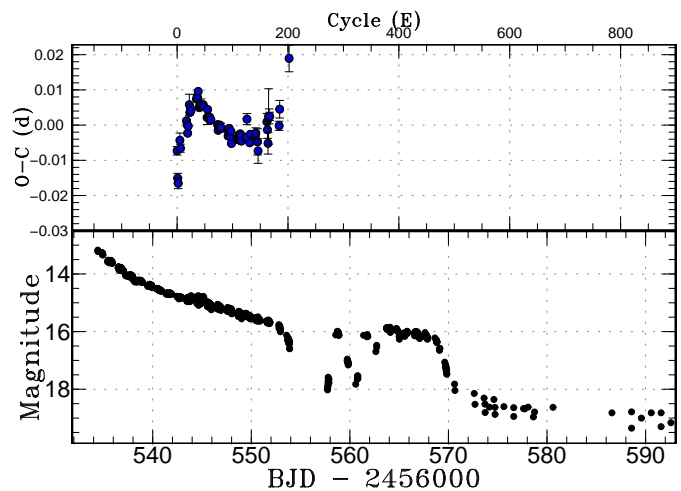


Fig. 43. $O - C$ diagram of superhumps in ASASSN-13ck (2013). (Upper): $O - C$ diagram. A period of 0.056238 d was used to draw this figure. (Lower): Light curve. The observations were binned to 0.012 d.

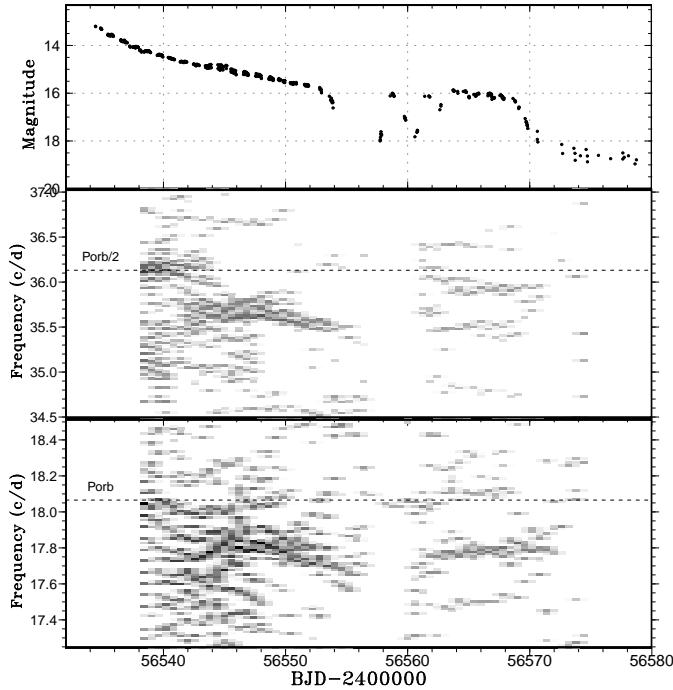


Fig. 44. Lasso analysis of ASASSN-13ck (2013). (Upper:) Light curve. The data were binned to 0.02 d. (Middle:) First harmonics of the superhump and orbital signals. (Lower:) Fundamental of the superhump and the orbital signal. The orbital signal was present both in the fundamental and the first harmonic during the earliest phase (early superhumps). The signal of (positive) superhumps with variable frequency was recorded during the superoutburst plateau. No indication of negative superhump was present. $\log \lambda = -8.8$ was used. The width of the sliding window and the time step used are 8 d and 0.6 d, respectively.

alog of SDSS (vsnet-alert 16354), the Guide Star Catalog (GSC), Version 2.3.2 has an object with a 21.4 mag. GALEX (Martin et al. 2005) also has a ultraviolet counterpart within 1'' [NUV and FUV magnitudes 22.07(3) and 21.6(4) mag, respectively].

We obtained a single-night observation of this object (vsnet-alert 16364; figure 45). Three superhump maxima were obtained: BJD 2456541.3818(7) ($N = 37$), 2456541.4441(2) ($N = 66$) and 2456541.5072(6) ($N = 36$). The best period by the PDM method is 0.0607(2) d.

3.38. ASASSN-13cz

This object was discovered by ASAS-SN survey on 2013 September 14 (vsnet-alert 16401). The coordinates are $15^{\text{h}}27^{\text{m}}55^{\text{s}}.3$, $+63^{\circ}27'53''.4$. Subsequent observations detected superhumps (vsnet-alert 16405; figure 46). The times of superhump maxima are listed in table 45. The period shown in table 2 is a result of the PDM analysis.

3.39. ASASSN-13da

This object was discovered by ASAS-SN survey on 2013 September 20 (vsnet-alert 16426). The coordinates are $19^{\text{h}}59^{\text{m}}18^{\text{s}}.03$, $-18^{\circ}33'31''.4$. The quiescent counterpart is

Table 44. Superhump maxima of ASASSN-13ck (2013)

E	max*	error	$O - C^{\dagger}$	N^{\ddagger}
0	56542.4669	0.0012	-0.0073	50
1	56542.5154	0.0014	-0.0150	57
2	56542.5701	0.0015	-0.0165	58
5	56542.7511	0.0021	-0.0043	15
6	56542.8051	0.0011	-0.0066	70
17	56543.4315	0.0006	0.0013	52
18	56543.4866	0.0003	0.0001	111
19	56543.5404	0.0002	-0.0023	104
20	56543.5987	0.0006	-0.0003	55
22	56543.7172	0.0030	0.0058	21
23	56543.7713	0.0002	0.0036	54
24	56543.8288	0.0003	0.0049	64
25	56543.8842	0.0005	0.0041	30
35	56544.4499	0.0006	0.0074	33
36	56544.5069	0.0002	0.0081	82
37	56544.5627	0.0002	0.0077	73
38	56544.6208	0.0010	0.0096	37
40	56544.7287	0.0006	0.0050	26
41	56544.7856	0.0003	0.0056	70
42	56544.8417	0.0004	0.0055	65
43	56544.8983	0.0015	0.0059	20
47	56545.1232	0.0002	0.0058	73
48	56545.1788	0.0004	0.0052	76
54	56545.5132	0.0020	0.0022	26
55	56545.5717	0.0003	0.0045	106
56	56545.6260	0.0003	0.0025	115
57	56545.6820	0.0003	0.0022	99
58	56545.7383	0.0004	0.0024	63
59	56545.7945	0.0003	0.0022	73
60	56545.8498	0.0004	0.0014	76
61	56545.9062	0.0007	0.0016	36
73	56546.5797	0.0004	0.0002	58
74	56546.6343	0.0005	-0.0015	69

*BJD-2400000.

† Against max = 2456542.4742 + 0.056238*E*.

‡ Number of points used to determine the maximum.

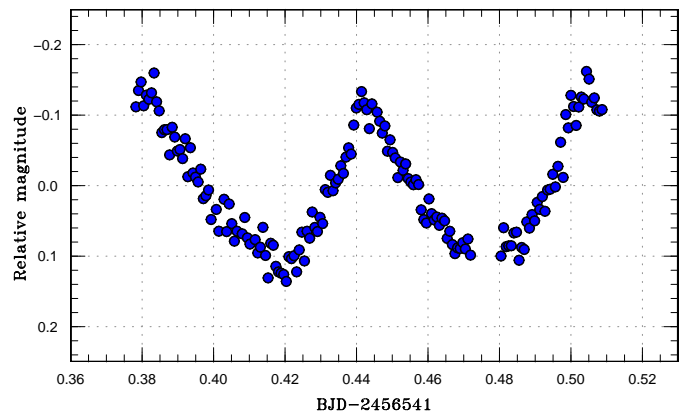
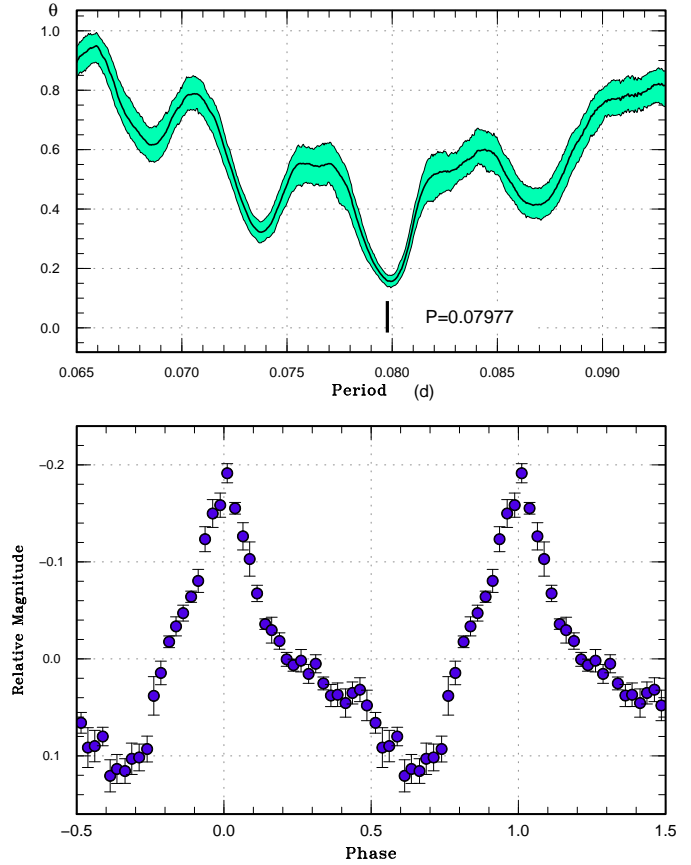


Fig. 45. Superhumps in ASASSN-13cv on 2013 September 5.

Table 44. Superhump maxima of ASASSN-13ck (2013) (continued)

E	max*	error	$O - C^\dagger$	N^\ddagger
75	56546.6915	0.0005	-0.0005	74
76	56546.7476	0.0005	-0.0007	62
77	56546.8046	0.0003	0.0001	77
78	56546.8598	0.0006	-0.0009	53
79	56546.9163	0.0013	-0.0007	31
91	56547.5905	0.0005	-0.0013	45
92	56547.6450	0.0005	-0.0031	66
93	56547.7026	0.0005	-0.0017	69
94	56547.7597	0.0005	-0.0009	55
95	56547.8142	0.0008	-0.0026	18
96	56547.8698	0.0011	-0.0032	22
97	56547.9275	0.0006	-0.0017	58
98	56547.9803	0.0007	-0.0052	57
110	56548.6569	0.0015	-0.0034	13
111	56548.7124	0.0005	-0.0041	48
112	56548.7701	0.0005	-0.0028	48
113	56548.8248	0.0009	-0.0042	35
114	56548.8829	0.0005	-0.0024	51
115	56548.9387	0.0006	-0.0028	76
116	56548.9933	0.0009	-0.0045	52
124	56549.4440	0.0004	-0.0036	59
125	56549.5005	0.0004	-0.0034	53
126	56549.5619	0.0016	0.0017	18
131	56549.8364	0.0009	-0.0050	50
132	56549.8950	0.0009	-0.0025	40
141	56550.4006	0.0007	-0.0031	33
142	56550.4577	0.0015	-0.0022	18
145	56550.6239	0.0037	-0.0047	15
146	56550.6776	0.0035	-0.0073	17
162	56551.5857	0.0024	0.0010	53
163	56551.6396	0.0024	-0.0013	59
164	56551.6921	0.0031	-0.0051	12

*BJD-2400000.

 \dagger Against max = 2456542.4742 + 0.056238 E . \ddagger Number of points used to determine the maximum.**Fig. 46.** Superhumps in ASASSN-13cz (2013). (Upper): PDM analysis. (Lower): Phase-averaged profile.**Table 44.** Superhump maxima of ASASSN-13ck (2013) (continued)

E	max*	error	$O - C^\dagger$	N^\ddagger
165	56551.7559	0.0079	0.0025	42
166	56551.8122	0.0021	0.0025	71
167	56551.8684	0.0012	0.0026	64
184	56552.8218	0.0013	-0.0001	28
185	56552.8827	0.0025	0.0046	26
202	56553.8532	0.0038	0.0190	61

*BJD-2400000.

 \dagger Against max = 2456542.4742 + 0.056238 E . \ddagger Number of points used to determine the maximum.**Table 45.** Superhump maxima of ASASSN-13cz (2013)

E	max*	error	$O - C^\dagger$	N^\ddagger
0	56550.3610	0.0004	0.0003	86
1	56550.4407	0.0004	0.0002	81
2	56550.5198	0.0005	-0.0006	82
13	56551.3986	0.0006	0.0001	50

*BJD-2400000.

 \dagger Against max = 2456550.3607 + 0.079834 E . \ddagger Number of points used to determine the maximum.

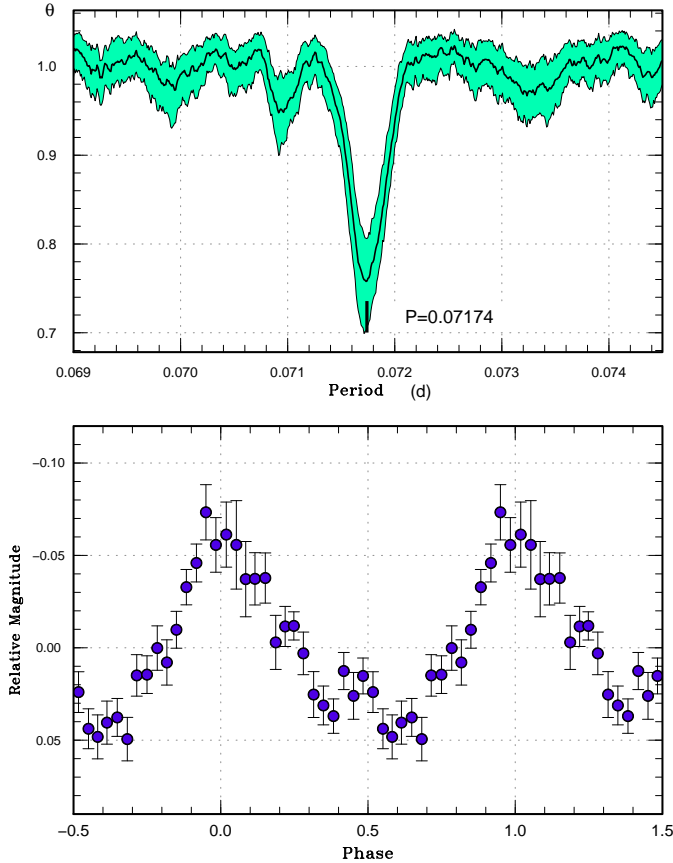


Fig. 47. Superhumps in ASASSN-13da (2013). (Upper): PDM analysis. (Lower): Phase-averaged profile.

a 21 mag object in CRTS. On the first three nights, only low-amplitude modulations were detected. Four days after the detection, fully grown superhumps appeared (vsnet-alert 16494; figure 47). This growth of superhumps was associated with the brightening of the system brightness. The times of superhump maxima are listed in table 46. The times for $E \leq 29$ were those for superhumps in the growing stage and they are likely stage A superhumps. Cycle counts for these maxima are uncertain. Although a PDM analysis of this segment yielded a possible period of 0.07300(5) d, this value was not included in table 2 due to its uncertainty. The decrease in $O - C$ for $E \geq 153$ suggests stage B-C transition.

3.40. ASASSN-14ac

This object was discovered by ASAS-SN survey on 2014 January 18 (Shappee et al. 2014). The coordinates are $07^{\text{h}}52^{\text{m}}54^{\text{s}}.9$, $+53^{\circ}05'31''.2$. The large outburst amplitude (~ 7 mag) and the blue SDSS counterpart ($u - g = -0.3$) was suggestive of a WZ Sge-type dwarf nova (vsnet-alert 16794). Although subsequent observations recorded some low amplitude modulations (vsnet-alert 16823, 16830), no distinct period was obtained. The object started to show ordinary superhumps 14 d after the discovery (vsnet-alert 16880, 16895; figure 48).

Table 46. Superhump maxima of ASASSN-13da (2013)

E	max*	error	$O - C^\dagger$	N^\ddagger
0	56556.5090	0.0025	0.0017	19
1	56556.5711	0.0047	-0.0079	20
29	56558.5871	0.0048	-0.0002	17
56	56560.5208	0.0010	-0.0032	19
57	56560.5976	0.0012	0.0019	20
70	56561.5317	0.0009	0.0036	19
71	56561.6015	0.0007	0.0016	19
98	56563.5360	0.0015	-0.0006	19
99	56563.6082	0.0014	-0.0001	15
112	56564.5350	0.0011	-0.0057	24
113	56564.6136	0.0021	0.0011	17
126	56565.5511	0.0016	0.0062	21
139	56566.4829	0.0111	0.0055	9
140	56566.5555	0.0018	0.0065	25
153	56567.4878	0.0212	0.0062	10
154	56567.5563	0.0010	0.0031	25
168	56568.5571	0.0014	-0.0004	26
181	56569.4737	0.0046	-0.0162	6
182	56569.5585	0.0024	-0.0031	26

*BJD-2400000.

† Against max = $2456556.5072 + 0.071728E$.

‡ Number of points used to determine the maximum.

The times of superhump maxima are listed in table 47. The early part of the observation clearly recorded stage A superhumps. The global light curve showed systematic brightening associated with the appearance of superhumps (see also figure 49). Although the later part of the superoutburst was not very well recorded, the P_{dot} of stage B superhumps was not strongly positive. The object started rapid fading from the plateau stage on February 17 (30 d after the discovery).

On March 1, E. Muyliaert recorded the object at 17.2 mag (unfiltered CCD magnitude), which appeared to be a post-superoutburst rebrightening. The type of the rebrightening, however, could not be determined.

Since the stage A superhumps of this object are well established, determination of the orbital period in quiescence is desired to estimate the mass ratio.

3.41. CSS J024354.0-160314

This object (=CSS131026:024354-160314, hereafter CSS J024354) was detected as a large-amplitude dwarf nova by CRTS on 2013 October 26 (vsnet-alert 16564). Subsequent observations detected superhumps (vsnet-alert 16600; figure 50). The times of superhump maxima are listed in table 48.

3.42. DDE 31

This dwarf nova was discovered by D. Denisenko in outburst (16.3 mag; all magnitudes for this object are unfiltered CCD magnitudes) on 2012 October 15 (vsnet-alert 15007). The coordinates are $02^{\text{h}}13^{\text{m}}17^{\text{s}}.18$, $+46^{\circ}06'03''.4$. On the next night, the object faded to 17.7 mag (B.

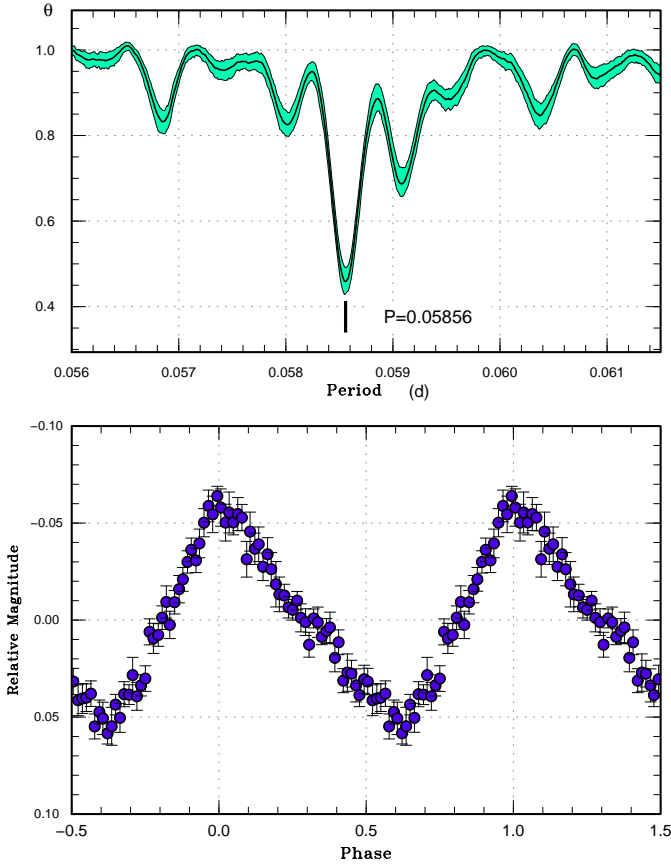


Fig. 48. Superhumps in ASASSN-14ac (2014). (Upper): PDM analysis for the interval BJD 2456692–2456701. (Lower): Phase-averaged profile.

Table 47. Superhump maxima of ASASSN-14ac (2014)

E	max*	error	$O - C^\dagger$	N^\ddagger
0	56689.1105	0.0023	-0.0364	43
1	56689.1686	0.0016	-0.0370	42
15	56690.0034	0.0006	-0.0245	32
52	56692.2034	0.0029	0.0023	17
53	56692.2656	0.0006	0.0058	31
54	56692.3279	0.0010	0.0094	31
55	56692.3847	0.0003	0.0074	24
56	56692.4400	0.0010	0.0040	23
57	56692.5074	0.0006	0.0127	31
58	56692.5630	0.0006	0.0096	30
68	56693.1495	0.0007	0.0087	25
69	56693.2077	0.0014	0.0081	39
70	56693.2673	0.0008	0.0090	47
71	56693.3261	0.0005	0.0091	31
72	56693.3863	0.0004	0.0106	32
83	56694.0294	0.0004	0.0076	42
84	56694.0876	0.0006	0.0071	42
85	56694.1463	0.0004	0.0070	42
86	56694.2066	0.0007	0.0086	50
87	56694.2665	0.0010	0.0098	42
88	56694.3246	0.0006	0.0091	31
89	56694.3837	0.0007	0.0095	31
90	56694.4382	0.0007	0.0053	18
151	56698.0078	0.0008	-0.0079	56
152	56698.0692	0.0010	-0.0052	50
153	56698.1300	0.0018	-0.0032	56
185	56700.0049	0.0009	-0.0077	38
186	56700.0588	0.0008	-0.0126	61
187	56700.1190	0.0016	-0.0111	61
188	56700.1737	0.0012	-0.0151	60

*BJD-2400000.

†Against max = 2456689.1469 + 0.058734E.

‡Number of points used to determine the maximum.

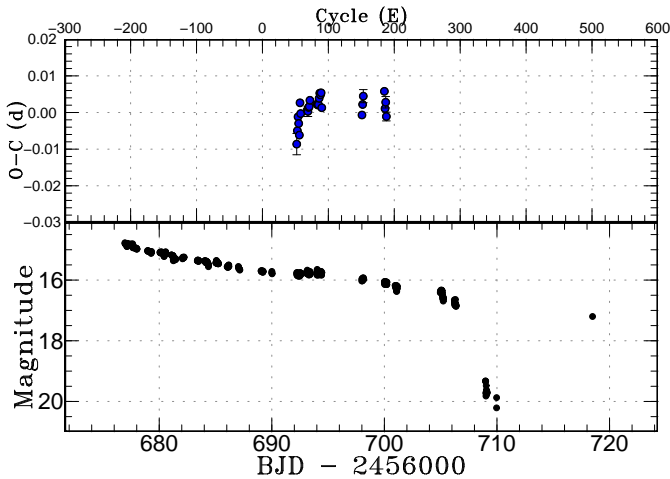


Fig. 49. $O - C$ diagram of superhumps in ASASSN-14ac (2014). (Upper): $O - C$ diagram. A period of 0.05855 d was used to draw this figure. (Lower): Light curve. The observations were binned to 0.012 d.

Table 48. Superhump maxima of CSS J024354 (2013)

E	max*	error	$O - C^\dagger$	N^\ddagger
0	56594.5208	0.0033	0.0094	143
1	56594.5645	0.0024	-0.0089	140
94	56600.3445	0.0009	-0.0020	80
126	56602.3336	0.0007	0.0007	121
127	56602.3953	0.0008	0.0003	143
128	56602.4548	0.0011	-0.0022	142
129	56602.5220	0.0093	0.0028	50

*BJD-2400000.

†Against max = 2456594.5114 + 0.062076E.

‡Number of points used to determine the maximum.

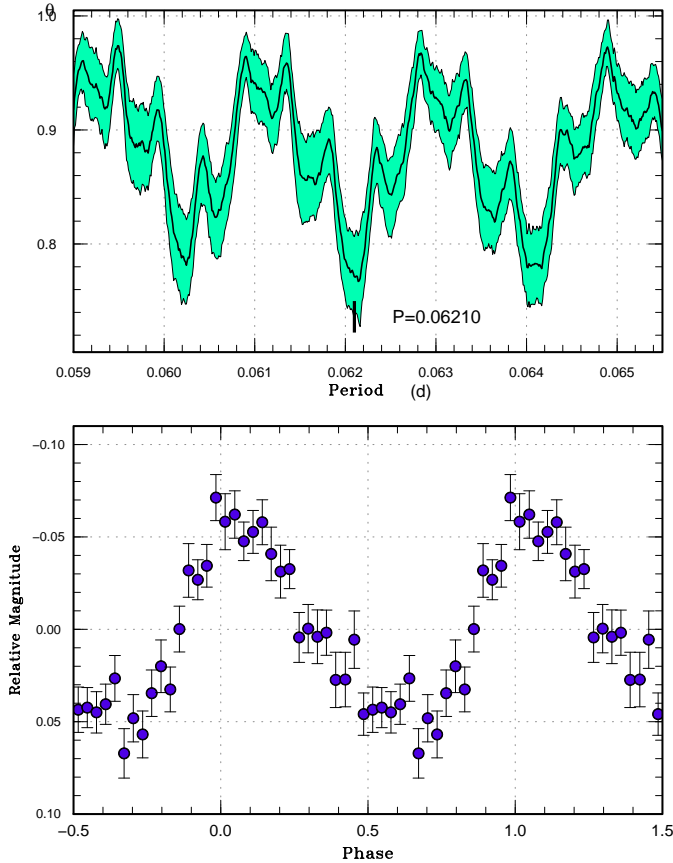


Fig. 50. Superhumps in CSS J024354 (2013). (Upper): PDM analysis. (Lower): Phase-averaged profile.

Staelen). On 2012 December 15, D. Denisenko again detected this object in outburst (16.2 mag) and reported a previous outburst on 2012 September 14 (17.0 mag, vsnet-alert 15170).

On 2014 January 4, D. Denisenko reported a brighter outburst (15.3 mag, vsnet-alert 16757). Time-resolved observations detected modulations resembling superoutburst (figure 51). Although a period of 0.073(3) d was inferred, the outburst faded rapidly (~ 1 mag d^{-1}) and the object was not detected brighter than 18.2 mag five nights later. This behavior was unusual for a superoutburst. Furthermore, an analysis of the SDSS colors (Kato et al. 2012b) yielded an expected orbital period longer than 0.1 d (it was also likely that these SDSS observations were not obtained in true quiescence, cf. vsnet-alert 15170). We therefore should wait another outburst to clarify the classification of this object.

3.4.3. MASTER OT J004527.52+503213.8

This object (hereafter MASTER J004527) was detected as a bright (12.5 mag) transient by the MASTER network (Gorbovskey et al. 2013) on 2013 September 17 (Denisenko et al. 2013c). The object has an 18–19 mag quiescent counterpart and the large outburst amplitude suggested a WZ Sge-type dwarf nova. The last non-

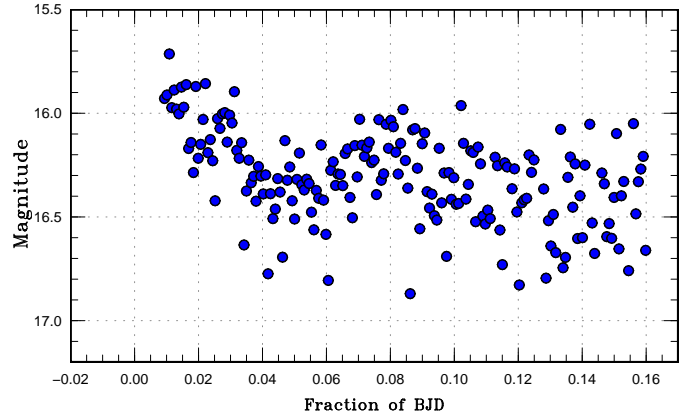


Fig. 51. Possible superhumps in DDE 31.

detection observation prior to the outburst was reported on September 13 (fainter than 18.5, vsnet-alert 16422).

Subsequent observations immediately detected superhumps (vsnet-alert 16423). The long (~ 0.081 d) superhump period, however, was not well compatible with the suggested WZ Sge-type classification (vsnet-alert 16425). Later observations yielded a slightly shorter superhump period (vsnet-alert 16433, 16434, 16459). A further decrease in the superhump period was reported on September 22 (vsnet-alert 16463, 16497). The object showed a single post-superoutburst rebrightening on October 6 (vsnet-alert 16513; figure 52).

The times of superhump maxima are listed in table 49. The decrease in the period around September 22 ($E \sim 50$; figure 52) may be either attributed to stage B-C transition (as in ordinary SU UMa-type dwarf novae) or stage A-B transition (as reported in likely period bouncers SSS J122221.7–311523, Kato et al. 2013b; OT J075418.7+381225 and OT J230425.8+062546, C. Nakata, in preparation). Since the large outburst amplitude of MASTER J004527 suggested the WZ Sge-type classification, the second possibility would deserve consideration. We consider that the former interpretation is more likely for several reasons: (1) The difference in the periods before and after the transition was 0.5%, which is typical for stage B-C transition (e.g. Kato et al. 2009), but is smaller than stage A-B transition (1.0–1.5%, cf. Nakata et al. 2013b). (2) There was a phase with a longer superhump period ($E \leq 7$), which can be considered as stage A. (3) The amplitudes of superhumps were much larger (0.2–0.3 mag; figure 53) than in superhumps in likely period bouncers (e.g. Kato et al. 2013b). We list the periods based on the former interpretation in table 2.

Following this interpretation of the superhump stages, the object can be recognized as an SU UMa-type dwarf nova (not a period bouncer) with a long orbital period and infrequent, large-amplitude outbursts. The object may resemble V1251 Cyg (Kato 1995a; Kato et al. 2009) or QY Per (Kato et al. 2009). Future monitoring of outbursts would be helpful in identifying the supercycle.

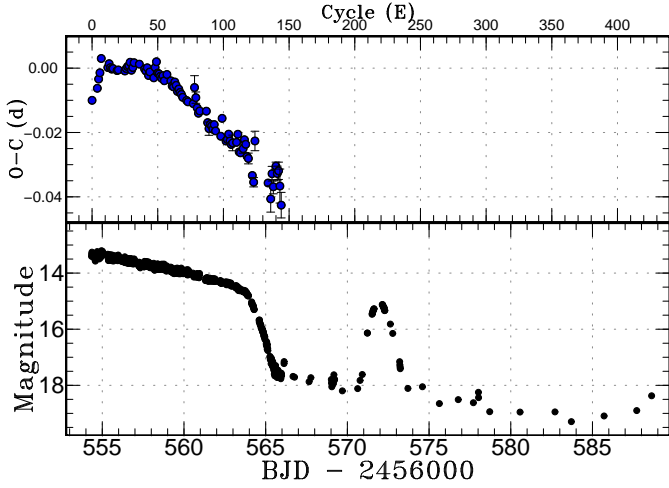


Fig. 52. $O-C$ diagram of superhumps in MASTER J004527 (2013). (Upper): $O-C$ diagram. A period of 0.08039 d was used to draw this figure. (Lower): Light curve. The observations were binned to 0.016 d.

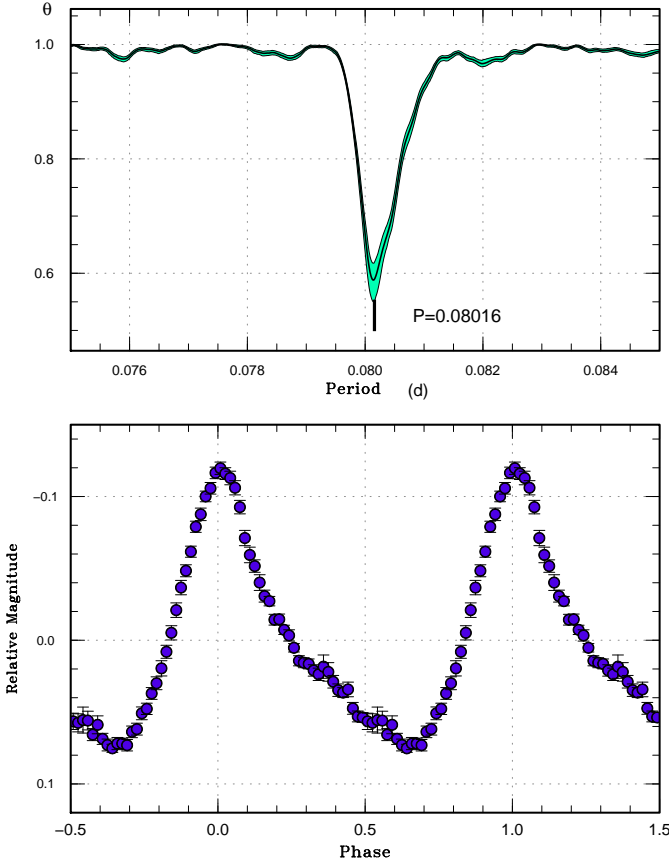


Fig. 53. Superhumps in MASTER J004527 (2013). (Upper): PDM analysis. (Lower): Phase-averaged profile.

Table 49. Superhump maxima of MASTER J004527 (2013)

E	max*	error	$O-C^\dagger$	N^\ddagger
0	56554.3649	0.0003	-0.0181	95
4	56554.6902	0.0002	-0.0132	226
5	56554.7735	0.0002	-0.0101	147
6	56554.8558	0.0002	-0.0079	124
7	56554.9406	0.0008	-0.0031	73
12	56555.3398	0.0002	-0.0045	197
13	56555.4214	0.0001	-0.0030	292
14	56555.5005	0.0001	-0.0040	386
15	56555.5804	0.0001	-0.0042	305
16	56555.6610	0.0002	-0.0037	310
19	56555.9016	0.0004	-0.0035	63
20	56555.9821	0.0003	-0.0030	59
25	56556.3838	0.0002	-0.0019	279
26	56556.4649	0.0002	-0.0009	279
27	56556.5459	0.0002	0.0000	171
28	56556.6266	0.0002	0.0006	202
29	56556.7080	0.0003	0.0019	190
30	56556.7859	0.0004	-0.0003	186
31	56556.8672	0.0003	0.0009	197
32	56556.9491	0.0006	0.0027	52
36	56557.2702	0.0003	0.0033	312
40	56557.5902	0.0006	0.0030	62
41	56557.6700	0.0004	0.0026	69
42	56557.7514	0.0005	0.0039	61
43	56557.8294	0.0005	0.0018	71
44	56557.9109	0.0005	0.0032	71
47	56558.1502	0.0004	0.0022	125
48	56558.2338	0.0003	0.0057	212
49	56558.3160	0.0003	0.0078	227
50	56558.3929	0.0003	0.0046	187
51	56558.4730	0.0003	0.0046	196
52	56558.5527	0.0003	0.0041	225

*BJD-2400000.

†Against max = $2456554.3830 + 0.080106E$.

‡Number of points used to determine the maximum.

3.44. MASTER OT J005740.99+443101.5

This object (hereafter MASTER J005740) was detected as a transient by the MASTER network on 2013 November 6 (Balanutsa et al. 2013a). Subsequent observations immediately detected early superhumps (vsnet-alert 16603, 16606, 16609). The large amplitude (0.4 mag) of early superhumps suggested a high inclination. There was also an eclipse-like feature in the light curve (vsnet-alert 16614; see also vsnet-alert 16603). On November 12–13, ordinary superhumps started to appear, which were accompanied by eclipses (vsnet-alert 16624; figure 54). After fading from the plateau, the eclipses became deeper (~ 1 mag, vsnet-alert 16640), implying that the white dwarf is eclipsed. This object became the first candidate WZ Sge-type dwarf nova showing the eclipse of the white dwarf.

We first obtained the eclipse ephemeris using observations other than the phase of early superhumps, since the profile of early superhumps is similar to, but known to be

Table 49. Superhump maxima of MASTER J004527 (2013) (continued)

E	max*	error	$O - C^\dagger$	N^\ddagger
53	56558.6324	0.0003	0.0037	256
54	56558.7136	0.0004	0.0049	130
55	56558.7924	0.0005	0.0036	61
57	56558.9552	0.0011	0.0061	24
60	56559.1944	0.0002	0.0050	209
61	56559.2731	0.0002	0.0037	263
62	56559.3533	0.0002	0.0037	144
63	56559.4352	0.0003	0.0055	128
64	56559.5145	0.0003	0.0047	169
65	56559.5930	0.0004	0.0031	66
66	56559.6741	0.0003	0.0041	206
67	56559.7535	0.0002	0.0034	188
68	56559.8333	0.0003	0.0030	68
69	56559.9127	0.0005	0.0024	70
72	56560.1529	0.0003	0.0023	120
73	56560.2329	0.0002	0.0021	137
77	56560.5539	0.0006	0.0027	56
78	56560.6393	0.0037	0.0080	42
79	56560.7165	0.0018	0.0051	28
80	56560.7938	0.0007	0.0023	61
81	56560.8725	0.0006	0.0009	69
82	56560.9536	0.0009	0.0019	37
87	56561.3555	0.0009	0.0032	104
88	56561.4323	0.0003	-0.0001	108
89	56561.5108	0.0021	-0.0017	30
90	56561.5925	0.0008	-0.0000	70
91	56561.6724	0.0005	-0.0002	69
92	56561.7518	0.0008	-0.0010	57
93	56561.8336	0.0007	0.0007	72
94	56561.9121	0.0008	-0.0009	68
98	56562.2320	0.0004	-0.0015	154
99	56562.3179	0.0006	0.0044	113

*BJD-2400000.

 † Against max = 2456554.3830 + 0.080106*E*. ‡ Number of points used to determine the maximum.

different from that of the eclipse (cf. Uemura et al. 2012). We obtained the following ephemeris

$$\text{Min}(\text{BJD}) = 2456617.36772(4) + 0.0561904(3)E \quad (4)$$

by using the MCMC modelling as in V893 Sco. Note that this ephemeris is not intended for long-term prediction, in contrast to other eclipsing dwarf novae treated in this paper, of eclipses since the eclipse profile is strongly affected by the varying superhumps and systematic variations in relation to the system brightness. The errors given in equation (4) is formal statistic ones, and the actual errors are expected to be larger due to the systematic errors.

The times of superhump maxima, determined after removing the within 0.07 orbital phases of eclipses, are listed in table 50. The $O - C$ diagram is presented in figure 57. The maxima for $E < 14$ are stage A superhumps with growing amplitudes. The maxima for $14 \leq E \leq 144$ are stage B superhumps. The times for $144 < E < 245$

Table 49. Superhump maxima of MASTER J004527 (2013) (continued)

E	max*	error	$O - C^\dagger$	N^\ddagger
102	56562.5520	0.0008	-0.0018	61
103	56562.6329	0.0008	-0.0010	65
104	56562.7149	0.0008	0.0009	52
105	56562.7932	0.0009	-0.0010	63
106	56562.8725	0.0006	-0.0018	70
107	56562.9534	0.0024	-0.0010	21
110	56563.1947	0.0005	0.0001	75
111	56563.2776	0.0007	0.0028	81
112	56563.3525	0.0006	-0.0024	149
113	56563.4326	0.0005	-0.0024	93
115	56563.5947	0.0014	-0.0005	64
116	56563.6779	0.0010	0.0026	124
117	56563.7569	0.0009	0.0014	87
118	56563.8335	0.0011	-0.0020	71
119	56563.9132	0.0017	-0.0024	66
122	56564.1491	0.0004	-0.0068	63
123	56564.2274	0.0014	-0.0087	84
124	56564.3206	0.0030	0.0045	17
134	56565.1115	0.0011	-0.0058	58
136	56565.2673	0.0041	-0.0101	27
137	56565.3555	0.0023	-0.0020	36
138	56565.4319	0.0022	-0.0058	35
140	56565.5990	0.0013	0.0012	71
141	56565.6772	0.0023	-0.0008	72
142	56565.7584	0.0027	0.0003	69
143	56565.8340	0.0053	-0.0042	73
144	56565.9085	0.0040	-0.0098	67

*BJD-2400000.

 † Against max = 2456554.3830 + 0.080106*E*. ‡ Number of points used to determine the maximum.

were not well determined because the amplitudes of superhumps became smaller and the profile was difficult to detect due to the orbital modulation. After $E = 245$, the amplitudes of superhumps grew again. These superhumps can be identified as stage C superhumps, which are not usually seen in WZ Sge-type dwarf novae (cf. Kato et al. 2009).

The period of early superhump by the PDM method was 0.056169(3) d (figure 55), which is 0.04% shorter than the orbital period. A summary of comparison of periods of early superhumps and orbital periods in various WZ Sge-type dwarf novae is given in subsection 4.4. The zero epoch in this figure is based on the ephemeris equation (4). Since the period of early superhumps and orbital period are very slightly different, we used the eclipse center nearest to the center of observation of early superhumps. The period used for phase-averaging is the period of early superhumps. The profile of these early superhumps and its implication is discussed in subsection 4.5.

The mean profile of stage B superhumps is shown in figure 56. Since the times of superhumps during the growing stage (stage A) were difficult to determine due to the orbital modulation, we also measured the period by the

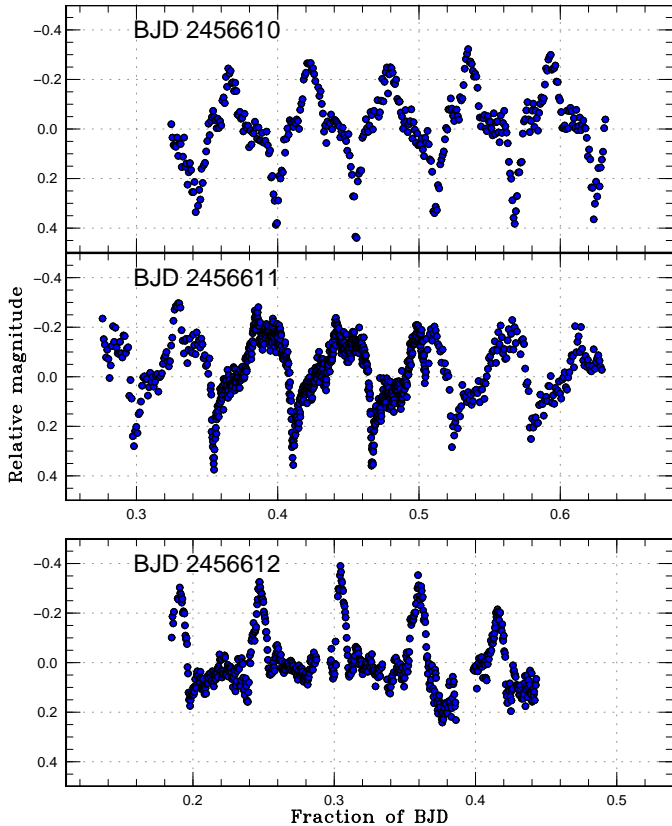


Fig. 54. Superhumps and eclipses in MASTER J005740 (2013). On the first night, eclipses were sharply detected. On the second night, eclipses became less apparent as the superhump maximum approaches the eclipses. On the third night, eclipses became inapparent.

PDM for the interval BJD 2456608–2456610. The resultant period was 0.05783(3) d. This value is slightly different from that of the $O-C$ analysis [0.05758(19) d, $E \leq 14$], which was likely more affected by the shorter period close to stage B. We therefore adopted the former period as the representative period of stage A. The resultant ε^* of 0.028(5) corresponds to $q=0.076(16)$.

A two-dimensional Lasso analysis is presented in figure 58. As in the eclipsing WZ Sge-type dwarf nova WZ Sge (Kato et al. 2014), the orbital signal was continuously seen. The superhump signal with decreasing frequencies (increasing periods) during the plateau phase of the superoutburst is also clearly visible.

3.45. MASTER OT J024847.86+501239.7

This object (hereafter MASTER J024847) was detected as a transient by the MASTER network on 2013 November 11 (Denisenko et al. 2013a). Subsequent observations immediately detected superhumps (vsnet-alert 16619; figure 59). A single-night observation yielded the following times of superhump maxima: BJD 2456609.3402(7) ($E = 62$), 2456609.4043(8) ($E = 62$), 2456609.4683(12) ($E = 65$). A PDM analysis yielded a period of 0.0644(3) d.

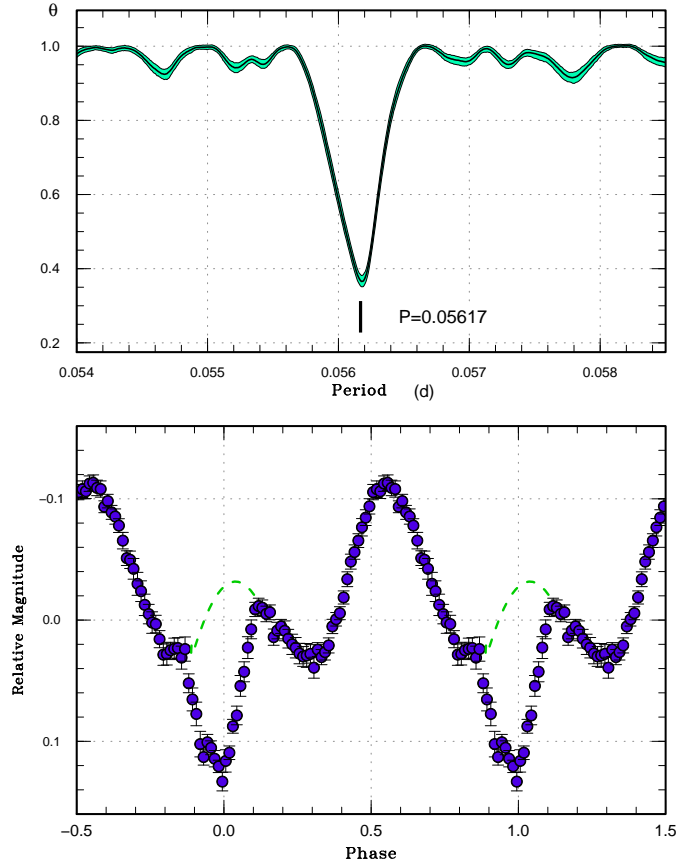


Fig. 55. Early superhumps in MASTER J005740 (2013). (Upper): PDM analysis. (Lower): Phase-averaged profile. The phase is relative to the eclipse ephemeris (see text for details). The dashed line represents a hypothetical hump maximum without an eclipse.

3.46. MASTER OT J061335.30+395714.7

This object (hereafter MASTER J061335) was detected as a bright (14.2 mag) transient by the MASTER network on 2013 October 15 (Vladimirov et al. 2013). After a period without strong modulations, growing superhumps were detected (vsnet-alert 16554, 16555, 16556, 16563, 16567; figure 60). The times of superhump maxima are listed in table 51. There are well-defined stages A-B-C (figure 61), although the period of stage A superhumps was not determined. Although early superhumps were potentially present during the first two nights, we could not detect the period due to the shortness of the observation. There was significant brightening around the stage B-C transition (figure 61).

3.47. MASTER OT J073208.11+064149.5

This object (hereafter MASTER J073208) was detected as a large-amplitude (~ 7 mag) transient by the MASTER network on 2013 December 29 (Balanutsa et al. 2013b). The object indeed showed short-period superhumps (vsnet-alert 16747, 16756). The times of superhump maxima are listed in table 52. Although a PDM

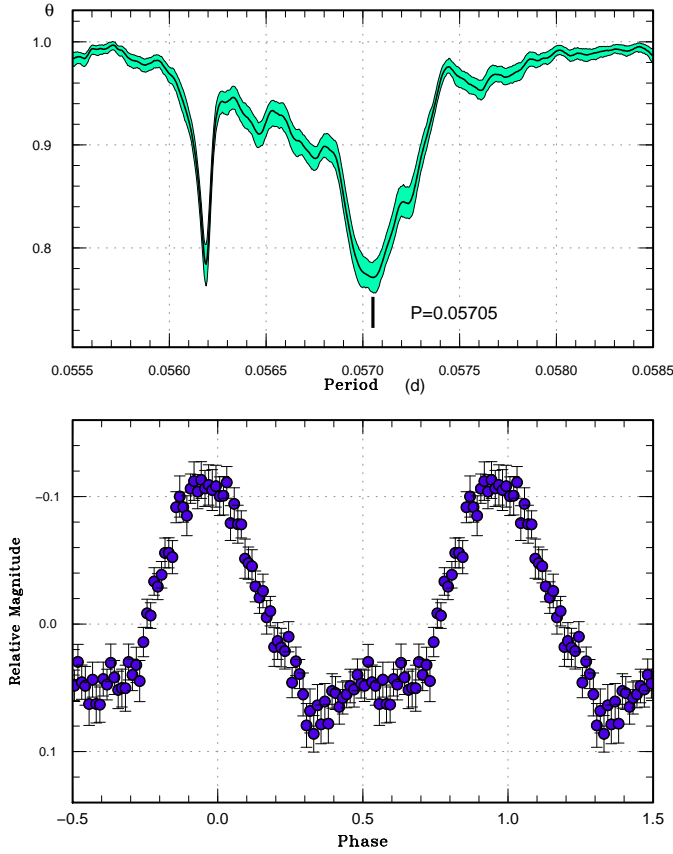


Fig. 56. Ordinary superhumps in MASTER J005740 (2013). The segment of stage B superhumps was used. (Upper): PDM analysis. (Lower): Phase-averaged profile. The sharp signal at 0.05619 d is the orbital period.

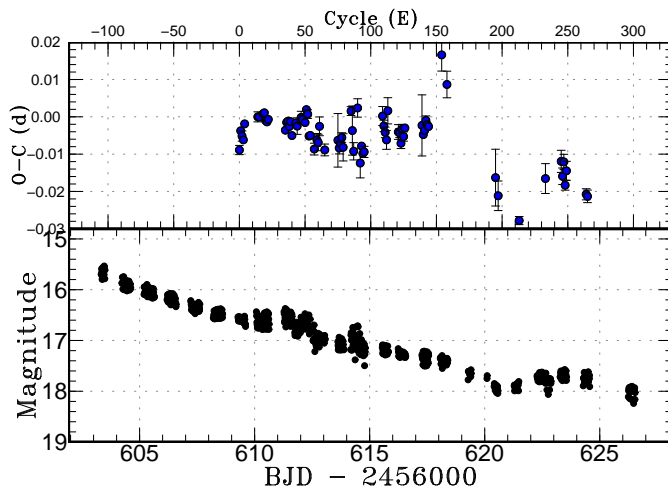


Fig. 57. $O-C$ diagram of superhumps in MASTER J005740 (2013). (Upper): $O-C$ diagram. A period of 0.05709 d was used to draw this figure. (Lower): Light curve. The observations were binned to 0.011 d.

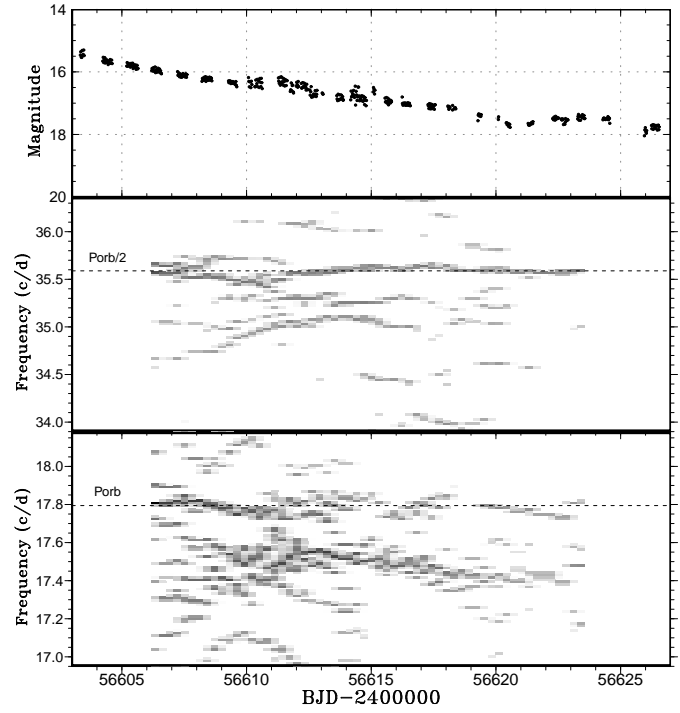


Fig. 58. Lasso analysis of MASTER J005740 (2013). (Upper): Light curve. The data were binned to 0.02 d. (Middle): First harmonics of the superhump and orbital signals. (Lower): Fundamental of the superhump and the orbital signal. The orbital signal was present both in the fundamental and the first harmonic. The signal of (positive) superhumps with variable frequency was recorded during the superoutburst plateau. No indication of negative superhump was present. $\log \lambda = -8.7$ was used. The width of the sliding window and the time step used are 6 d and 0.3 d, respectively.

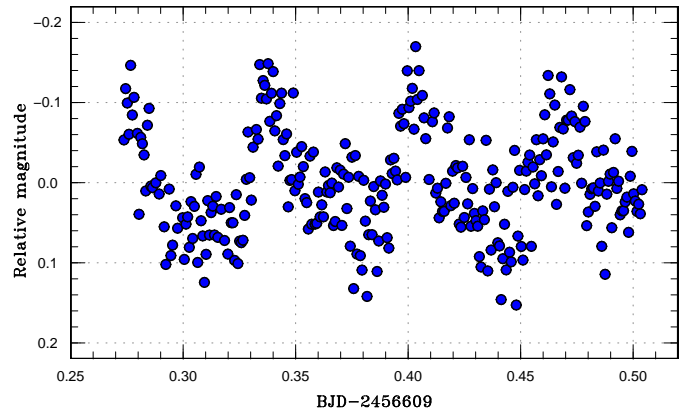


Fig. 59. Superhumps in MASTER J024847.

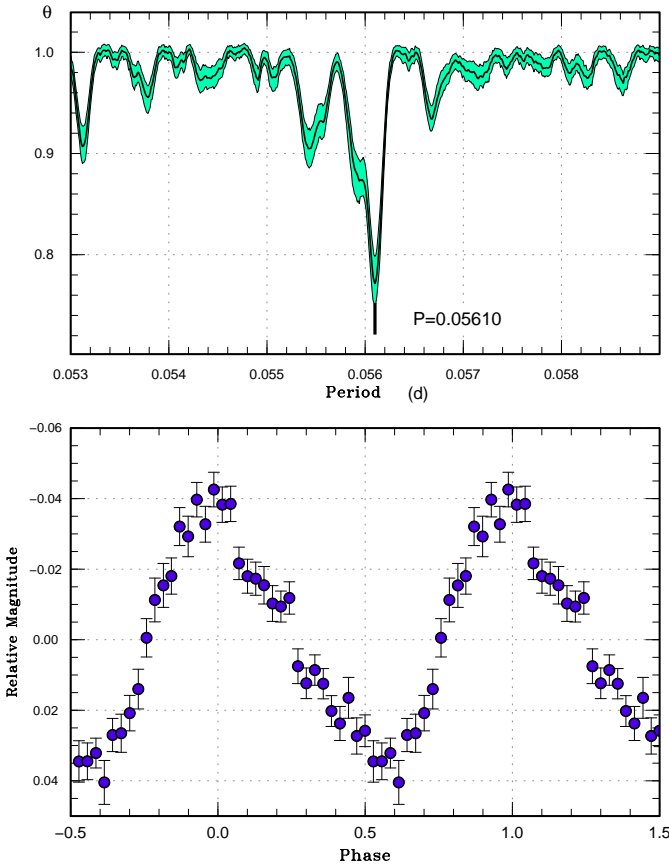


Fig. 60. Possible early superhumps in MASTER J061335 (2013). (Upper): PDM analysis. (Lower): Phase-averaged profile.

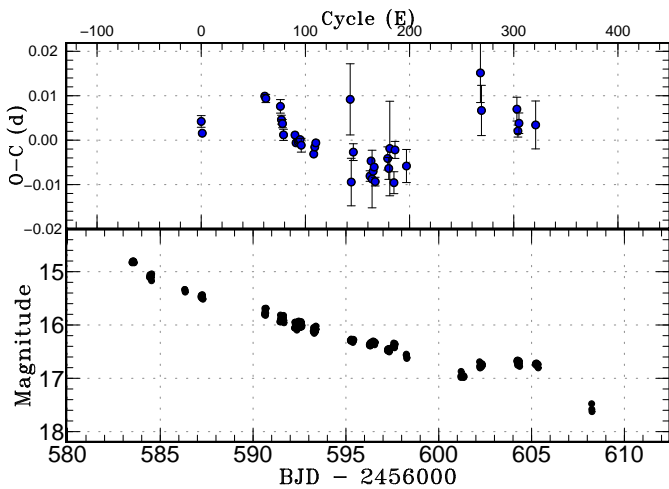


Fig. 61. $O - C$ diagram of superhumps in MASTER J061335 (2013). (Upper): $O - C$ diagram. A period of 0.056114 d was used to draw this figure. (Lower): Light curve. The observations were binned to 0.011 d.

Table 50. Superhump maxima of MASTER J005740 (2013)

E	max*	error	$O - C^\dagger$	phase ‡	N^\S
0	56609.3288	0.0012	-0.0089	70	
1	56609.3910	0.0008	-0.0036	71	
2	56609.4467	0.0014	-0.0050	64	
3	56609.5028	0.0008	-0.0060	54	
4	56609.5642	0.0008	-0.0016	46	
14	56610.1370	0.0013	0.0008	35	
15	56610.1940	0.0007	0.0008	35	
18	56610.3661	0.0005	0.0019	50	
19	56610.4235	0.0005	0.0022	50	
20	56610.4785	0.0005	0.0002	48	
21	56610.5352	0.0005	-0.0001	51	
22	56610.5930	0.0007	0.0006	53	
35	56611.3323	0.0007	-0.0016	51	
36	56611.3915	0.0003	0.0006	193	
37	56611.4489	0.0005	0.0009	198	
38	56611.5045	0.0005	-0.0005	139	
39	56611.5629	0.0008	0.0009	45	
40	56611.6163	0.0008	-0.0028	44	
43	56611.7909	0.0010	0.0008	37	
44	56611.8472	0.0022	0.0000	35	
47	56612.0208	0.0016	0.0025	31	
48	56612.0773	0.0013	0.0019	25	
50	56612.1907	0.0006	0.0013	46	
51	56612.2512	0.0005	0.0048	103	
52	56612.3071	0.0012	0.0037	75	
53	56612.3583	0.0006	-0.0022	95	
54	56612.4155	0.0005	-0.0020	86	
57	56612.5832	0.0016	-0.0055	30	
59	56612.6998	0.0017	-0.0029	28	
60	56612.7562	0.0022	-0.0035	30	
61	56612.8176	0.0025	0.0009	17	

*BJD-2400000.

† Against max = 2456609.3376 + 0.057035 E .

‡ Orbital phase.

§ Number of points used to determine the maximum.

analysis favors a period of 0.05878(2) d, a shorter alias of 0.05722(2) d is not excluded.

3.48. MASTER OT J095018.04-063921.9

This object (hereafter MASTER J095018) was detected as a 14.1-mag transient by the MASTER network on 2013 November 11 (Rufanov et al. 2013). Subsequent observations immediately detected superhumps (vsnet-alert 16631, 16659; figure 63). Although a period of 0.06681(3) d was initially reported, a re-analysis of the data clarified that this is the double value of the true variation (see also figure 63). A PDM analysis of the entire data yielded a period of 0.033409(4) d (figure 64). The profile, however, is unlike that of ordinary superhumps, but resembles that of early superhumps with double maxima (cf. Kato 2002). An $O - C$ analysis did not show significant period variation.

The period suggests a system with a compact, evolved

Table 50. Superhump maxima of MASTER J005740 (2013)
(continued)

E	max*	error	$O - C^\dagger$	phase ‡	N^\S
65	56613.0396	0.0016	-0.0053	28	
75	56613.6132	0.0072	-0.0021	29	
76	56613.6682	0.0016	-0.0041	50	
77	56613.7265	0.0009	-0.0028	50	
78	56613.7852	0.0013	-0.0012	50	
79	56613.8396	0.0036	-0.0038	50	
85	56614.1919	0.0012	0.0062	31	
86	56614.2438	0.0066	0.0011	25	
87	56614.2953	0.0023	-0.0044	24	
90	56614.4781	0.0025	0.0073	27	
92	56614.5781	0.0034	-0.0067	8	
93	56614.6390	0.0010	-0.0030	40	
94	56614.6940	0.0010	-0.0049	73	
95	56614.7516	0.0015	-0.0044	63	
101	56615.0939	0.0027	-0.0043	83	
109	56615.5609	0.0026	0.0064	27	
110	56615.6153	0.0015	0.0038	63	
111	56615.6708	0.0014	0.0022	65	
112	56615.7257	0.0025	0.0001	31	
113	56615.7905	0.0035	0.0079	26	
121	56616.2415	0.0020	0.0026	17	
122	56616.2984	0.0012	0.0024	69	
123	56616.3527	0.0014	-0.0002	85	
124	56616.4136	0.0012	0.0036	69	
125	56616.4687	0.0012	0.0016	37	
126	56616.5280	0.0010	0.0039	37	
139	56617.2709	0.0082	0.0054	19	
140	56617.3255	0.0009	0.0030	38	
141	56617.3837	0.0009	0.0041	47	
142	56617.4435	0.0012	0.0069	45	
143	56617.4995	0.0006	0.0058	47	

*BJD-2400000.

 † Against max = 2456609.3376 + 0.057035E. ‡ Orbital phase. § Number of points used to determine the maximum.

secondary like SBS 1108+574 (Kato et al. 2013a; Littlefield et al. 2013; Carter et al. 2013). If the present variation is indeed early superhumps, the present observation becomes the first to detect early superhumps in such systems. We leave this possibility for future observations since we could not follow the later stage, when ordinary superhumps were expected. On the last two nights (November 24 and 25), the double-wave modulation became less apparent and waves with a period of ~ 0.08 d seemed to appear. We were not, however, confident in the presence of this periodicity due to the limited signal-to-ratio for this faint object.

3.49. MASTER OT J141143.46+262051.5

This object (hereafter MASTER J141143) was detected as a transient (15.4 mag) by the MASTER network on 2013 February 13 (Shumkov et al. 2013). The object was again detected in outburst on 2014 January 30.

Table 50. Superhump maxima of MASTER J005740 (2013)
(continued)

E	max*	error	$O - C^\dagger$	phase ‡	N^\S
144	56617.5561	0.0010	0.0053	33	
154	56618.1461	0.0043	0.0251	23	
158	56618.3666	0.0036	0.0174	24	
195	56620.4539	0.0076	-0.0056	45	
197	56620.5633	0.0040	-0.0103	34	
213	56621.4701	0.0011	-0.0161	23	
233	56622.6231	0.0040	-0.0038	26	
245	56623.3129	0.0029	0.0016	45	
246	56623.3660	0.0022	-0.0023	53	
247	56623.4269	0.0020	0.0016	84	
248	56623.4778	0.0013	-0.0046	65	
249	56623.5386	0.0025	-0.0008	46	
264	56624.3887	0.0015	-0.0063	46	
265	56624.4452	0.0017	-0.0068	45	

*BJD-2400000.

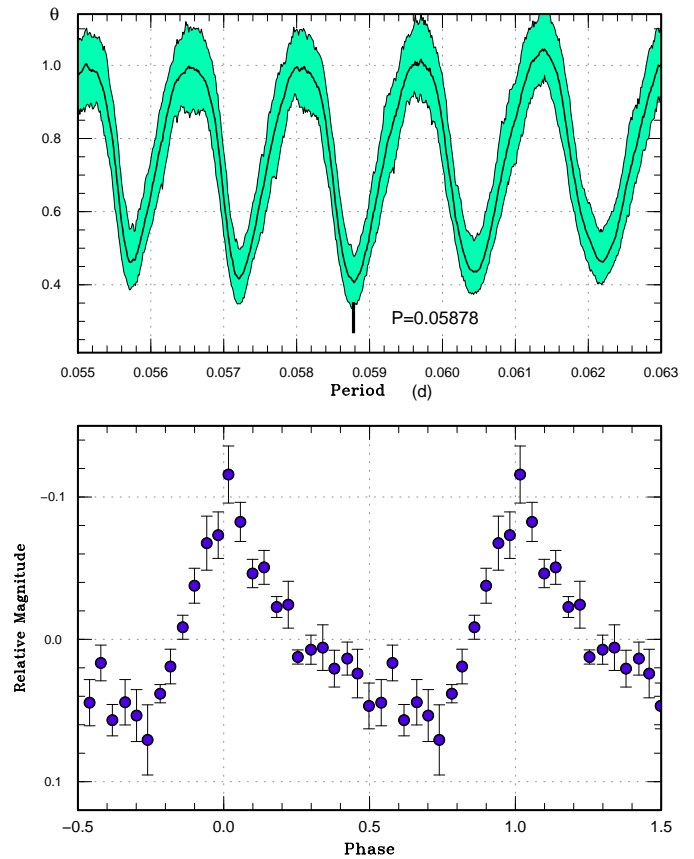
 † Against max = 2456609.3377 + 0.057035E. ‡ Orbital phase. § Number of points used to determine the maximum.**Fig. 62.** (Early?) superhumps in MASTER J073208 (2013).
(Upper): PDM analysis. (Lower): Phase-averaged profile.

Table 51. Superhump maxima of MASTER J061335 (2013)

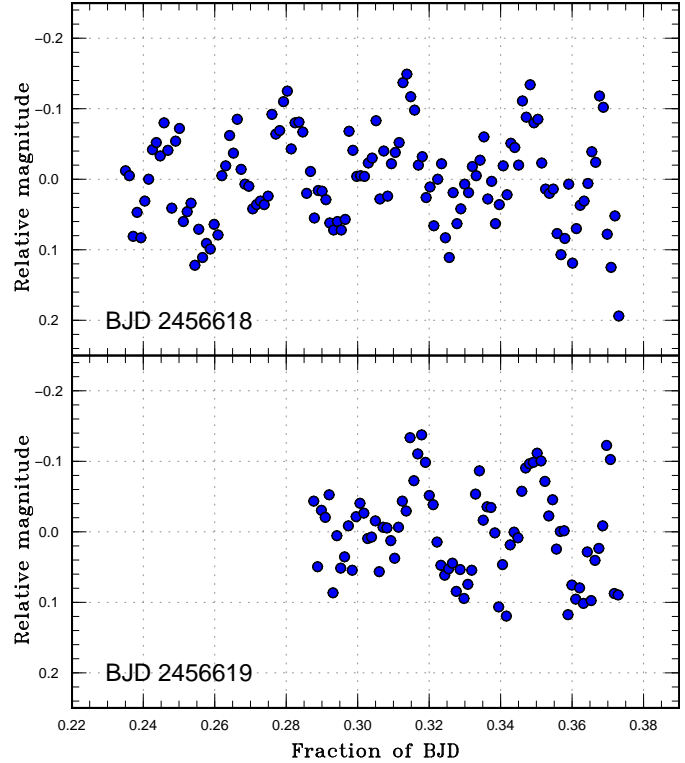
E	max*	error	$O - C^\dagger$	N^\ddagger
0	56587.2100	0.0013	0.0042	119
1	56587.2635	0.0007	0.0016	167
61	56590.6387	0.0007	0.0099	56
62	56590.6942	0.0009	0.0094	37
76	56591.4781	0.0015	0.0076	32
77	56591.5312	0.0010	0.0047	31
78	56591.5864	0.0009	0.0038	30
79	56591.6400	0.0013	0.0012	21
90	56592.2572	0.0008	0.0012	41
91	56592.3116	0.0008	-0.0006	41
93	56592.4240	0.0007	-0.0004	35
94	56592.4804	0.0007	-0.0001	90
95	56592.5368	0.0007	0.0002	74
96	56592.5916	0.0015	-0.0011	30
108	56593.2630	0.0009	-0.0031	46
109	56593.3207	0.0006	-0.0015	101
110	56593.3777	0.0004	-0.0006	51
143	56595.2393	0.0080	0.0093	36
144	56595.2768	0.0053	-0.0094	33
146	56595.3958	0.0019	-0.0026	31
162	56596.2882	0.0012	-0.0080	58
163	56596.3477	0.0008	-0.0046	95
164	56596.3997	0.0065	-0.0087	27
165	56596.4576	0.0006	-0.0069	67
166	56596.5147	0.0005	-0.0060	77
167	56596.5675	0.0010	-0.0092	39
179	56597.2461	0.0026	-0.0040	35
180	56597.3000	0.0025	-0.0063	41
181	56597.3606	0.0106	-0.0018	20
185	56597.5773	0.0025	-0.0095	23
186	56597.6408	0.0019	-0.0021	19
197	56598.2544	0.0037	-0.0057	50
268	56602.2595	0.0067	0.0153	41
269	56602.3072	0.0057	0.0068	40
303	56604.2153	0.0027	0.0071	36
304	56604.2665	0.0014	0.0022	41
305	56604.3244	0.0023	0.0040	41
321	56605.2218	0.0054	0.0036	44

*BJD-2400000.

 † Against max = 2456587.2058 + 0.056114*E*. ‡ Number of points used to determine the maximum.**Table 52.** Superhump maxima of MASTER J073208 (2013)

E	max*	error	$O - C^\dagger$	N^\ddagger
0	56658.3918	0.0018	-0.0028	15
1	56658.4553	0.0006	0.0018	40
2	56658.5134	0.0007	0.0010	23
37	56660.5747	0.0007	0.0031	20
38	56660.6273	0.0011	-0.0031	42

*BJD-2400000.

 † Against max = 2456658.3947 + 0.058836*E*. ‡ Number of points used to determine the maximum.**Fig. 63.** Example of (early?) superhumps in MASTER J095018 on two nights.

The outburst was caught in the early stage (vsnet-alert 16852). The only available observation on February 5 showed superhumps with amplitudes of 0.15 mag (vsnet-alert 16881). The period was determined by the PDM method to be 0.064(1) d. The times of superhump maxima were BJD 2456693.5806(9) ($N = 35$) and 2456693.6466(9) ($N = 33$).

3.50. MASTER OT J162323.48+782603.3

This object (hereafter MASTER J162323) was detected as a bright (13.0-mag) transient by the MASTER network on 2013 December 9 (Denisenko et al. 2013b). There were a number of past ROSAT chance observations, recording a relatively soft source with variable intensity (vsnet-alert 16698). Subsequent observations immediately detected modulation (vsnet-alert 16703) which were followed by growing superhumps (vsnet-alert 16706, 16716, 16717, 16723; figure 66). The times of superhump maxima are listed in table 53. They were clear stages A and B. There was no variation of the superhump period around the rapid fading. There was an apparent decrease in the period 5 d after the fading (around $E = 200$). We interpret the superhumps up to $E = 192$ to be stage B superhumps and listed the period in table 2. The resultant P_{dot} of $+3.9(9) \times 10^{-5}$ for stage B again makes another example of a positive P_{dot} in a long- P_{orb} system [such examples include GX Cas (Kato et al. 2012a), V1239 Her, OT J145921.8+354806, OT J214738.4+244553 (Kato et al.

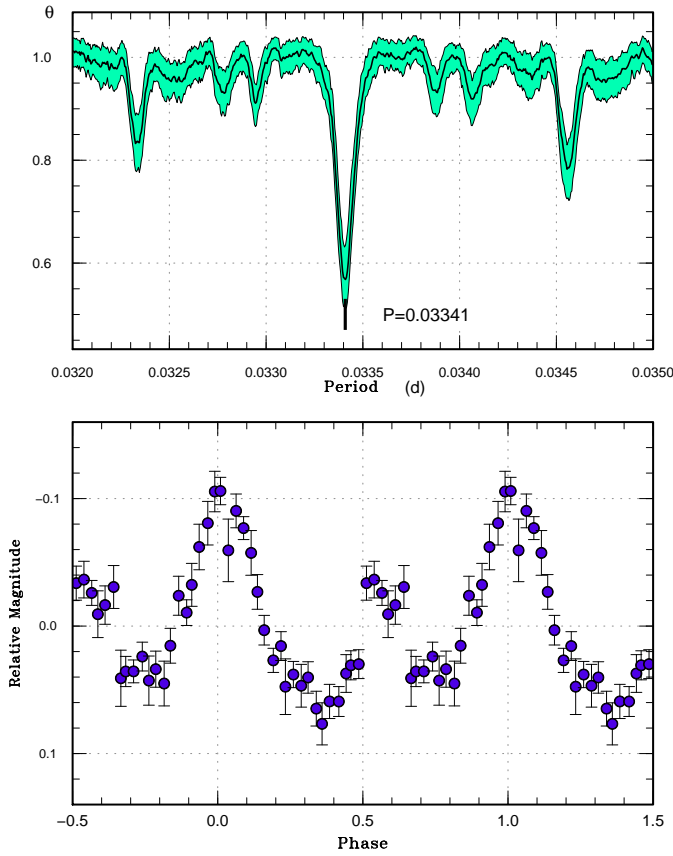


Fig. 64. (Early?) superhumps in MASTER J095018 (2013). (Upper): PDM analysis. (Lower): Phase-averaged profile.

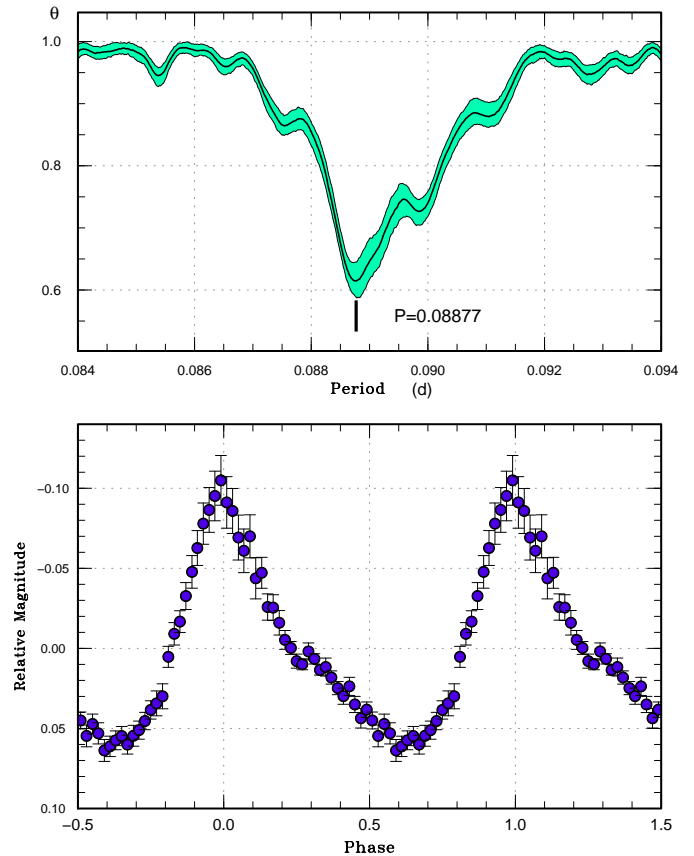


Fig. 66. Superhumps in MASTER J162323 during the superoutburst plateau (2013). (Upper): PDM analysis. (Lower): Phase-averaged profile.

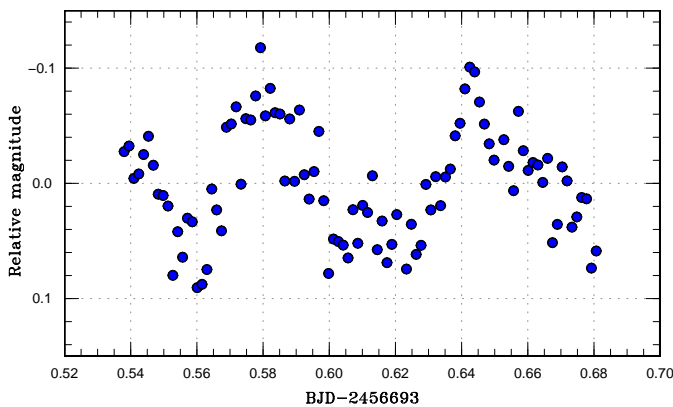


Fig. 65. Superhumps in MASTER J141143 on 2014 February 5.

2013a), V444 Peg, CSS J203937.7–042907, MASTER OT J212624.16+253827.2 (Kato et al. 2014)].

The quiescent SDSS colors suggest an orbital period of 0.072 d based on Kato et al. (2012b). This relatively long orbital period for an SU UMA-type dwarf nova is in agreement with the present observation. The object was twice detected in outburst in 2012 by MASTER data (Denisenko et al. 2013b). The supercycle appears to be less than 1 yr. Being bright and frequently outbursting, future observations including the determination of the orbital period, will be promising.

3.51. MASTER OT J234843.23+250250.4

This object (hereafter MASTER J234843) was detected as a 14.4-mag transient by the MASTER network on 2013 October 29 (Shurpakov et al. 2013). The object has a faint, blue ($g = 20.2$, $g - r = -0.1$) SDSS counterpart. Five previous outbursts were recorded by CRTS.

Subsequent observations detected modulations resembling early superhumps (vsnet-alert 16577, 16578). Later observation, however, indicated that the period was the half of what was initially suggested (figure 67), and the object was recognized as a CV below the period minimum (vsnet-alert 16608; the superhump profile is shown in figure 68). The times of superhump maxima based on this in-

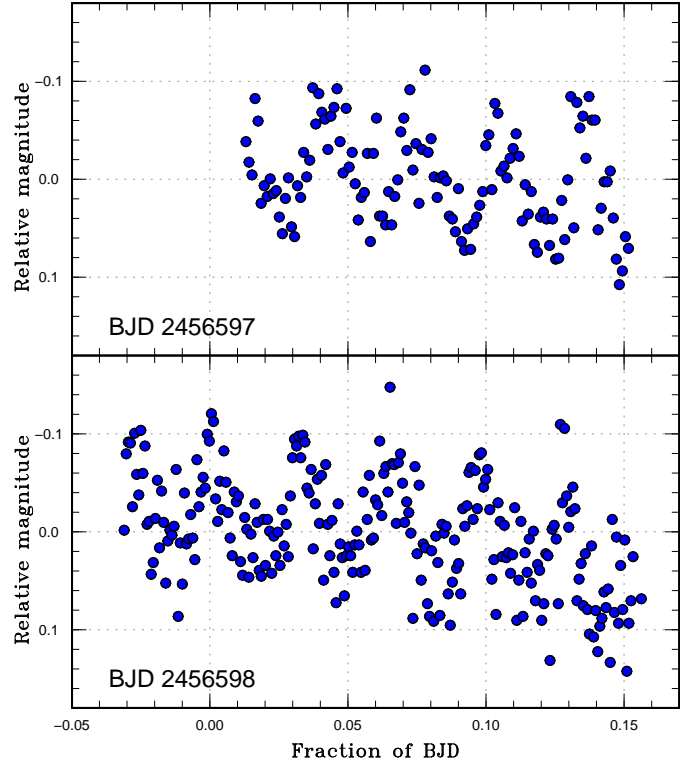
Table 53. Superhump maxima of MASTER J162323 (2013)

E	max*	error	$O - C^\dagger$	N^\ddagger
0	56637.5690	0.0011	-0.0542	94
1	56637.6655	0.0020	-0.0464	86
2	56637.7684	0.0012	-0.0323	46
19	56639.3104	0.0006	0.0021	40
20	56639.3987	0.0002	0.0017	177
21	56639.4874	0.0003	0.0017	157
22	56639.5749	0.0008	0.0005	12
23	56639.6642	0.0007	0.0011	12
30	56640.2879	0.0010	0.0040	17
31	56640.3795	0.0002	0.0069	159
32	56640.4681	0.0003	0.0068	165
33	56640.5578	0.0003	0.0078	112
35	56640.7456	0.0014	0.0182	9
42	56641.3661	0.0028	0.0179	24
44	56641.5352	0.0003	0.0096	66
45	56641.6238	0.0008	0.0095	25
46	56641.7088	0.0009	0.0059	12
56	56642.6015	0.0007	0.0116	56
57	56642.6897	0.0015	0.0112	16
67	56643.5716	0.0012	0.0062	10
68	56643.6643	0.0019	0.0102	15
79	56644.6320	0.0031	0.0023	15
98	56646.3168	0.0005	0.0020	73
99	56646.4037	0.0005	0.0003	112
101	56646.5840	0.0018	0.0032	12
102	56646.6708	0.0010	0.0012	15
135	56649.5986	0.0057	0.0024	16
136	56649.6894	0.0021	0.0044	16
143	56650.3106	0.0012	0.0048	44
153	56651.2012	0.0055	0.0086	28
154	56651.2825	0.0012	0.0012	50
155	56651.3732	0.0011	0.0031	50
156	56651.4641	0.0063	0.0053	13
180	56653.5948	0.0027	0.0075	13
181	56653.6807	0.0100	0.0047	13
187	56654.2236	0.0044	0.0155	18
188	56654.3132	0.0028	0.0164	13
192	56654.6519	0.0030	0.0004	21
223	56657.3771	0.0015	-0.0238	30
224	56657.4603	0.0018	-0.0293	28
244	56659.2330	0.0013	-0.0304	14

*BJD-2400000.

†Against max = 2456637.6232 + 0.088689*E*.

‡Number of points used to determine the maximum.

**Fig. 67.** Example of superhumps in MASTER J234843 on two nights.

terpretation are listed in table 54. Although the data were not sufficient, the $O - C$ values suggest that there was a stage B-C transition around $E = 252$ as in SBS 1108+574, a similar ultrashort- P_{orb} dwarf nova (Kato et al. 2013a). The outburst light curve and $O - C$ diagram are presented in figure 69.

Although spectroscopic observation is needed to see whether this object is hydrogen-rich or not, we suspect that this object is a binary containing hydrogen in the secondary with an evolved core rather than a hydrogen-depleted AM CVn-type binary, since the known AM CVn-type objects with this P_{orb} do not show outbursts (cf. Solheim 2010; Ramsay et al. 2012). Further detailed observations will clarify the nature of this object.

3.52. OT J013741.1+220312

This object was detected as a transient of unknown type by CRTS (=CSS140104:013741+220312, hereafter OT J013741) on 2014 January 4. There was no previous outburst detection in CRTS. Subsequent observations detected double-wave early superhumps with a mean period of 0.05854(2) d (vsnet-alert 16765, 16769; figure 70). Only the stage of early superhumps was observed.

3.53. OT J210016.0-024258

This object was detected as a transient by CRTS (=CSS130905:210016-024258, hereafter OT J210016) on 2013 September 5. The quiescent counterpart has an

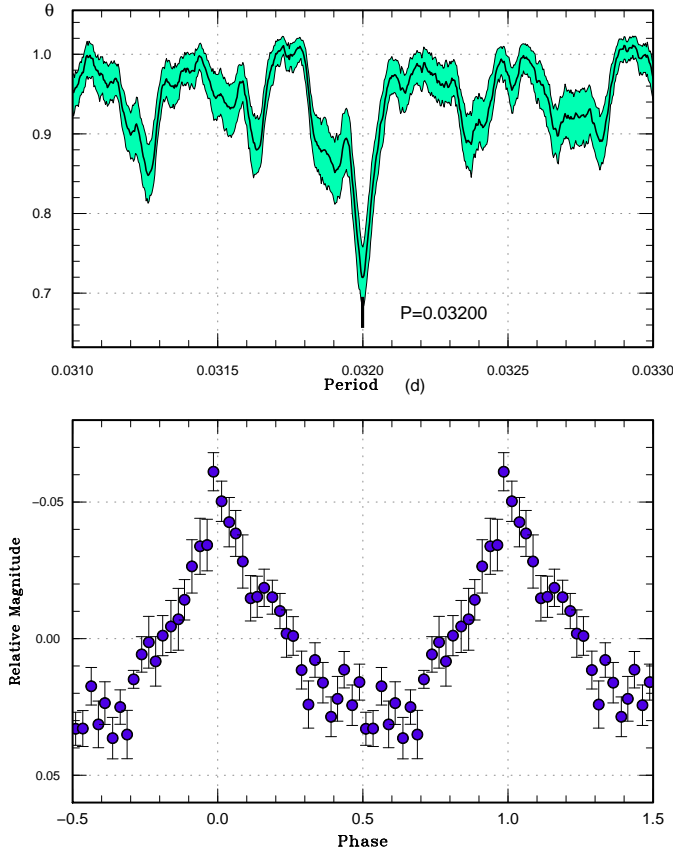


Fig. 68. Superhumps in MASTER J234843 during the superoutburst plateau (2013). (Upper): PDM analysis. (Lower): Phase-averaged profile.

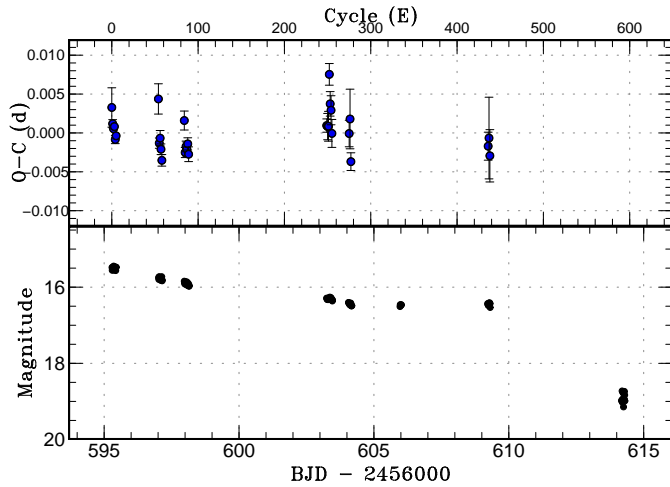


Fig. 69. $O - C$ diagram of superhumps in MASTER J234843 (2013). (Upper): $O - C$ diagram. A period of 0.031997 d was used to draw this figure. (Lower): Light curve. The observations were binned to 0.010 d.

Table 54. Superhump maxima of MASTER J234843 (2013)

E	max*	error	$O - C^\dagger$	N^\ddagger
0	56595.2868	0.0025	0.0032	13
1	56595.3167	0.0005	0.0011	33
2	56595.3480	0.0004	0.0005	26
3	56595.3803	0.0004	0.0008	34
4	56595.4106	0.0005	-0.0009	29
5	56595.4431	0.0005	-0.0004	26
54	56597.0157	0.0019	0.0043	15
55	56597.0420	0.0007	-0.0014	23
56	56597.0747	0.0010	-0.0007	23
57	56597.1052	0.0007	-0.0021	23
58	56597.1358	0.0007	-0.0036	23
84	56597.9728	0.0012	0.0015	22
85	56598.0007	0.0006	-0.0026	34
86	56598.0335	0.0007	-0.0018	34
87	56598.0651	0.0009	-0.0021	34
88	56598.0978	0.0008	-0.0015	35
89	56598.1285	0.0009	-0.0028	34
249	56603.2517	0.0009	0.0009	22
250	56603.2836	0.0017	0.0007	28
251	56603.3156	0.0019	0.0008	28
252	56603.3543	0.0014	0.0075	19
253	56603.3825	0.0016	0.0037	26
254	56603.4137	0.0019	0.0028	28
255	56603.4427	0.0018	-0.0001	28
275	56604.0826	0.0017	-0.0002	23
276	56604.1165	0.0038	0.0017	22
277	56604.1430	0.0011	-0.0038	24
436	56609.2325	0.0018	-0.0018	15
437	56609.2655	0.0053	-0.0008	17
438	56609.2952	0.0034	-0.0030	16

*BJD-2400000.

\dagger Against max = 2456595.2835 + 0.031997 E .

\ddagger Number of points used to determine the maximum.

SDSS magnitude of $g = 19.9$, implying a dwarf nova with a large outburst amplitude (vsnet-alert 16347).

Low amplitude modulations resembling early superhumps were recorded until September 12 (vsnet-alert 16362; figure 71). Starting from September 16, ordinary superhumps appeared (vsnet-alert 16420, 16430; figure 72). The times of ordinary superhumps are listed in table 55. Although the earliest epochs may contain stage A superhumps, we could not convincingly detect stage A. Since $E = 0$ and $E = 1$ were likely obtained during the growing stage of superhumps, we excluded these epochs when determining P_{dot} of stage B superhumps.

The object rapidly faded from the superoutburst plateau on September 29. It showed a post-superoutburst rebrightening on October 6 (around 17.4 mag, all magnitudes during this rebrightening were unfiltered CCD magnitudes; vsnet-alert 16525). The snapshot CCD observations indicate that this object was already bright bright on October 1 (16.86 mag) and October 4 (17.55 mag). These observations indicate that the faint state follow-

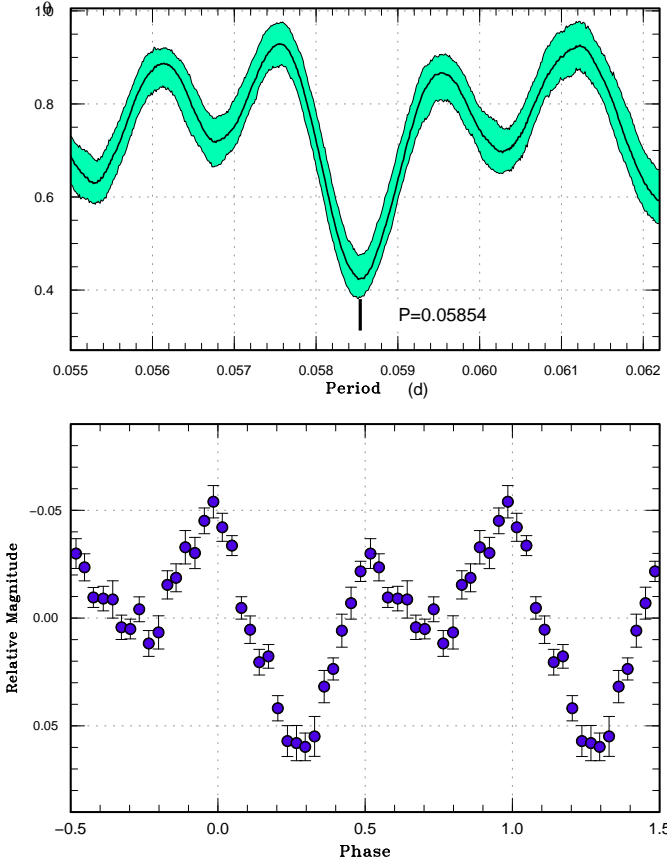


Fig. 70. Early superhumps in OT J013741 (2013). (Upper): PDM analysis. (Lower): Phase-averaged profile.

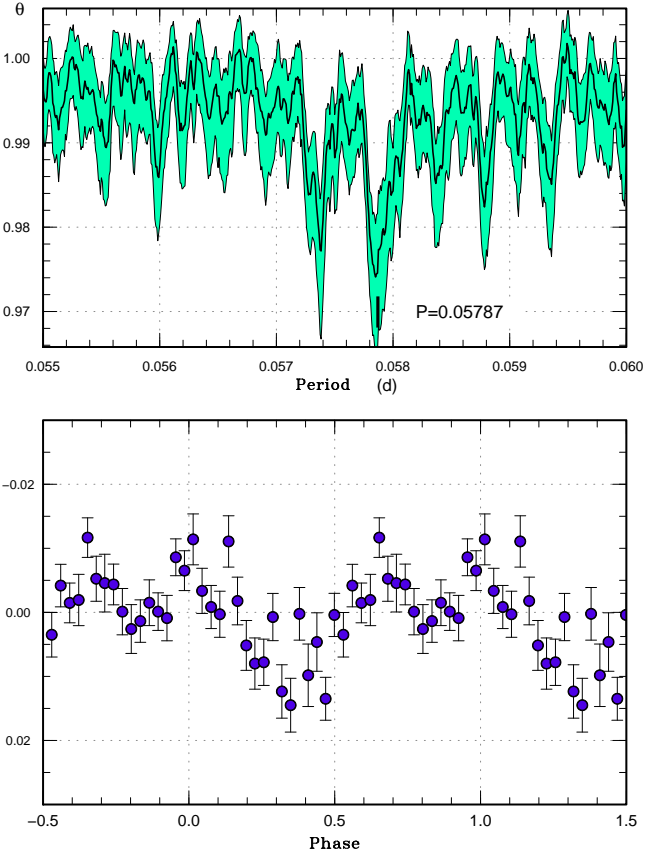


Fig. 71. Possible early superhumps in OT J210016 (2013). (Upper): PDM analysis. The rejection rate for bootstrapping was reduced to 0.3. (Lower): Phase-averaged profile.

ing the superoutburst plateau lasted less than 2 d. This fading was probably a “dip”-type between the main superoutburst and long rebrightening as in the WZ Sge-type dwarf nova AL Com (1995, cf. Nogami et al. 1997). The WZ Sge-type nature is supported by the likely presence of early superhumps, the large outburst amplitude and the lack of past outburst detections in the CRTS data.

3.54. PNV J19150199+0719471

This object (hereafter PNV J191501) was detected as a possible nova of 10.8 mag on 2013 May 31.5974 UT (Itagaki et al. 2013).⁶ The object was detected at 9.8 mag on May 30.721 UT by T. Kojima. The object was identified as an H α emission object IPHAS J191502.09+071947.6 ($r=18.503$, Drew et al. 2005), and the color and large proper motion suggested a dwarf nova rather than a classical nova (vsnet-alert 15768). The object was then regarded as a good candidate for a WZ Sge-type dwarf nova (vsnet-alert 15776). Although subsequent observations detected small variations suggestive of early superhumps (vsnet-alert 15778, 15785, 15788), the period was difficult to determine due to the low amplitude. We will deal with this issue later.

⁶ See also <<http://www.cbat.eps.harvard.edu/unconf/followups/J19150199+0719471.html>>.

Table 55. Superhump maxima of OT J210016 (2013)

E	max*	error	$O - C^\dagger$	N^\ddagger
0	56552.0076	0.0014	-0.0070	40
1	56552.0764	0.0018	0.0033	61
17	56553.0093	0.0007	-0.0001	60
18	56553.0705	0.0006	0.0027	61
34	56554.0039	0.0014	-0.0002	47
35	56554.0678	0.0014	0.0052	47
57	56555.3469	0.0013	-0.0030	47
58	56555.4057	0.0010	-0.0027	46
59	56555.4675	0.0015	0.0006	47
60	56555.5296	0.0030	0.0042	17
108	56558.3312	0.0109	-0.0030	17
109	56558.3908	0.0008	-0.0019	44
110	56558.4503	0.0010	-0.0008	45
160	56561.3796	0.0012	0.0027	31

*BJD-2400000.

[†]Against max = 2456552.0146 + 0.058514E.

[‡]Number of points used to determine the maximum.

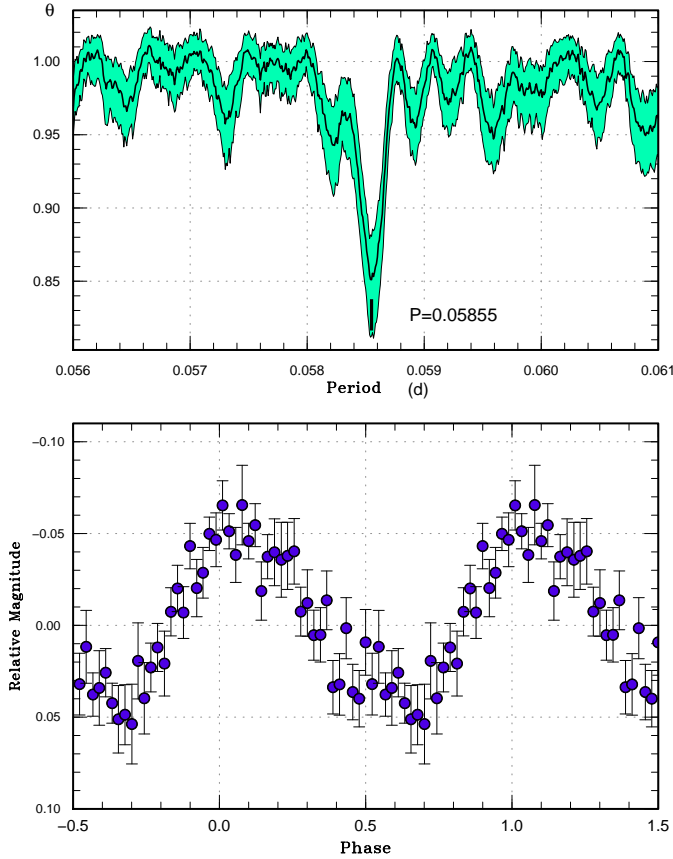


Fig. 72. Ordinary superhumps in OT J210016 (2013). (Upper): PDM analysis. (Lower): Phase-averaged profile.

In the meantime, low-resolution spectra confirmed the dwarf nova-type classification (vsnet-alert 15779). The spectrum showed double-peak $H\beta$ emission line and a $CIII/NIII$ emission line, suggesting that this object is a WZ Sge-type dwarf nova with a moderate inclination (vsnet-alert 15782). Further spectroscopic observation were also reported (vsnet-alert 15787, 15800). The latter spectrum showed Balmer series in absorption with emission cores in $H\alpha$ and $H\beta$. Nakata et al. (2013a) also reported a UV spectrum taken by Swift satellite.

Six days after the discovery, modulations suggesting growing superhumps appeared (vsnet-alert 15815; the actual variations could be detected two days earlier). The times of superhump maxima during the superoutburst plateau are listed in table 56. The profile is shown in figure 73. There were remarkably well-sampled stage B and C. The existence of stage C in a WZ Sge-type dwarf nova is rather exceptional. Although stage A was detected, the lack of observation for 1 d due to the bad weather prevented us from measuring the period of stage A superhumps from the $O-C$ analysis. A PDM analysis for an interval of BJD 2456449–2456452 yielded a period of 0.05883(6) d with an amplitude of 0.015 mag.

After rapid fading from the superoutburst, the superhump signal became strong again. The times of these

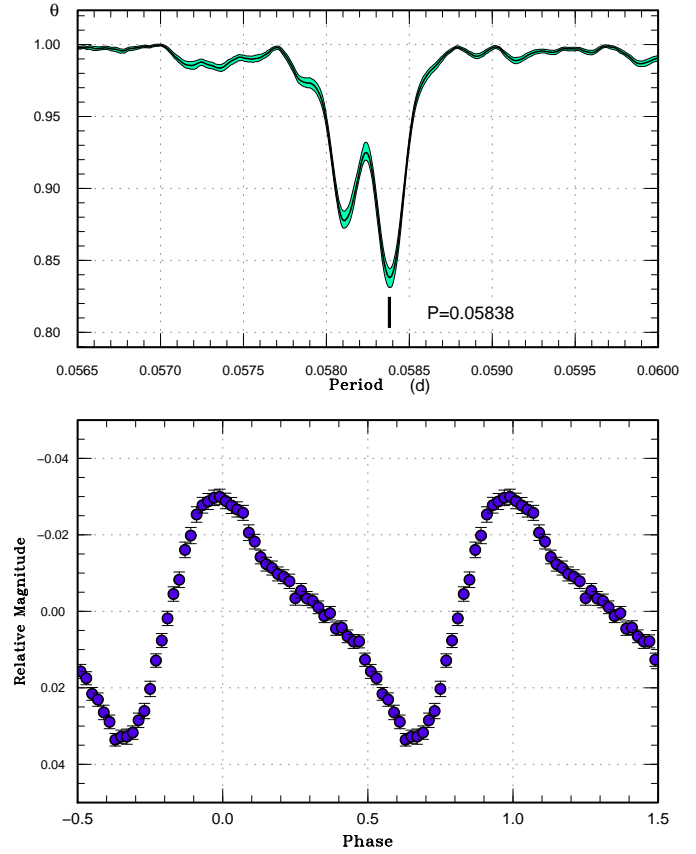


Fig. 73. Ordinary superhumps in PNV J191501 (2013). (Upper): PDM analysis. (Lower): Phase-averaged profile.

post-superoutburst superhumps are listed in table 57. The data indicate that there was a phase ~ 0.5 jump between BJD 2456472.295 and BJD 2456472.688. The combined $O-C$ diagram (figure 74) indicate, however, the superhumps in the post-superoutburst stage are on a smooth extension of stage C superhumps. The signal of reversed phases (likely corresponding to “traditional” late superhumps) appeared only briefly near the rapid fading.

The signal of early superhumps was very weak and the period of 0.05706(2) d is the only candidate period in the region of the period of early superhumps expected from the superhump period (figure 75). Although the fractional excess of stage A superhumps based on the $O-C$ analysis corresponds to $q=0.095(4)$, this measurement suffers from uncertainties arising from the low amplitudes of both early superhumps and stage A superhumps. Future determination of the orbital period will be necessary to confirm this value.

A two dimensional Lasso analysis is presented in figure 76. The superhumps with increasing frequencies (decreasing periods) after the superoutburst are clearly seen. The overall behavior resembles that of an SU UMa-type dwarf nova rather than an extreme WZ Sge-type dwarf nova (cf. WZ Sge in Kato et al. 2014) except for the possible presence of early superhumps.

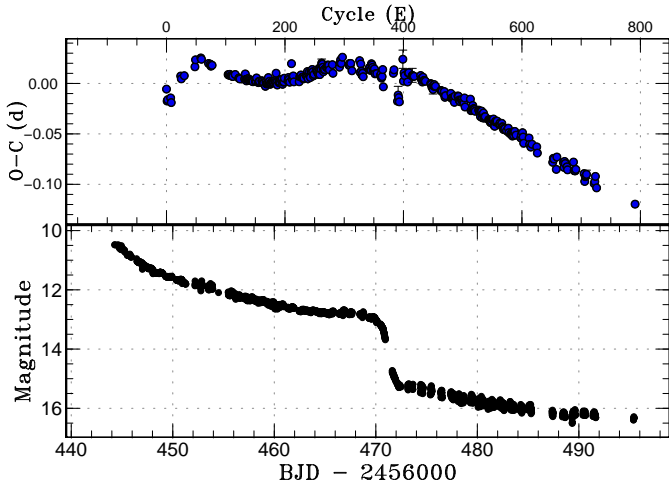


Fig. 74. $O - C$ diagram of superhumps in PNV J191501 (2013). (Upper): $O - C$ diagram. A period of 0.05835 d was used to draw this figure. (Lower): Light curve. The observations were binned to 0.010 d.

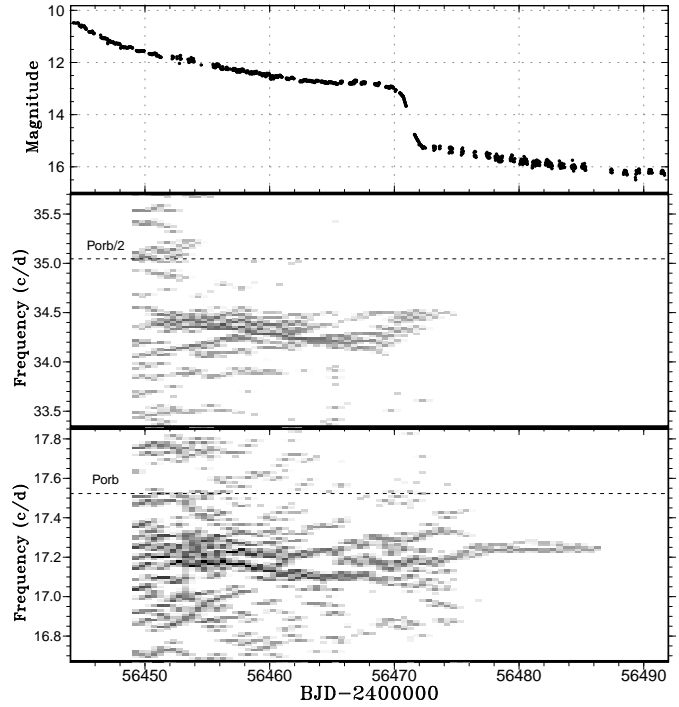


Fig. 76. Lasso analysis of PNV J191501 (2013). (Upper:) Light curve. The data were binned to 0.02 d. (Middle:) First harmonics of the superhump and possible orbital signals. (Lower:) Fundamental of the superhump and the possible orbital signal. The orbital signal was present only in the initial part of the outburst. The signal of (positive) superhumps with variable frequency was recorded during the superoutburst plateau and post-superoutburst stage. No indication of negative superhump was present. $\log \lambda = -8.0$ was used. The width of the sliding window and the time step used are 10 d and 0.5 d, respectively.

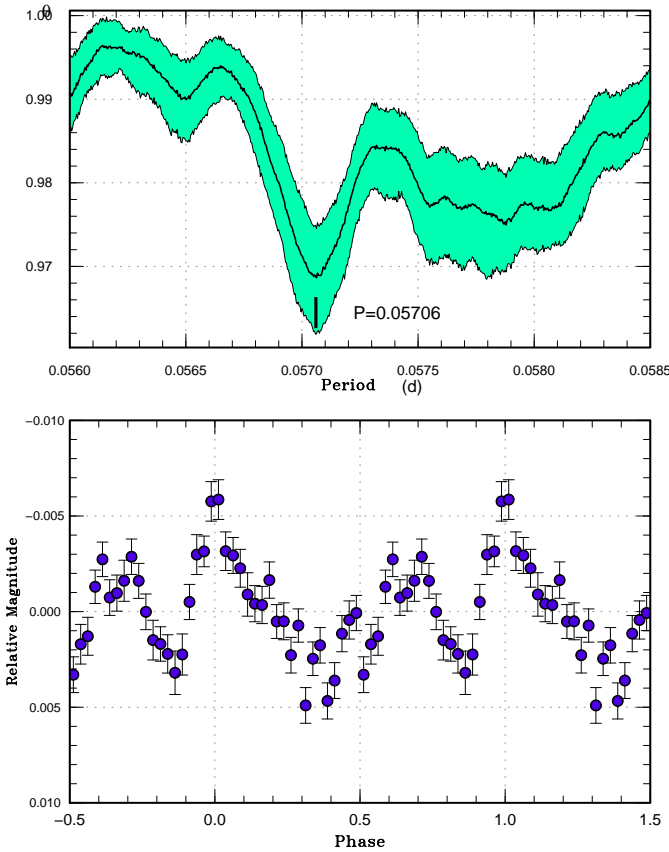


Fig. 75. Possible early superhumps in PNV J191501 (2013). (Upper): PDM analysis. (Lower): Phase-averaged profile.

3.55. SSS J094327.3–272038

This object (=SSS111226:094327–272039, hereafter SSS J094327) was discovered as a transient object by CRTS Siding Spring Survey (SSS) on 2011 December 26 at an unfiltered CCD magnitude of 16.6. The object, however, showed several outbursts reaching $V = 12.8$ in ASAS-3 data (vsnet-alert 14013). There is also an X-ray counterpart 1RXS J094326.1–272035. The past outburst behavior suggested an SU UMa-type dwarf nova. The 2011 December outburst brightened to 14.7 mag (unfiltered CCD) and was observed for one night which possibly showed superhumps (vsnet-alert 14034).

The 2014 outburst was visually detected by A. Pearce on January 29. The bright magnitude (13.1 mag) immediately suggested a superoutburst (vsnet-alert 16842). Subsequent observations indeed detected superhumps (vsnet-alert 16853, 16859, 16867; figure 77). The times of superhump maxima are listed in table 59. The epochs for $E \leq 2$ were likely stage A superhumps. There were likely stages B and C. Despite that the object experienced a rapid fading from the superoutburst, no phase jump (corresponding to “traditional” late superhumps) was ob-

Table 56. Superhump maxima of PNV J191501 (2013)

E	max*	error	$O - C^\dagger$	N^\ddagger
0	56449.3764	0.0010	-0.0056	221
1	56449.4229	0.0025	-0.0175	222
2	56449.4826	0.0010	-0.0162	211
7	56449.7761	0.0018	-0.0146	64
8	56449.8298	0.0012	-0.0193	313
24	56450.7898	0.0009	0.0064	124
25	56450.8453	0.0019	0.0035	154
30	56451.1402	0.0006	0.0065	784
48	56452.1993	0.0005	0.0146	98
49	56452.2646	0.0009	0.0215	126
58	56452.7916	0.0005	0.0230	32
59	56452.8486	0.0002	0.0217	51
71	56453.5446	0.0002	0.0170	63
74	56453.7190	0.0003	0.0162	38
75	56453.7754	0.0003	0.0142	53
76	56453.8347	0.0003	0.0151	89
77	56453.8929	0.0002	0.0150	99
104	56455.4592	0.0014	0.0048	45
105	56455.5171	0.0002	0.0042	92
106	56455.5754	0.0002	0.0042	92
107	56455.6345	0.0003	0.0049	108
109	56455.7499	0.0002	0.0035	97
110	56455.8079	0.0002	0.0031	114
111	56455.8665	0.0001	0.0033	113
112	56455.9241	0.0002	0.0025	113
116	56456.1595	0.0003	0.0044	651
122	56456.5059	0.0003	0.0005	181
123	56456.5645	0.0003	0.0006	101
124	56456.6218	0.0003	-0.0004	89
132	56457.0887	0.0002	-0.0007	238
133	56457.1520	0.0030	0.0043	183
134	56457.2050	0.0001	-0.0011	586

*BJD-2400000.

†Against max = 2456449.3820 + 0.058389*E*.

‡Number of points used to determine the maximum.

Table 56. Superhump maxima of PNV J191501 (2013) (continued)

E	max*	error	$O - C^\dagger$	N^\ddagger
135	56457.2618	0.0001	-0.0027	566
136	56457.3217	0.0002	-0.0012	97
137	56457.3803	0.0003	-0.0010	192
138	56457.4391	0.0003	-0.0006	221
139	56457.4958	0.0002	-0.0022	303
140	56457.5550	0.0003	-0.0015	121
141	56457.6122	0.0002	-0.0026	105
143	56457.7287	0.0003	-0.0029	132
144	56457.7872	0.0002	-0.0028	156
145	56457.8450	0.0002	-0.0034	163
146	56457.9028	0.0002	-0.0040	124
150	56458.1365	0.0004	-0.0039	234
151	56458.1950	0.0004	-0.0037	394
152	56458.2567	0.0009	-0.0004	77
155	56458.4271	0.0003	-0.0052	44
156	56458.4866	0.0005	-0.0041	33
157	56458.5451	0.0003	-0.0039	66
161	56458.7791	0.0003	-0.0035	137
162	56458.8365	0.0003	-0.0045	183
163	56458.8933	0.0003	-0.0061	180
164	56458.9516	0.0003	-0.0062	98
167	56459.1236	0.0025	-0.0094	83
168	56459.1862	0.0002	-0.0051	199
169	56459.2426	0.0002	-0.0071	204
170	56459.3015	0.0002	-0.0066	202
171	56459.3604	0.0003	-0.0061	201
172	56459.4240	0.0007	-0.0009	72
173	56459.4773	0.0003	-0.0059	172
174	56459.5371	0.0003	-0.0046	181
175	56459.5924	0.0002	-0.0077	183
176	56459.6519	0.0009	-0.0066	71
177	56459.7101	0.0010	-0.0067	15
178	56459.7702	0.0006	-0.0051	142

*BJD-2400000.

†Against max = 2456449.3820 + 0.058389*E*.

‡Number of points used to determine the maximum.

served.

Although the period could not be determined, the 2011 observations were compatible with a period ~ 0.07 d.

In table 58, we summarized the past outbursts from the ASAS-3 data. Many of the detected outbursts were superoutbursts and the shortest intervals between superoutburst was ~ 390 d.

3.56. TCP J23382254-2049518

This object (hereafter TCP J233822) was discovered as a transient object by K. Itagaki on 2013 September 28 at an unfiltered CCD magnitude of 13.6.⁷ The object is identical with a blue SDSS object ($g = 21.5$, $g - r = -0.2$) and a GALEX ultraviolet source GALEX J233822.5-204951 (vsnet-alert 16468). The large outburst amplitude already suggested the WZ Sge-type classification.

⁷ <<http://www.cbat.eps.harvard.edu/unconf/followups/J23382254-2049518.html>>.

The object initially showed early superhumps (vsnet-alert 16486, 16489, 16496, 16528; figure 78). Twelve days after the discovery, the object started to show ordinary superhumps (vsnet-alert 16520, 16529, 16532, 16536; figure 79). The times of superhump maxima are listed in table 60, in which stage A-B transition is clearly seen (also figure 80). For the epochs $E \geq 222$, there was some evidence of shortening of the period. This part may correspond to stage C superhumps.

The fractional superhump excess (in frequency) for stage A superhumps was $\epsilon^* = 0.0231(14)$. This value corresponds to $q = 0.061(4)$, suggesting that the object is near the period minimum or somewhat passed the period minimum.

The object showed two post-superoutburst rebrightenings (figure 80). It is rare to see multiple post-superoutburst rebrightenings in such a short- P_{orb} system

Table 56. Superhump maxima of PNV J191501 (2013) (continued)

E	max*	error	$O - C^\dagger$	N^\ddagger
179	56459.8276	0.0004	-0.0060	147
180	56459.8857	0.0004	-0.0063	147
181	56459.9445	0.0005	-0.0059	129
183	56460.0628	0.0004	-0.0043	81
184	56460.1196	0.0003	-0.0059	94
185	56460.1869	0.0008	0.0030	421
186	56460.2359	0.0005	-0.0065	614
187	56460.2919	0.0010	-0.0088	370
190	56460.4692	0.0002	-0.0067	228
191	56460.5278	0.0003	-0.0064	208
192	56460.5861	0.0003	-0.0065	176
193	56460.6474	0.0008	-0.0036	108
195	56460.7645	0.0005	-0.0033	91
196	56460.8177	0.0007	-0.0085	232
197	56460.8783	0.0005	-0.0063	241
198	56460.9369	0.0006	-0.0061	79
199	56460.9989	0.0006	-0.0025	22
205	56461.3464	0.0009	-0.0053	70
206	56461.4080	0.0023	-0.0021	176
207	56461.4647	0.0004	-0.0038	207
208	56461.5200	0.0005	-0.0069	196
211	56461.7135	0.0024	0.0114	72
212	56461.7574	0.0006	-0.0031	161
213	56461.8138	0.0009	-0.0050	179
214	56461.8763	0.0013	-0.0009	247
215	56461.9288	0.0019	-0.0068	146
224	56462.4541	0.0014	-0.0070	76
225	56462.5174	0.0010	-0.0021	92
226	56462.5758	0.0011	-0.0021	87
227	56462.6359	0.0012	-0.0004	120
229	56462.7502	0.0007	-0.0029	153
230	56462.8088	0.0008	-0.0026	195
231	56462.8654	0.0004	-0.0045	251

*BJD-2400000.

 † Against max = 2456449.3820 + 0.058389*E*. ‡ Number of points used to determine the maximum.**Table 56.** Superhump maxima of PNV J191501 (2013) (continued)

E	max*	error	$O - C^\dagger$	N^\ddagger
232	56462.9244	0.0010	-0.0038	89
236	56463.1602	0.0005	-0.0016	208
237	56463.2184	0.0006	-0.0018	210
238	56463.2811	0.0012	0.0026	208
239	56463.3324	0.0009	-0.0045	257
240	56463.3952	0.0008	-0.0001	251
241	56463.4557	0.0011	0.0020	84
242	56463.5102	0.0007	-0.0019	63
243	56463.5670	0.0007	-0.0035	61
244	56463.6315	0.0020	0.0026	102
246	56463.7500	0.0014	0.0043	64
247	56463.8061	0.0018	0.0020	59
248	56463.8603	0.0010	-0.0021	112
249	56463.9201	0.0018	-0.0007	43
253	56464.1579	0.0007	0.0035	206
254	56464.2148	0.0008	0.0020	206
255	56464.2735	0.0007	0.0024	204
256	56464.3298	0.0006	0.0002	209
257	56464.3869	0.0008	-0.0011	248
258	56464.4514	0.0010	0.0051	151
259	56464.5034	0.0023	-0.0013	131
260	56464.5692	0.0012	0.0061	61
261	56464.6256	0.0011	0.0041	98
262	56464.6899	0.0040	0.0100	65
263	56464.7471	0.0014	0.0089	104
264	56464.8025	0.0028	0.0058	162
265	56464.8564	0.0008	0.0014	191
266	56464.9168	0.0015	0.0033	84
267	56464.9753	0.0009	0.0035	76
270	56465.1522	0.0011	0.0053	117
271	56465.2116	0.0012	0.0062	115
272	56465.2715	0.0008	0.0078	121
273	56465.3290	0.0015	0.0069	226

*BJD-2400000.

 † Against max = 2456449.3820 + 0.058389*E*. ‡ Number of points used to determine the maximum.

(cf. Nakata et al. 2013b).

4. Discussion

We first report in this section general statistical properties of the sample together with the earlier sample as in Kato et al. (2014). We then deals with new topics which arose in this paper.

4.1. Period Derivatives during Stage B

Figure 81 represents updated relation between P_{dot} for stage B versus P_{orb} . Most of the objects with $P_{\text{orb}} < 0.085$ d followed the general trend reported in Kato et al. (2013a). Some objects with P_{orb} longer than 0.085 d show negative P_{dot} while some of them show large positive P_{dot} (as we will see in subsection 4.7, some of these objects may have been contaminated by stage A superhumps). We

could add a new sample MASTER J162323 to the latter group. We can say that most of objects $P_{\text{orb}} < 0.080$ d have positive P_{dot} for stage B.

4.2. Mass Ratios from Stage A Superhumps

It has been proposed that the binary mass ratios can be estimated from the stage A superhumps, which are considered to reflect the dynamical precession rate at the radius of the 3:1 resonance (Kato, Osaki 2013b). Stage A superhumps recorded in the present study are listed in table 62. In table 61, we list the new estimates of mass ratios from in this paper. A updated summary of q estimates is shown in figure 82, in which measurements in Nakata et al. (2013b) are also included. The Kepler DNe shown in this figures are V516 Lyr (Kato, Osaki 2013a), KIC 7524178 (Kato, Osaki 2013c) and the unusual short- P_{orb} object GALEX J194419.33+491257.0 in the field of KIC

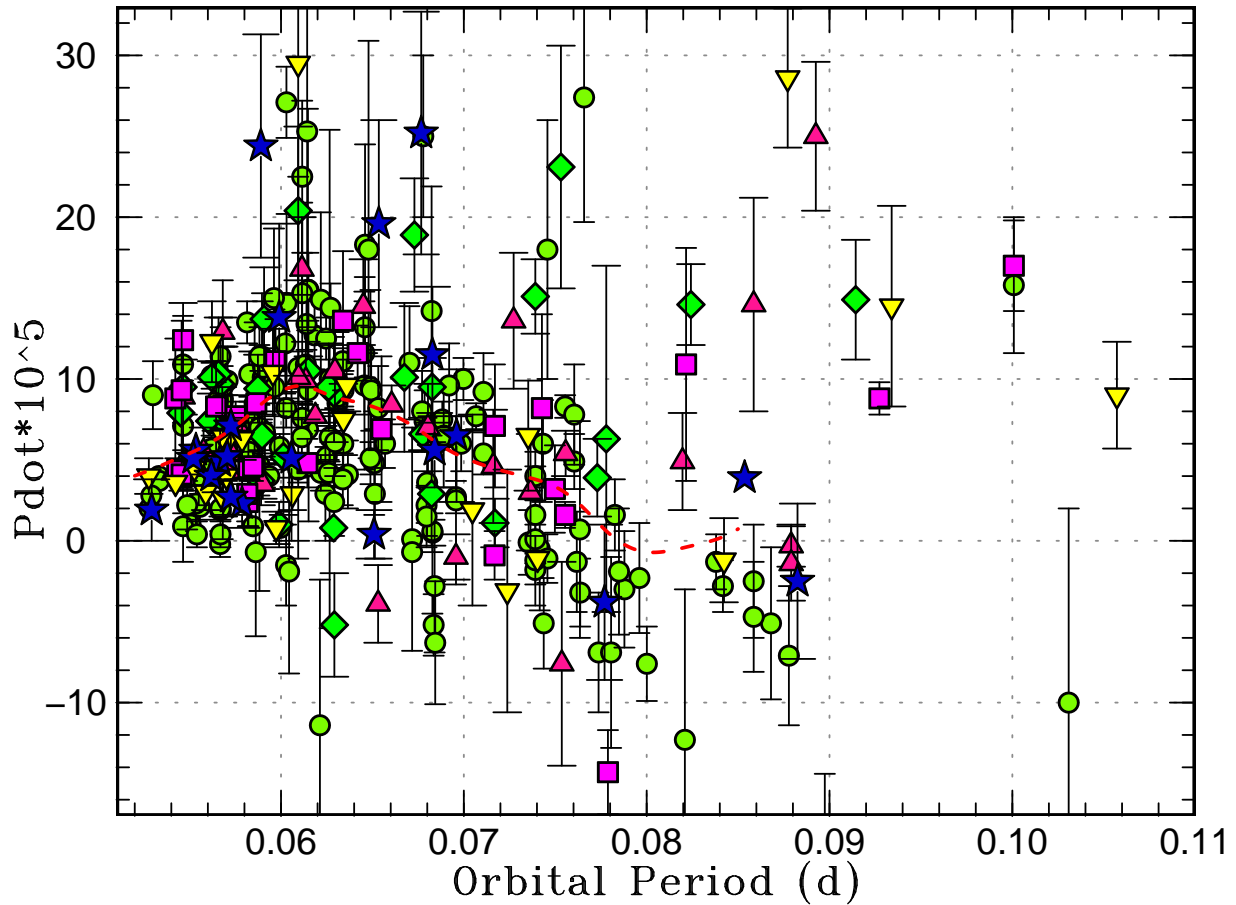


Fig. 81. P_{dot} for stage B versus P_{orb} . Filled circles, filled diamonds, filled triangles, filled squares, filled lower-pointed triangles and filled stars represent samples in Kato et al. (2009), Kato et al. (2010), Kato et al. (2012a), Kato et al. (2013a), Kato et al. (2014) and this paper, respectively. The curve represents the spline-smoothed global trend.

11412044 (Kato, Osaki 2014) (located at $P_{\text{orb}}=0.05282$ d, $q=0.14$).

4.3. WZ Sge-Type Stars

The WZ Sge-type dwarf novae in this study are listed in table 63. In figure 83, we showed the relation between P_{dot} and P_{orb} for the entire set of WZ Sge-type dwarf novae. This figure is an updated version of figure 86 of Kato et al. (2014). We here use the types of superoutburst in terms of rebrightenings as introduced in Imada et al. (2006) and Kato et al. (2009): type-A outburst (long-duration rebrightening), type-B outburst (multiple discrete rebrightenings), type-C outburst (single rebrightening) and type-D outburst (no rebrightening) (see e.g. figure 35 in Kato et al. 2009). The type-E outburst (superoutburst with early superhumps and another superoutburst with ordinary superhumps) has been introduced since Kato et al. (2014). The new data have confirmed the trend in that each subtype of the rebrightening pattern clusters in this diagram. Objects with type B (multiple) rebrightenings have a high concentration around $P_{\text{orb}}=0.060$ d. Nakata et al. (2013b) indicated that at least two objects with type B rebrightening are not period bouncers but lie on the ordinary track of CV evolution before the period minimum.

If this interpretation applies to the majority of the objects with type B rebrightening, these objects may be in a stage of CV evolution between short-period SU UMa-type dwarf novae and extreme WZ Sge-type dwarf novae near the period minimum.

4.4. Comparison of Periods of Early Superhumps and Orbital Periods

Although early superhumps have been documented (e.g. Kato et al. 1996; Patterson et al. 1996; Kato et al. 2001; Ishioka et al. 2002; Patterson et al. 2002; Kato 2002) as double-wave modulations having periods very close to the orbital period, there has been no summary of comparison between the period of early superhumps and the orbital period. We therefore make a study using the WZ Sge-type dwarf novae with well-established orbital period.

The periods of early superhumps of AL Com (2001), HV Vir (2008) were estimated from the data in Ishioka et al. (2002), Kato et al. (2009), respectively. The orbital period of BW Scl has been refined using quiescent observations (MLF, HaC, SPE and AAVSO data) between 2004 September and 2013 September, 14070 measurements). The orbital period of EZ Lyn is a revised one using post-superoutburst eclipses reported in Kato et al. (2012a).

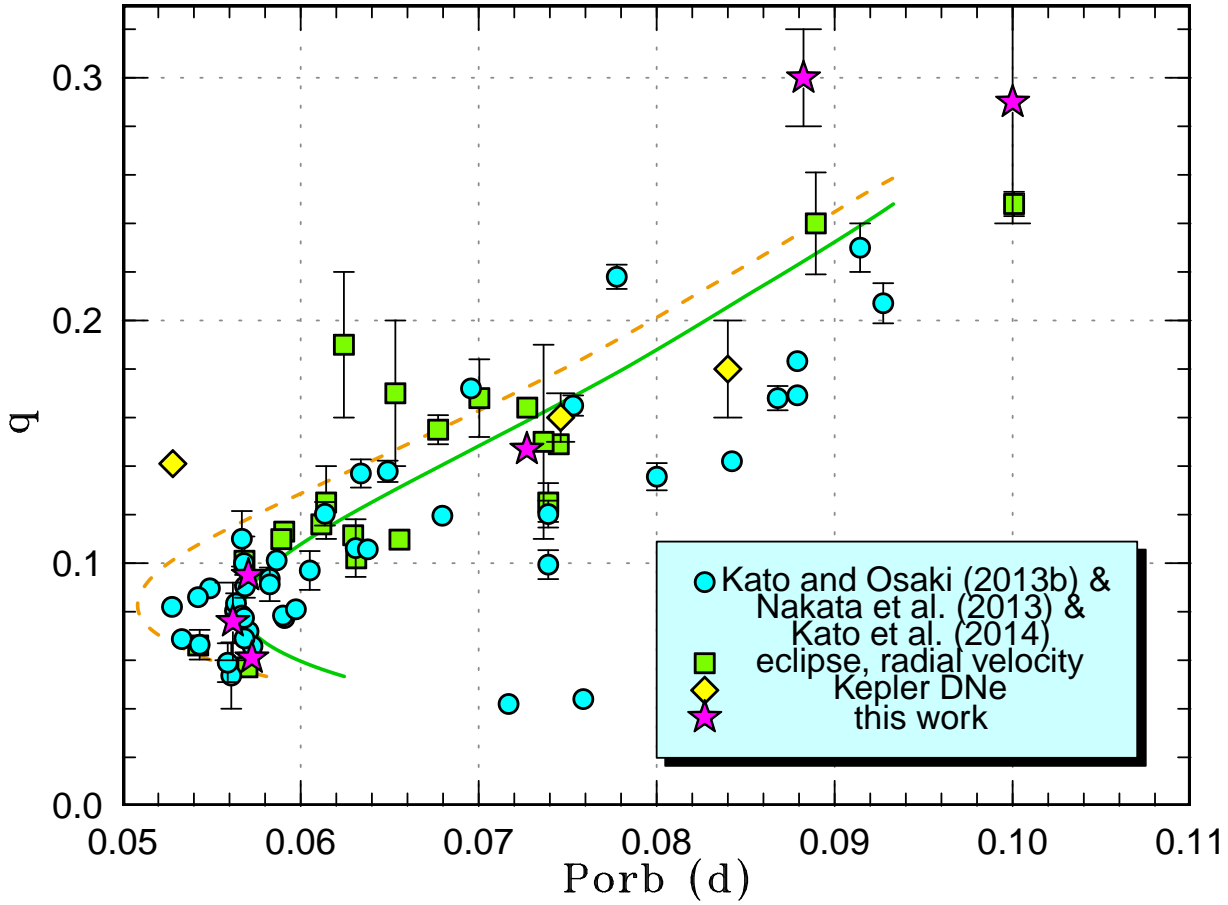


Fig. 82. Mass ratio versus orbital period. The dashed and solid curves represent the standard and optimal evolutionary tracks in Knigge et al. (2011), respectively. The filled circles, filled squares, filled stars, filled diamonds represent q values from a combination of the estimates from stage A superhumps published in three preceding sources (Kato, Osaki 2013b; Nakata et al. 2013b; Kato et al. 2014), known q values from quiescent eclipses or radial-velocity study (see Kato, Osaki 2013b for the data source), q estimated in this work and dwarf novae in the Kepler data (see text for the complete reference), respectively.

Table 63. Parameters of WZ Sge-type superoutbursts.

Object	Year	P_{SH}	P_{orb}	P_{dot}^*	err [*]	ϵ	Type [†]	N_{reb}^{\ddagger}	delay [§]	Max	Min
UZ Boo	2013	0.062066	–	5.1	5.1	–	B	4	3	12.5	19.7
AL Com	2013	0.057323	0.056669	4.9	1.9	0.012	A	1(2)	7	12.7	19.8
ASASSN-13ck	2013	0.056186	0.055348	5.6	0.4	0.015	A	1(3)	≥ 8	12.9	20.8
ASASSN-14ac	2014	0.058550	–	–1.7	1.2	–	–	≥ 1	≥ 14	14.5	21.6
MASTER J005740	2013	0.057067	0.056190	4.0	1.0	0.016	–	–	≥ 6	15.4	20.9
OT J210016	2013	0.058502	0.05787	2.3	1.5	0.011	–	–	–	14.2	19.9
PNV J191501	2013	0.058382	0.05706	5.2	0.2	0.023	D	0	≥ 7	9.8	18.5
TCP J233822	2013	0.057868	0.057255	2.7	1.1	0.011	B	2	≥ 12	13.6	21.5

*Unit 10^{-5} .

[†]A: long-lasting rebrightening; B: multiple rebrightenings; C: single rebrightening; D: no rebrightening.

[‡]Number of rebrightenings.

[§]Days before ordinary superhumps appeared.

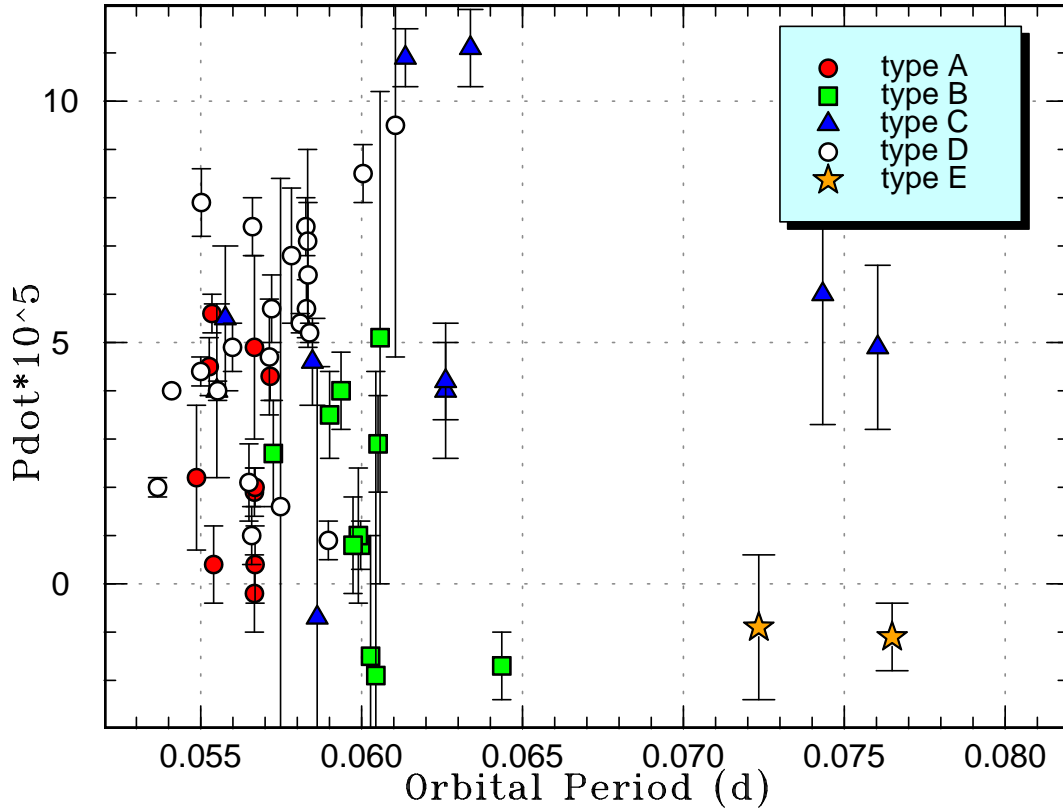


Fig. 83. P_{dot} versus P_{orb} for WZ Sge-type dwarf novae. Symbols represent the type (cf. Kato et al. 2009) of outburst: type-A (filled circles), type-B (filled squares), type-C (filled triangles), type-D (open circles) and type-E (filled stars) which show double superoutburst as shown in Kato et al. (2013b).

The orbital period of AL Com is an updated one using observations of early superhumps in three superoutbursts (subsection 3.11).

The result is summarized in table 64. Although all the objects showed statistically significant negative ε for early superhumps, the period deficit is very small (an order of 0.05%). This result has confirmed the finding in Ishioka et al. (2002). Since the period deficit is very small, the periods of early superhumps can be considered as the orbital periods to an accuracy of 0.1%. If more accuracy is needed and the orbital period is not known, we propose to estimate the orbital period by assuming ε of -0.05% .

4.5. Eclipses during the Phase of Early Superhumps

In the light curve of early superhumps in MASTER J005740 (figure 55), there are sharp structures (kinks in the light curve) around orbital phases -0.15 and 0.15 . They suggest that the phases between -0.15 and 0.15 were affected by the eclipse. We can propose a hypothetical uneclipsed hump structure (assuming that larger and smaller humps are separated equally) as the dashed line in the figure 55.

It has been a mystery why eclipses are not evident during the stage of early superhumps in such a high inclination system such as WZ Sge (Patterson et al. 2002), despite that eclipses appear more strongly after the appearance of ordinary superhumps. While Patterson et al.

(2002) suggested the enhanced hot spot as the origin of eclipses during the phase of ordinary superhumps, Osaki, Meyer (2003) suggested that what is eclipsed is the superhump light source rather than the enhanced hot spot. In the interpretation of Osaki, Meyer (2003), the source of early superhumps, which Osaki, Meyer (2002) interpret as the two-armed dissipation pattern of the 2:1 Lindblad resonance cannot be eclipsed because this pattern is located azimuthally far away from the secondary star. The present observation indicates that the broad eclipse was located close the expected eclipse center, which suggest that (the axisymmetric component of) the bright disk, rather than the enhanced hot spot, is eclipsed. This picture smoothly fits the interpretation by Osaki, Meyer (2003), and the mystery of the apparent absence of the eclipse during the phase of early superhumps is solved.

In Uemura et al. (2012), the eclipse of the disk was considered in the model. This effect was, however, not so large in the model parameters of V455 And, which apparently has a lower inclination than in MASTER J005740, and its effect was difficult to distinguish from the uneclipsed light curve of early superhumps. Our new observation in a system of higher inclination now presents more convincing evidence against the greatly increased mass-transfer in the WZ Sge-type outburst.

Table 64. Periods of Early Superhumps

Object	P_{orb} (d)	P_{ESH}^* (d)	$\varepsilon_{\text{ESH}}^\dagger$	References
V455 And (2007)	0.05630921(1)	0.0562675(18)	-0.00074(3)	Kato et al. (2009)
AL Com (1995)	0.056668589(9)	0.05666(2)	-0.0002(4)	this work; Kato et al. (1996)
AL Com (2001)	0.056668589(9)	0.056660(4)	-0.00015(7)	this work
AL Com (2013)	0.056668589(9)	0.056660(8)	-0.00015(14)	this work
EZ Lyn (2010)	0.05900495(3)	0.058973(6)	-0.00054(10)	Kato et al. (2012a)
BW Scl (2011)	0.05432391(1)	0.054308(2)	-0.00029(4)	this work; Kato et al. (2013a)
WZ Sge (2001)	0.0566878460(3)	0.056656(2)	-0.00057(4)	Patterson et al. (2002); Ishioka et al. (2002).
HV Vir (1992)	0.057069(6)	0.05698(8)	-0.0016(14)	Patterson et al. (2003); Kato et al. (2001)
HV Vir (2008)	0.057069(6)	0.056991(7)	-0.0014(1)	this work
MASTER J005740 (2013)	0.0561904(3)	0.056169(3)	-0.0038(5)	this work

*Period of early superhumps.

†Fractional excess of early superhumps.

Table 56. Superhump maxima of PNV J191501 (2013) (continued)

E	max*	error	$O - C^\dagger$	N^\ddagger
274	56465.3880	0.0016	0.0075	112
275	56465.4417	0.0014	0.0028	112
280	56465.7386	0.0033	0.0077	15
281	56465.7884	0.0019	-0.0008	15
292	56466.4363	0.0010	0.0048	135
293	56466.4991	0.0005	0.0092	156
294	56466.5604	0.0006	0.0121	136
295	56466.6151	0.0004	0.0085	118
297	56466.7380	0.0028	0.0145	16
308	56467.3717	0.0008	0.0060	111
309	56467.4320	0.0012	0.0079	136
310	56467.4883	0.0007	0.0058	88
311	56467.5487	0.0009	0.0078	63
313	56467.6581	0.0006	0.0004	34
326	56468.4267	0.0007	0.0100	62
327	56468.4734	0.0006	-0.0017	124
328	56468.5401	0.0010	0.0066	87
329	56468.5915	0.0009	-0.0004	60
330	56468.6457	0.0008	-0.0046	66
331	56468.7059	0.0041	-0.0028	15
332	56468.7609	0.0020	-0.0062	17
342	56469.3528	0.0013	0.0019	79
343	56469.4120	0.0008	0.0027	194
344	56469.4674	0.0008	-0.0003	224
345	56469.5263	0.0005	0.0002	151
346	56469.5906	0.0009	0.0061	151
347	56469.6476	0.0015	0.0047	64
348	56469.7037	0.0013	0.0024	96
349	56469.7592	0.0007	-0.0005	127
350	56469.8181	0.0008	0.0000	172
351	56469.8773	0.0010	0.0009	161
352	56469.9307	0.0016	-0.0041	64
355	56470.1060	0.0009	-0.0041	77

*BJD-2400000.

†Against max = 2456449.3820 + 0.058389*E*.

‡Number of points used to determine the maximum.

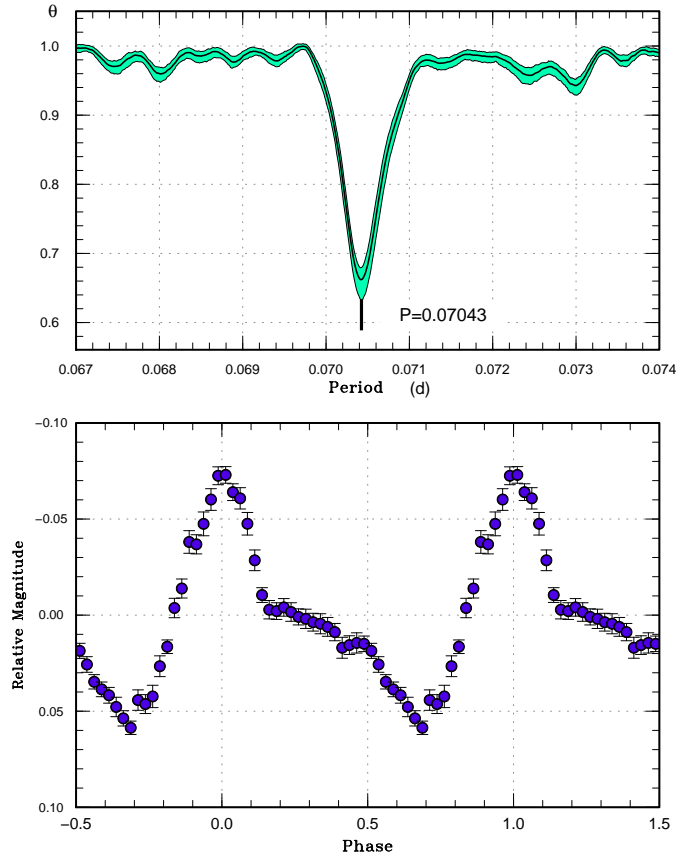
**Fig. 77.** Superhumps in SSS J094327 (2014). (Upper): PDM analysis. (Lower): Phase-averaged profile.

Table 56. Superhump maxima of PNV J191501 (2013) (continued)

E	max*	error	$O - C^\dagger$	N^\ddagger
361	56470.4542	0.0013	-0.0062	63
362	56470.5139	0.0015	-0.0049	61
363	56470.5683	0.0009	-0.0088	59
364	56470.6282	0.0035	-0.0073	64
365	56470.6935	0.0014	-0.0004	93
366	56470.7348	0.0012	-0.0175	180

*BJD-2400000.

 † Against max = 2456449.3820 + 0.058389 E . ‡ Number of points used to determine the maximum.**Table 57.** Superhump maxima of PNV J191501 (2013) (post-superoutburst)

E	max*	error	$O - C^\dagger$	N^\ddagger
0	56471.7401	0.0018	-0.0068	185
1	56471.8019	0.0026	-0.0030	210
7	56472.1209	0.0024	-0.0322	61
8	56472.1853	0.0086	-0.0258	62
9	56472.2412	0.0021	-0.0280	62
10	56472.2953	0.0011	-0.0319	77
16	56472.6877	0.0090	0.0124	23
17	56472.7242	0.0029	-0.0091	84
18	56472.7908	0.0019	-0.0005	224
19	56472.8465	0.0006	-0.0029	202
24	56473.1319	0.0020	-0.0076	59
25	56473.1993	0.0004	0.0018	123
26	56473.2578	0.0008	0.0023	119
32	56473.6053	0.0069	0.0017	27
33	56473.6628	0.0014	0.0012	50
34	56473.7212	0.0013	0.0015	56
35	56473.7793	0.0004	0.0016	125
46	56474.4220	0.0005	0.0061	84
47	56474.4768	0.0006	0.0028	104
48	56474.5360	0.0004	0.0041	108
49	56474.5906	0.0009	0.0006	116
50	56474.6537	0.0022	0.0057	86
51	56474.7087	0.0006	0.0027	104
52	56474.7671	0.0004	0.0031	161
54	56474.8831	0.0004	0.0030	184
63	56475.4060	0.0006	0.0038	28
64	56475.4634	0.0003	0.0031	77
65	56475.5192	0.0004	0.0009	65
67	56475.6335	0.0044	-0.0009	20
68	56475.6953	0.0015	0.0030	51
69	56475.7551	0.0006	0.0047	103
70	56475.8115	0.0004	0.0030	133
71	56475.8702	0.0003	0.0037	138

*BJD-2400000.

 † Against max = 2456471.7470 + 0.058021 E . ‡ Number of points used to determine the maximum.**Table 57.** Superhump maxima of PNV J191501 (2013) (post-superoutburst) (continued)

E	max*	error	$O - C^\dagger$	N^\ddagger
80	56476.3910	0.0013	0.0024	20
81	56476.4493	0.0004	0.0027	63
82	56476.5068	0.0005	0.0022	54
85	56476.6795	0.0015	0.0008	18
86	56476.7401	0.0005	0.0034	73
87	56476.7928	0.0008	-0.0020	135
88	56476.8527	0.0009	-0.0000	128
97	56477.3801	0.0007	0.0052	42
98	56477.4338	0.0005	0.0008	63
99	56477.4919	0.0014	0.0009	69
100	56477.5498	0.0004	0.0008	45
101	56477.6096	0.0006	0.0026	62
102	56477.6669	0.0003	0.0018	95
103	56477.7214	0.0009	-0.0017	125
104	56477.7859	0.0005	0.0048	97
109	56478.0779	0.0013	0.0066	44
110	56478.1357	0.0009	0.0064	60
111	56478.1905	0.0006	0.0032	62
112	56478.2476	0.0008	0.0023	63
113	56478.3054	0.0007	0.0021	62
115	56478.4241	0.0006	0.0048	102
116	56478.4828	0.0008	0.0054	85
117	56478.5384	0.0009	0.0030	83
118	56478.5980	0.0007	0.0046	85
119	56478.6540	0.0006	0.0025	44
120	56478.7177	0.0006	0.0082	54
121	56478.7671	0.0008	-0.0004	91
130	56479.3000	0.0016	0.0104	26
131	56479.3469	0.0006	-0.0007	39
132	56479.4057	0.0005	0.0000	99
133	56479.4658	0.0006	0.0021	97
134	56479.5271	0.0018	0.0054	83
135	56479.5821	0.0005	0.0023	85

*BJD-2400000.

 † Against max = 2456471.7470 + 0.058021 E . ‡ Number of points used to determine the maximum.

4.6. Model of the Eclipse during Early Superhumps

We further studied whether a simple model can reproduce the depth of the eclipse in MASTER J005740 during the phase of early superhumps. We adopted $q=0.076$ from our measurement using stage A superhumps (it is well-known that q and inclination are in strong relation in modeling the eclipse light curve, and the uncertainty in q can be reasonably neglected by allowing a free selection of the inclination). We assumed that the disk radius is the radius of the 2:1 resonance ($0.615A$ in the case of $q=0.076$). We assumed flat and axisymmetric geometry and a standard disk having a surface luminosity with a radial dependence $\propto r^{-3/4}$ (assuming that we observed the Rayleigh-Jeans tail of the emission from the hot disk). Although all of these assumptions are rough, they will not seriously affect the results. We constructed the eclipse light curve using the Roche geometry. We could

Table 57. Superhump maxima of PNV J191501 (2013) (post-superoutburst) (continued)

E	max*	error	$O - C^\dagger$	N^\ddagger
136	56479.6407	0.0013	0.0029	74
137	56479.6981	0.0021	0.0023	28
138	56479.7548	0.0008	0.0010	68
144	56480.1060	0.0010	0.0041	60
145	56480.1632	0.0006	0.0032	61
146	56480.2200	0.0005	0.0020	62
147	56480.2746	0.0005	-0.0014	60
148	56480.3384	0.0024	0.0044	31
149	56480.3968	0.0006	0.0047	50
150	56480.4486	0.0012	-0.0015	67
151	56480.5103	0.0005	0.0022	71
152	56480.5700	0.0006	0.0039	64
153	56480.6232	0.0007	-0.0009	63
154	56480.6828	0.0008	0.0007	20
155	56480.7413	0.0006	0.0011	79
161	56481.0886	0.0007	0.0003	61
162	56481.1461	0.0008	-0.0002	63
163	56481.2036	0.0009	-0.0007	62
164	56481.2606	0.0010	-0.0017	60
165	56481.3203	0.0007	-0.0001	52
166	56481.3779	0.0011	-0.0005	23
167	56481.4387	0.0006	0.0022	51
168	56481.4971	0.0005	0.0027	69
169	56481.5559	0.0008	0.0035	47
170	56481.6079	0.0007	-0.0026	43
171	56481.6654	0.0020	-0.0031	46
172	56481.7281	0.0010	0.0016	58
173	56481.7872	0.0015	0.0027	63
174	56481.8456	0.0008	0.0030	65
175	56481.9040	0.0011	0.0034	67
179	56482.1338	0.0006	0.0011	77
180	56482.1938	0.0006	0.0031	109
181	56482.2501	0.0008	0.0014	125

*BJD-2400000.

 † Against max = 2456471.7470 + 0.058021E. ‡ Number of points used to determine the maximum.

reproduce the eclipse depth of 0.16 mag from the assumed secondary maximum of early superhumps and the bottom of the eclipse (as seen from figure 55) by assuming the inclination of 81.5 ± 0.5 . The total duration of the eclipse was 0.28 binary phase, which is in agreement with the observation. Under these parameters, the white dwarf is marginally eclipsed, which is also in agreement with the observational suggestion.

The model light curve is shown in table 84. This model assumes that the standard disk is eclipsed by the secondary and the early superhumps are simply added to the light curve (i.e. we assume that the light source of the early superhumps is not eclipsed). The two maxima of early superhumps are approximated by sine curves having different amplitudes (the secondary maximum is assumed to have the half amplitude of the primary maximum). The resultant light curve appears to well reproduce the

Table 57. Superhump maxima of PNV J191501 (2013) (post-superoutburst) (continued)

E	max*	error	$O - C^\dagger$	N^\ddagger
183	56482.3686	0.0010	0.0038	69
184	56482.4235	0.0007	0.0007	111
185	56482.4814	0.0007	0.0006	108
186	56482.5375	0.0006	-0.0013	57
187	56482.5969	0.0009	0.0001	38
188	56482.6550	0.0011	0.0001	28
191	56482.8280	0.0003	-0.0009	100
194	56483.0056	0.0016	0.0026	35
195	56483.0595	0.0014	-0.0015	27
198	56483.2330	0.0007	-0.0021	117
199	56483.2923	0.0026	-0.0008	66
200	56483.3513	0.0009	0.0002	39
201	56483.4062	0.0007	-0.0029	108
202	56483.4676	0.0004	0.0005	108
203	56483.5236	0.0017	-0.0016	61
204	56483.5855	0.0006	0.0023	39
205	56483.6442	0.0025	0.0030	25
207	56483.7573	0.0006	0.0000	94
215	56484.2213	0.0024	-0.0001	111
216	56484.2824	0.0046	0.0030	55
218	56484.4016	0.0014	0.0061	21
219	56484.4556	0.0015	0.0021	24
220	56484.5078	0.0013	-0.0037	24
229	56485.0381	0.0019	0.0044	55
230	56485.0901	0.0011	-0.0016	56
232	56485.2041	0.0027	-0.0036	99
234	56485.3237	0.0010	-0.0001	38
242	56485.7879	0.0005	-0.0001	110
243	56485.8401	0.0010	-0.0059	108
269	56487.3480	0.0019	-0.0065	24
270	56487.4103	0.0006	-0.0022	40
271	56487.4680	0.0017	-0.0026	25

*BJD-2400000.

 † Against max = 2456471.7470 + 0.058021E. ‡ Number of points used to determine the maximum.

basic characteristics of the observation (figure 55). The sharp minimum around phase 0.0 reflects the eclipse of the central part of the disk; the less clear appearance of this feature in observation may have been the result of the self-occultation of the central part of the disk.

4.7. Stage A Superhumps in Long-Period Systems

In subsections 3.14 and 3.10, probable stage A superhumps were detected in the long- P_{orb} systems MN Dra and GZ Cnc. The identification of stage A superhumps in the former system is almost certain because growing amplitudes of the superhumps were detected.

This finding appears to contradict the earlier interpretation that stage A superhumps reflecting the radius of the 3:1 resonance in high- q systems are difficult to detect because the tidal effect is stronger in higher- q systems and the eccentric region spreads more quickly than in low- q systems (Kato, Osaki 2013b). In MN Dra and GZ Cnc,

Table 57. Superhump maxima of PNV J191501 (2013) (post-superoutburst) (continued)

E	max*	error	$O - C^\dagger$	N^\ddagger
275	56487.6911	0.0012	-0.0115	60
276	56487.7617	0.0005	0.0010	110
287	56488.3981	0.0010	-0.0008	42
288	56488.4516	0.0005	-0.0053	41
289	56488.5159	0.0006	0.0009	45
290	56488.5721	0.0006	-0.0008	45
293	56488.7439	0.0006	-0.0031	93
294	56488.7993	0.0007	-0.0057	88
304	56489.3905	0.0017	0.0053	70
305	56489.4405	0.0012	-0.0027	70
306	56489.4985	0.0006	-0.0028	45
307	56489.5569	0.0004	-0.0024	46
308	56489.6166	0.0007	-0.0007	46
322	56490.4293	0.0012	-0.0003	44
323	56490.4799	0.0018	-0.0077	48
324	56490.5430	0.0008	-0.0026	46
325	56490.6023	0.0007	-0.0014	47
326	56490.6620	0.0042	0.0003	30
339	56491.4113	0.0008	-0.0046	46
340	56491.4717	0.0005	-0.0023	45
341	56491.5352	0.0009	0.0032	45
343	56491.6406	0.0010	-0.0075	43
408	56495.4172	0.0025	-0.0022	40

*BJD-2400000.

 † Against max = 2456471.7470 + 0.058021*E*. ‡ Number of points used to determine the maximum.**Table 59.** Superhump maxima of SSS J094327 (2014)

E	max*	error	$O - C^\dagger$	N^\ddagger
0	56689.0954	0.0013	-0.0073	123
1	56689.1697	0.0010	-0.0036	112
14	56690.0889	0.0003	0.0000	140
15	56690.1581	0.0003	-0.0012	142
16	56690.2310	0.0003	0.0012	142
17	56690.3007	0.0003	0.0005	140
18	56690.3716	0.0005	0.0009	81
28	56691.0753	0.0004	0.0002	136
29	56691.1462	0.0003	0.0006	141
43	56692.1327	0.0003	0.0010	142
44	56692.2032	0.0005	0.0010	142
45	56692.2741	0.0004	0.0015	141
46	56692.3434	0.0005	0.0004	138
50	56692.6270	0.0009	0.0023	22
51	56692.6971	0.0007	0.0019	24
52	56692.7674	0.0009	0.0018	19
53	56692.8385	0.0015	0.0024	22
57	56693.1213	0.0006	0.0035	142
58	56693.1913	0.0006	0.0030	143
59	56693.2610	0.0010	0.0022	141
60	56693.3325	0.0006	0.0034	132
65	56693.6825	0.0009	0.0012	23
66	56693.7536	0.0009	0.0018	19
72	56694.1758	0.0031	0.0014	76
78	56694.5904	0.0052	-0.0067	11
79	56694.6640	0.0011	-0.0036	23
80	56694.7388	0.0013	0.0008	20
81	56694.8097	0.0016	0.0013	21
82	56694.8773	0.0021	-0.0016	16
85	56695.0884	0.0012	-0.0018	137
86	56695.1567	0.0012	-0.0039	141
87	56695.2272	0.0011	-0.0038	142
88	56695.3007	0.0016	-0.0008	78

*BJD-2400000.

 † Against max = 2456689.1028 + 0.070440*E*. ‡ Number of points used to determine the maximum.**Table 58.** Outbursts of SSS J094327

JD-2400000	Maximum (V)	Duration	Type
51926	13.1	12	Super
52440	12.8	>3	Super?
53005	13.8	1*	Normal?
53385	12.8	11	Super
53776	13.0	>7	Super
54182	13.1	>8	Super
54667	13.6	2	Normal
54796	13.3	1*	Normal?

*Single detection.

however, the q values are probably critically close to the condition in which the 3:1 resonance occurs, and the resonance may be weak enough to be confined to the radius of the 3:1 resonance for longer time than in ordinary SU UMa-type dwarf novae. This possibility needs to be studied further. Although some of objects recorded in our past study with long P_{orb} and large negative P_{dot} may have been the similar ones, we could not find as convincing case as MN Dra. Since almost all of these systems lack determination of the orbital period, future measurements of the orbital periods may provide a clue to interpret this phenomenon.

4.8. Negative Superhumps in VW Hydri

In recent series of papers (Osaki, Kato 2013a; Osaki, Kato 2013b; Osaki, Kato 2014), it has been demonstrated using the Kepler data that the state with negative super-

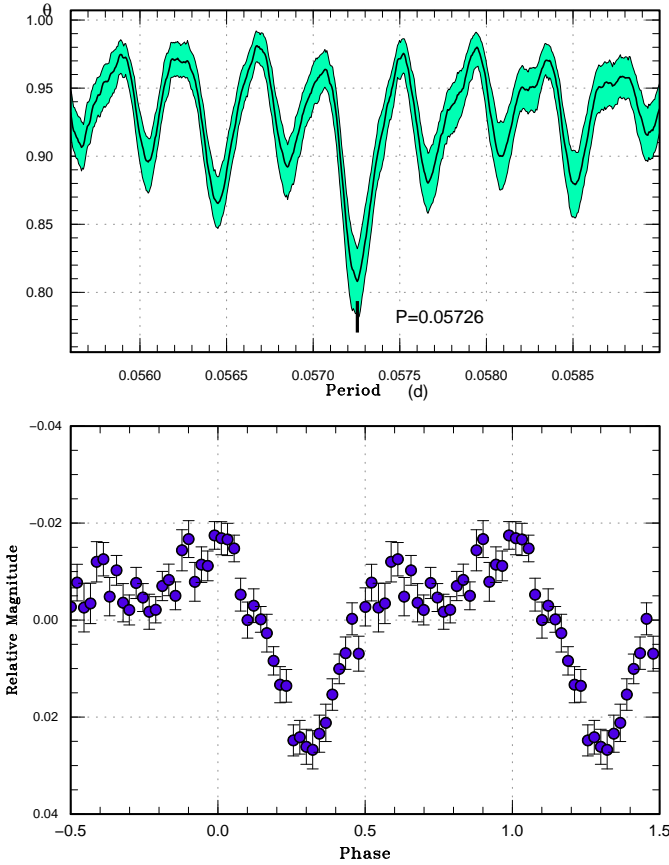


Fig. 78. Early superhumps in TCP J233822 (2013). (Upper): PDM analysis. (Lower): Phase-averaged profile.

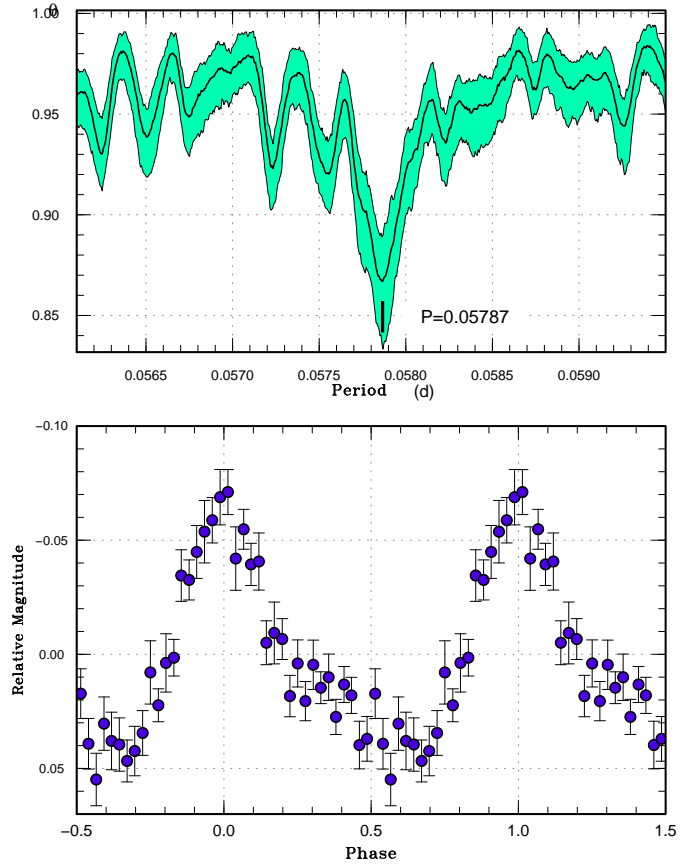


Fig. 79. Ordinary superhumps in TCP J233822 (2013). The interval of BJD 2456577.6–2456593 was used. (Upper): PDM analysis. (Lower): Phase-averaged profile.

humps tend to suppress normal outbursts in V1504 Cyg and V344 Lyr. The same phenomenon is also reported in ER UMa (Ohshima et al. 2012; Zemko et al. 2013; Ohshima et al. 2014). This phenomenon has been interpreted as a result of the decreased mass supply to the outermost part of the accretion disk when the disk is tilted, thereby reducing the occurrence of thermal instability in the outer part of the disk (Osaki, Kato 2013a; Ohshima et al. 2014). Osaki, Kato (2013a) called the supercycle type S (short intervals between normal outbursts) type L (long intervals between normal outbursts), the nomenclature originally introduced by Smak (1985) for VW Hyi. Although the result in V1504 Cyg and V344 Lyr suggests that the same mechanism is responsible for type S and L supercycle in VW Hyi, this has not yet been demonstrated by observation.

We conducted an intensive campaign on VW Hyi in 2012–2013 to test this possibility. Since the start of the campaign in 2012 October 29, no outburst was detected (for a duration of 25 d) until the next superoutburst starting on November 23 (the superoutburst reported in subsection 3.18). Although the observations were not as dense as our CCD campaign, visual observations by the AAVSO observers did not detect an outburst since the last recorded outburst on September 9. If there was no

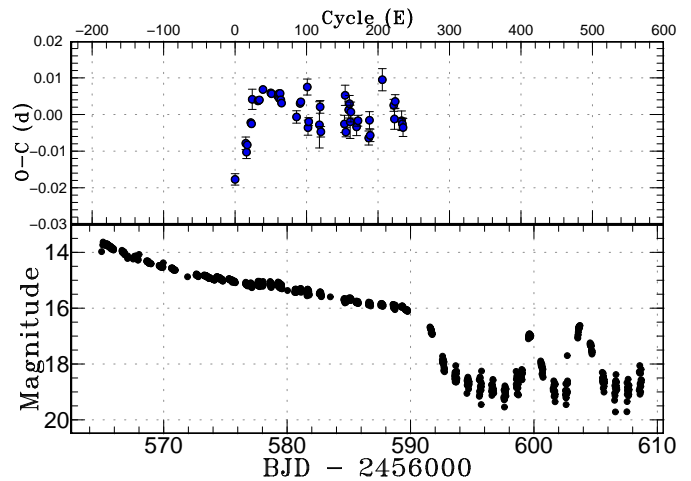


Fig. 80. $O - C$ diagram of superhumps in TCP J233822 (2013). (Upper): $O - C$ diagram. A period of 0.057913 d was used to draw this figure. (Lower): Light curve. The observations were binned to 0.011 d.

Table 60. Superhump maxima of TCP J233822 (2013)

E	max*	error	$O - C^\dagger$	N^\ddagger
0	56575.7668	0.0016	-0.0178	28
15	56576.6453	0.0017	-0.0079	14
16	56576.7008	0.0017	-0.0103	15
17	56576.7607	0.0010	-0.0083	28
22	56577.0564	0.0007	-0.0023	27
23	56577.1140	0.0009	-0.0026	37
24	56577.1786	0.0028	0.0041	15
32	56577.6414	0.0006	0.0037	13
33	56577.6995	0.0007	0.0038	14
34	56577.7575	0.0005	0.0039	27
39	56578.0499	0.0008	0.0068	20
50	56578.6861	0.0008	0.0058	18
51	56578.7437	0.0006	0.0056	25
60	56579.2642	0.0004	0.0048	124
61	56579.3229	0.0006	0.0056	123
62	56579.3795	0.0004	0.0043	133
63	56579.4388	0.0007	0.0057	134
64	56579.4949	0.0008	0.0039	133
65	56579.5520	0.0007	0.0030	133
86	56580.7644	0.0017	-0.0007	30
91	56581.0576	0.0007	0.0030	11
92	56581.1159	0.0010	0.0034	15
101	56581.6412	0.0022	0.0074	13
102	56581.6880	0.0021	-0.0037	14
103	56581.7476	0.0011	-0.0020	28
118	56582.6154	0.0063	-0.0029	12
119	56582.6782	0.0017	0.0020	13
120	56582.7293	0.0014	-0.0048	21
153	56584.6426	0.0024	-0.0027	19
154	56584.7083	0.0028	0.0051	29
155	56584.7562	0.0013	-0.0049	72
159	56584.9939	0.0022	0.0012	12

*BJD-2400000.

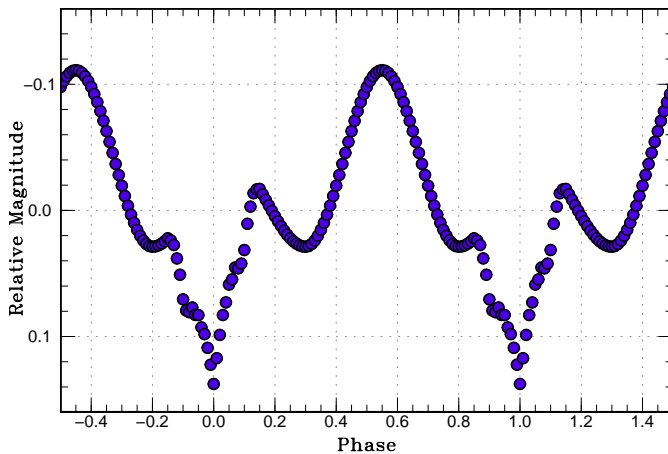
 † Against max = 2456575.7845 + 0.057913E. ‡ Number of points used to determine the maximum.**Table 60.** Superhump maxima of TCP J233822 (2013) (continued)

E	max*	error	$O - C^\dagger$	N^\ddagger
160	56585.0535	0.0022	0.0029	15
161	56585.1065	0.0045	-0.0021	11
162	56585.1671	0.0027	0.0006	15
170	56585.6263	0.0024	-0.0035	15
172	56585.7438	0.0015	-0.0018	31
187	56586.6078	0.0019	-0.0065	14
188	56586.6706	0.0023	-0.0017	13
189	56586.7244	0.0017	-0.0058	22
206	56587.7241	0.0030	0.0094	23
222	56588.6437	0.0016	0.0024	13
223	56588.6979	0.0028	-0.0013	17
224	56588.7606	0.0019	0.0034	19
233	56589.2765	0.0027	-0.0018	133
234	56589.3336	0.0016	-0.0027	134
235	56589.3905	0.0024	-0.0037	132

*BJD-2400000.

 † Against max = 2456575.7845 + 0.057913E. ‡ Number of points used to determine the maximum.**Table 61.** New estimates for the binary mass ratio from stage A superhumps

Object	ε^* (stage A)	q from stage A
GZ Cnc	0.089(7)	0.30(2)
MN Dra	0.078, 0.092	0.29(5)
DT Oct	0.050(2)	0.147(7)
MASTER J005740	0.028(5)	0.076(16)
PNV J191501	0.0344(12)	0.095(4)
TCP J233822	0.0231(14)	0.061(4)

**Fig. 84.** Model light curve of the early superhump and eclipse of MASTER J005740.**Table 62.** Superhump Periods during Stage A

Object	Year	period (d)	err
UZ Boo	2013	0.06210	0.00005
GZ Cnc	2014	0.09690	0.00030
AL Com	2013	0.05859	0.00009
MN Dra	2012	0.10993	0.00009
MN Dra	2013	0.10822	0.00013
DT Oct	2014	0.07271	-
ASASSN-13ck	2013	0.05700	0.00010
ASASSN-14ac	2014	0.05952	0.00003
MASTER J004527	2013	0.08210	0.00035
MASTER J005740	2013	0.05783	0.00034
MASTER J162323	2013	0.09134	0.00055
PNV J191501	2013	0.05909	0.00008
TCP J233822	2013	0.05861	0.00008

outburst between them, the interval of normal outbursts may be as long as ~ 70 d. Since VW Hyi undergoes normal outbursts as frequently as every 11–23 d in type S supercycles (cf. Smak 1985), in which intervals shorter than 23 d were considered as type S and those longer than ~ 30 d were type L), the state before the 2012 superoutburst was most likely type L.

A PDM analysis of the observation BJD 2456229–2456254 (quiescence before the 2012 superoutburst) after subtracting the mean orbital variation yielded a period of 0.07265(3) d, 2.2% shorter than the orbital period. Another candidate period is 0.07829(3) d, which is a one-day alias of the 0.07265 d period. Although there remains a possibility that 0.07829 d is the true period and the 0.07265 d period is a one-day alias signal, we consider this possibility less likely because the similar signal was also observed after the superoutburst (figure 86). In this interval, the negative superhump was the strongest signal after subtracting the orbital modulations, and there is no remaining ambiguity of a one-day alias. The periods of negative superhumps determined for different segments of the data after subtraction of the orbital signal are listed in table 65. During the superoutburst, the period of negative superhumps could not be determined because it was located close to the one-day alias of the (positive) superhump period.

The mean profile (figure 85) is also characteristic of negative superhumps (cf. Osaki, Kato 2013a; Osaki, Kato 2013b) with a slower rise to the maximum and a faster decline to the minimum. The co-existence of orbital humps and negative superhumps, which is also recorded both in V1504 Cyg and V344 Lyr, suggests that some of the stream hits the outermost part of the disk to produce the hot spot while some part of the stream reaches the inner disk to produce negative superhumps (cf. Wood, Burke 2007).

A two-dimensional Lasso analysis (figure 87) shows a signal of negative superhumps with a frequency around 13.75 cycle d^{-1} before the superoutburst. A possible signal of negative superhumps with frequencies around 13.65–13.70 cycle d^{-1} was also detected after the superoutburst. The decrease in the frequency (also evident as an increase in period in table 65) is compatible of the shrinkage of the accretion disk after the superoutburst. As reported in Osaki, Kato (2013a), the precession frequency of a tilted disk can be expressed as follows (Larwood 1998):

$$\nu_{\text{NSH}}/\nu_{\text{orb}} = 1 + \left(\frac{3}{7} \frac{q}{\sqrt{1+q}} \cos\theta \right) \left(\frac{R_d}{A} \right)^{3/2}, \quad (5)$$

where ν_{NSH} and ν_{orb} are the frequency for the negative superhump and binary orbital frequency, respectively, R_d the disk radius, A is the binary separation, θ is the tilt angle of the disk to the binary orbital plane. The smallest $|\varepsilon^*|$ (equivalent to $\nu_{\text{NSH}}/\nu_{\text{orb}}$) before the superoutburst was 0.024 and the largest $|\varepsilon^*|$ after the superoutburst was 0.020. This difference can be explained by a 13 percent shrinkage of the disk radius after the superoutburst.

Table 65. Period of negative superhumps in VW Hyi (2012)

JD–2400000	Period (d)	Error (d)	Amplitude (mag)
56229–56239	0.07252	0.00003	0.05
56240–56254	0.07266	0.00002	0.04
56269–56279	0.07261	0.00003	0.10
56285–56302	0.07279	0.00003	0.07
56305–56327	0.07275	0.00002	0.07
56339–56361	–	–	–
56365–56374	0.07271	0.00005	0.05

Assuming $q=0.21(2)$ (from radial-velocity study by Smith et al. 2006) and a small tilt angle ($\cos\theta \sim 1$), these two values of $|\varepsilon^*|$ correspond to the disk radii of 0.42(1) A and 0.39(1) A , respectively.⁸

For comparison, a two-dimensional Lasso analysis of the 2011 data is also shown in figure 88. No clear signal of negative superhumps was detected, although the analysis is noisy due to the poorer coverage than in the 2012 observation and the persistence of positive superhumps which interferes the detection of other signals when the data are sparse.

We conclude that type L supercycle in VW Hyi (reduced number of normal outbursts) is associated with the presence of negative superhumps as in V1504 Cyg and V344 Lyr, and the tilt in the disk can be regarded as a cause of the varying frequency of normal outbursts.

5. Summary

In addition to basic data of superhumps of the objects observed in this paper, the major findings we obtained can be summarized as follows.

- We report the detection of negative superhumps in quiescence of VW Hyi in 2012. We conclude that type L supercycle in VW Hyi (reduced number of normal outbursts) is associated with the presence of negative superhumps as in V1504 Cyg and V344 Lyr.
- MASTER J005740 is the first eclipsing WZ Sge-type dwarf nova showing the probable eclipse of the white dwarf. The sharp structure in the profile of the early superhumps is interpreted as the eclipse of the accretion disk, which has been difficult to distinguish from the profile of the early superhump itself in other WZ Sge-type dwarf novae. The symmetric profile of the eclipse indicates that the disk itself, not the enhanced hot spot, is eclipsed. This finding gives observational support to Osaki, Meyer (2003) who interpreted that the source of the early superhumps is not the hot spot as suggested by an en-

⁸ Smith et al. (2006) suggested that this q value is highly insecure. We used this value since there is no other direct determination of the q value, and the q determined from stage B superhumps (Patterson et al. 2005) has unknown uncertainty.

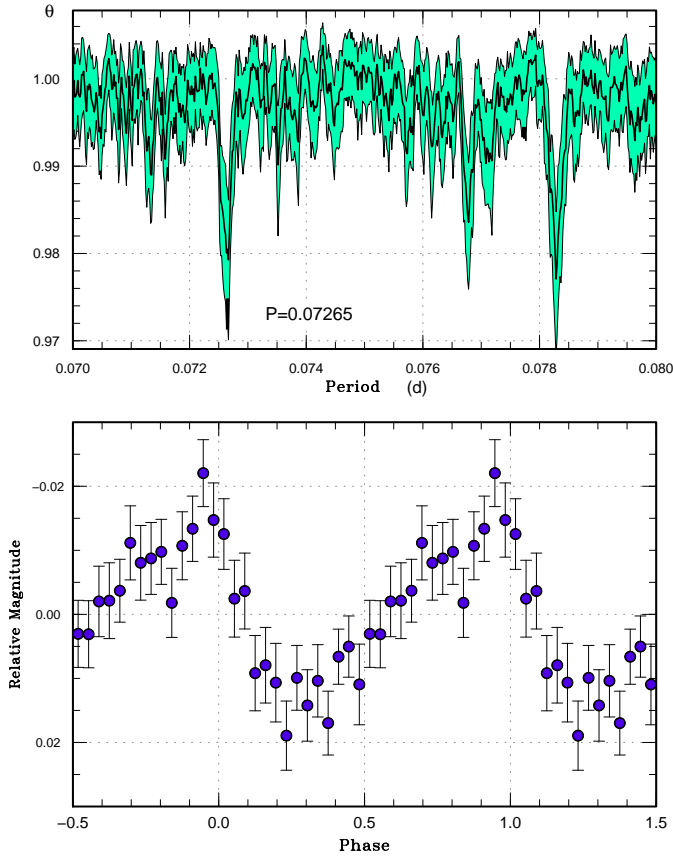


Fig. 85. Negative superhumps in VW Hyi (2012). The observation BJD 2456229–2456584 (quiescence before the 2012 superoutburst) was analyzed after subtracting the mean orbital variation. (Upper): PDM analysis. (Lower): Phase-averaged profile.

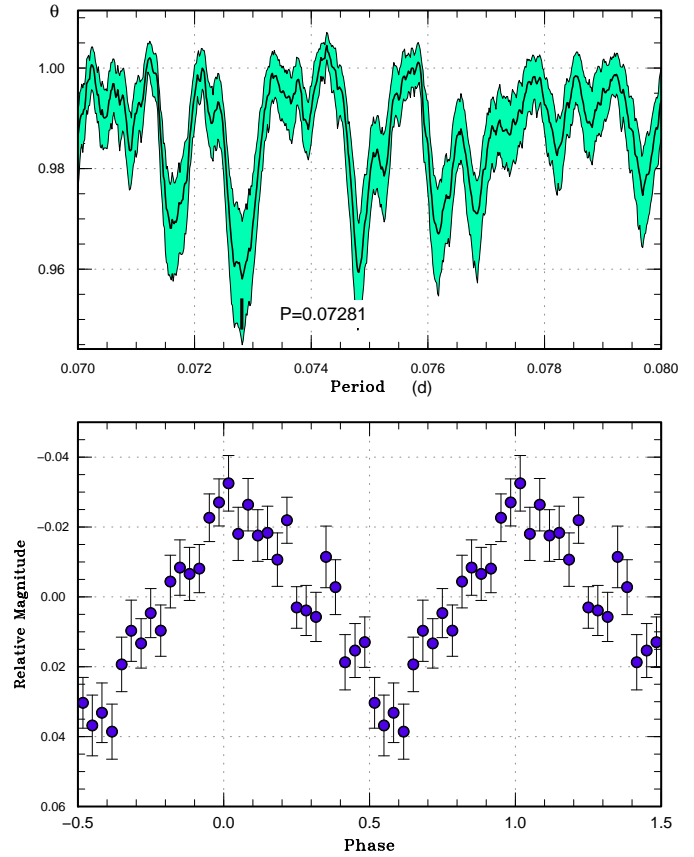


Fig. 86. Negative superhumps in VW Hyi (2012). The observation BJD 2456282–2456302 (quiescence between the first two normal outbursts after the superoutburst) was analyzed after subtracting the mean orbital variation. (Upper): PDM analysis. (Lower): Phase-averaged profile.

hanced mass-transfer model (Patterson et al. 1981). We also provided a model calculation of the eclipse light curve of this object during the phase of early superhumps.

- We detected stage A superhumps with growing amplitudes in MN Dra and likely stage A (from the $O-C$ diagram) in GZ Cnc, both of which have long orbital periods. The stage A superhumps in these systems lasted longer than expected. We interpreted that the 3:1 resonance was confined in the region of excitement because these objects have mass-ratios critically close to the condition in which the tidal instability occurs. This may provide an interpretation of large negative period derivatives recorded in the past in systems with long orbital periods.
- The 2013 superoutburst of UZ Boo was followed by four post-superoutburst rebrightening as was observed in the 2003 superoutburst. This observation suggests that the pattern of rebrightening tends to be reproducible in the same object.
- The WZ Sge-type dwarf novae AL Com and ASASSN-13ck showed a long-lasting (plateau-type) rebrightening. In the early phase of the rebrighten-

ing, both objects showed a precursor-like outburst, suggesting that the long-lasting rebrightening is triggered by a precursor outburst. Both objects showed small dip(s) during the rebrightening.

- We have reviewed the observation of early superhumps of WZ Sge-type dwarf novae and found that the fractional superhump excesses for early superhumps have a typical value of -0.05% .
- We have succeeded in detecting a positive period derivative of superhumps in the helium CV CP Eri. This object also showed oscillation-type rebrightenings.
- We have established the long-sought superoutburst of the eclipsing dwarf nova V893 Sco after fifteen years since the rediscovery.

This work was supported by the Grant-in-Aid “Initiative for High-Dimensional Data-Driven Science through Deepening of Sparse Modeling” from the Ministry of Education, Culture, Sports, Science and Technology (MEXT) of Japan. The authors are grateful to observers of VSNET Collaboration and VSOLJ observers who supplied vital data. We acknowledge with thanks the variable

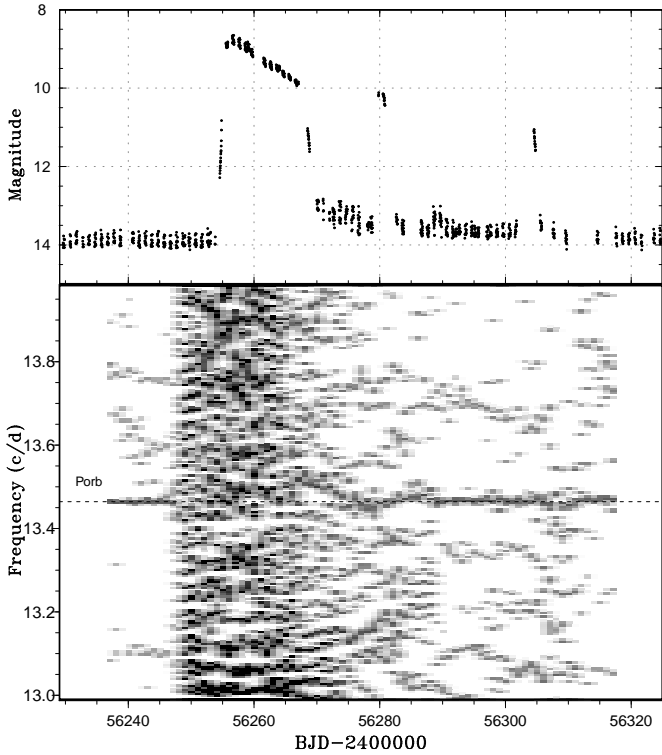


Fig. 87. Two-dimensional Lasso period analysis of VW Hyi (2012). (Upper:) Light curve. The data were binned to 0.02 d. (Lower:) Lasso period analysis of the superhump and the orbital signal. The signal of negative superhumps with a frequency around $13.75 \text{ cycle d}^{-1}$ before the superoutburst was recorded. A possible signal of negative superhumps with frequencies around $13.65\text{--}13.70 \text{ cycle d}^{-1}$ was also detected after the superoutburst. $\log \lambda = -7.8$ was used. The width of the sliding window and the time step used are 15 d and 1 d, respectively.

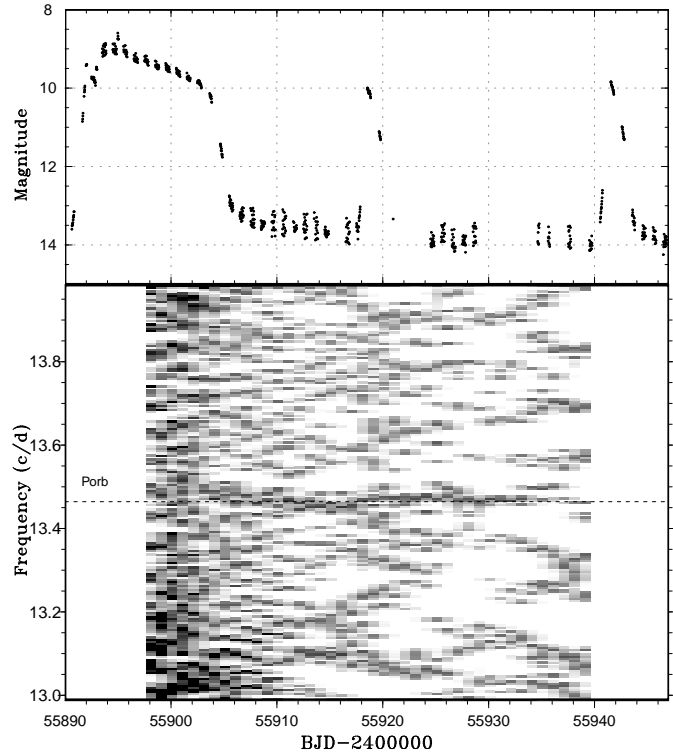


Fig. 88. Two-dimensional Lasso period analysis of VW Hyi (2011). See figure 87 for the explanation. No strong signal of negative superhumps was detected.

star observations from the AAVSO International Database contributed by observers worldwide and used in this research. This work is deeply indebted to outburst detections and announcement by a number of variable star observers worldwide, including participants of CVNET and BAA VSS alert. We thank Dr. Brian Skiff for making historical materials about WX Hyi available to us. The CCD operation of the Bronberg Observatory is partly sponsored by the Center for Backyard Astrophysics. The CCD operation by Peter Nelson is on loan from the AAVSO, funded by the Curry Foundation. We are grateful to the Catalina Real-time Transient Survey team for making their real-time detection of transient objects available to the public.

References

- Abbott, T. M. C., Robinson, E. L., Hill, G. J., & Haswell, C. A. 1992, *ApJ*, 399, 680
- Andronov, I. L. 1986, *Astron. Tsirk.*, 1432, 6
- Antipin, S. V., & Pavlenko, E. P. 2002, *A&A*, 391, 565
- Araujo-Betancor, S., et al. 2005, *A&A*, 430, 629
- Armstrong, E., Patterson, J., & Kemp, J. 2012, *MNRAS*, 421, 2310
- Aungwerojwit, A., et al. 2006, *A&A*, 455, 659
- Avery, R., & Sievers, J. 1968, *Bamberg Veröff.*, 7, 76
- Bailey, J. 1979a, *MNRAS*, 188, 681
- Bailey, J. 1979b, *MNRAS*, 189, 41P
- Balanutsa, P., et al. 2013a, *Astron. Telegram*, 5555
- Balanutsa, P., et al. 2013b, *Astron. Telegram*, 5708
- Bateson, F. M. 1976, *IBVS*, 1161
- Bateson, F. M. 1982a, *Publ. Variable Stars Sect. R. Astron. Soc. New Zealand*, 10, 24
- Bateson, F. M. 1982b, *Publ. Variable Stars Sect. R. Astron. Soc. New Zealand*, 10, 12
- Bateson, F. M. 1998, *Publ. Variable Stars Sect. R. Astron. Soc. New Zealand*, 23, 44
- Bertola, F. 1964, *Annales d'Astrophysique*, 27, 298
- Bertola, F. 1965, *IBVS*, 103, 1
- Bond, H. E., Kemper, E., & Mattei, J. A. 1982, *ApJ*, 260, L79
- Boyd, D., Oksanen, A., & Henden, A. 2006, *J. Br. Astron. Assoc.*, 116, 187
- Bruch, A. 1989, *A&AS*, 78, 145
- Bruch, A., Fischer, F.-J., & Wilmsen, U. 1987, *A&AS*, 70, 481
- Bruch, A., Steiner, J. E., & Gneiding, C. D. 2000, *PASP*, 112, 237
- Cannizzo, J. K., Still, M. D., Howell, S. B., Wood, M. A., & Smale, A. P. 2010, *ApJ*, 725, 1393
- Cannon, A. J. 1925, *Harvard Coll. Obs. Bull.*, 825, 1
- Carter, P. J., et al. 2013, *MNRAS*, 431, 372
- Chen, J.-S., Liu, X.-W., & Wei, M.-Z. 1991, *A&A*, 242, 397
- Cleveland, W. S. 1979, *J. Amer. Statist. Assoc.*, 74, 829
- Demartino, R., Kocyla, D., Pridmore, C., & Wetherbee, E. 1996, *IBVS*, 4322, 1
- Denisenko, D., et al. 2013a, *Astron. Telegram*, 5572

- Denisenko, D., et al. 2013b, *Astron. Telegram*, 5643
 Denisenko, D., et al. 2013c, *Astron. Telegram*, 5399
 Denisenko, D. V., & Sokolovsky, K. V. 2011, *Astron. Lett.*, 37, 91
 Downes, R., Webbink, R. F., & Shara, M. M. 1997, *PASP*, 109, 345
 Downes, R. A. 1990, *AJ*, 99, 339
 Downes, R. A., Webbink, R. F., Shara, M. M., Ritter, H., Kolb, U., & Duerbeck, H. W. 2001, *PASP*, 113, 764
 Drake, A. J., et al. 2009, *ApJ*, 696, 870
 Drew, J. E., et al. 2005, *MNRAS*, 362, 753
 Duerbeck, H. W. 1987, *Space Sci. Rev.*, 45, 1
 Fernie, J. D. 1989, *PASP*, 101, 225
 Filin, A. Y., & Satyrvoldiev, V. 1975, *Perem. Zvezdy*, 20, 161
 Fisher, W. J. H., Walker, W. S. G., Jones, A. F., & Nelson, P. 1971, *IAU Circ.*, 2348, 2
 Gill, C. D., & O'Brien, T. J. 1998, *MNRAS*, 300, 221
 Glasby, J. S. 1970, *The Dwarf Novae* (London: Constable)
 Gorbovskoy, E. S., et al. 2013, *Astron. Rep.*, 57, 233
 Green, R. F., Ferguson, D. H., Liebert, J., & Schmidt, M. 1982, *PASP*, 94, 560
 Haro, G., & Luyten, W. J. 1962, *Boletín de los Observatorios de Tonantzintla y Tacubaya*, 3, 37
 Harvey, D., Skillman, D. R., Patterson, J., & Ringwald, F. A. 1995, *PASP*, 107, 551
 Hirose, M., & Osaki, Y. 1990, *PASJ*, 42, 135
 Hoffmeister, C. 1936, *Astron. Nachr.*, 259, 37
 Hoffmeister, C. 1949, *Erg. Astron. Nachr.*, 12, 12
 Hoffmeister, C. 1957, *Mitteil. Veränderl. Sterne*, 1, 245
 Hoffmeister, C. 1967, *Astron. Nachr.*, 289, 205
 Howell, S. B., De Young, J., Mattei, J. A., Foster, G., Szkody, P., Cannizzo, J. K., Walker, G., & Fierce, E. 1996, *AJ*, 111, 2367
 Howell, S. B., Dobrzycka, D., Szkody, P., & Kreidl, T. J. 1991, *PASP*, 103, 300
 Howell, S. B., & Szkody, P. 1990, *ApJ*, 356, 623
 Iida, M., & York, D. 1994, *IAU Circ.*, 6056, 3
 Imada, A., Kubota, K., Kato, T., Nogami, D., Maehara, H., Nakajima, K., Uemura, M., & Ishioka, R. 2006, *PASJ*, 58, L23
 Ishioka, R., Kato, T., Uemura, M., Iwamatsu, H., Matsumoto, K., Martin, B. E., Billings, G. W., & Novak, R. 2001, *PASJ*, 53, L51
 Ishioka, R., et al. 2002, *A&A*, 381, L41
 Itagaki, K., et al. 2013, *Cent. Bur. Electron. Telegrams*, 3554, 1
 Kato, T. 1995a, *IBVS*, 4152
 Kato, T. 1995b, *IBVS*, 4242
 Kato, T. 1996, *IBVS*, 4369
 Kato, T. 2002, *PASJ*, 54, L11
 Kato, T., et al. 2002a, *A&A*, 396, 929
 Kato, T., et al. 2013a, *PASJ*, 65, 23
 Kato, T., et al. 2014, *PASJ*, 66, 30
 Kato, T., Hanson, G., Poyner, G., Muylaert, E., Reszelski, M., & Dubovsky, P. A. 2000, *IBVS*, 4932
 Kato, T., Haseda, K., Takamizawa, K., Kazarovets, E. V., & Samus, N. N. 1998a, *IBVS*, 4585
 Kato, T., et al. 2009, *PASJ*, 61, S395
 Kato, T., Ishioka, R., & Uemura, M. 2002b, *PASJ*, 54, 1029
 Kato, T., & Kunjaya, C. 1995, *PASJ*, 47, 163
 Kato, T., Lipkin, Y., Retter, A., & Leibowitz, E. 1998b, *IBVS*, 4602
 Kato, T., & Maehara, H. 2013, *PASJ*, 65, 76
 Kato, T., et al. 2012a, *PASJ*, 64, 21
 Kato, T., Maehara, H., & Uemura, M. 2012b, *PASJ*, 64, 62
 Kato, T., et al. 2010, *PASJ*, 62, 1525
 Kato, T., Matsumoto, K., & Uemura, M. 2002c, *IBVS*, 5262
 Kato, T., Monard, B., Hamsch, F.-J., Kiyota, S., & Maehara, H. 2013b, *PASJ*, 65, L11
 Kato, T., et al. 2004a, *MNRAS*, 347, 861
 Kato, T., Nogami, D., Baba, H., Masuda, S., Matsumoto, K., & Kunjaya, C. 1999, in *Disk Instabilities in Close Binary Systems*, ed. S. Mineshige, & J. C. Wheeler (Tokyo: Universal Academy Press), p. 45
 Kato, T., Nogami, D., Baba, H., Matsumoto, K., Arimoto, J., Tanabe, K., & Ishikawa, K. 1996, *PASJ*, 48, L21
 Kato, T., Nogami, D., & Masuda, S. 1996, *PASJ*, 48, L5
 Kato, T., Nogami, D., Matsumoto, K., & Baba, H. 2004b, *PASJ*, 56, S109
 Kato, T., & Osaki, Y. 2013a, *PASJ*, 65, 97
 Kato, T., & Osaki, Y. 2013b, *PASJ*, 65, 115
 Kato, T., & Osaki, Y. 2013c, *PASJ*, 65, L13
 Kato, T., & Osaki, Y. 2014, *PASJ*, 66, L5
 Kato, T., Sekine, Y., & Hirata, R. 2001, *PASJ*, 53, 1191
 Kato, T., et al. 2002d, *A&A*, 395, 541
 Kato, T., Stubbings, R., Pearce, A., Nelson, P., & Monard, B. 2001a, *IBVS*, 5119, 1
 Kato, T., & Uemura, M. 2012, *PASJ*, 64, 122
 Kato, T., Uemura, M., Buczynski, D., & Schmeer, P. 2001b, *IBVS*, 5123
 Kato, T., Uemura, M., Ishioka, R., Nogami, D., Kunjaya, C., Baba, H., & Yamaoka, H. 2004c, *PASJ*, 56, S1
 Kazarovets, E. V., Samus, N. N., Durlevich, O. V., Kireeva, N. N., & Pastukhova, E. N. 2008, *IBVS*, 5863, 1
 Kholopov, P. N., et al. 1985, *General Catalogue of Variable Stars*, fourth edition (Moscow: Nauka Publishing House)
 Klose, S. 1995, *ApJ*, 446, 357
 Knigge, C., Baraffe, I., & Patterson, J. 2011, *ApJS*, 194, 28
 Knigge, R., & Bauernfeind, H. 1967, *Bamberg Veröff.*, 6, 45
 Kukarkin, B. V. 1971, *IAU Circ.*, 2319, 2
 Kukarkin, B. V., et al. 1969, *General Catalogue of Variable Stars*, third edition (Moscow: Astronomical Council of the Academy of Sciences in the USSR)
 Kunjaya, C., Kinugasa, K., Ishioka, R., Kato, T., Iwamatsu, H., & Uemura, M. 2001, *IBVS*, 5128
 Kuulkers, E., Howell, S. B., & van Paradijs, J. 1996, *ApJ*, 462, L87
 Larwood, J. 1998, *MNRAS*, 299, L32
 Littlefair, S. P., Dhillon, V. S., Marsh, T. R., & Gänsicke, B. T. 2006, *MNRAS*, 371, 1435
 Littlefield, C., et al. 2013, *AJ*, 145, 145
 Liu, Wu., & Hu, J. Y. 2000, *ApJS*, 128, 387
 Liu, Wu., Hu, J. Y., Zhu, X. H., & Li, Z. Y. 1999, *ApJS*, 122, 243
 Lubow, S. H. 1991, *ApJ*, 381, 259
 Lucchetti, S. C., & Usher, P. D. 1972, *IBVS*, 696, 1
 Luyten, W. J. 1932, *Astron. Nachr.*, 245, 211
 Luyten, W. J., & Haro, G. 1959, *PASP*, 71, 469
 Martin, D. C., et al. 2005, *ApJ*, 619, L1
 Mason, E., & Howell, S. 2003, *A&A*, 403, 699
 Mason, E., Skidmore, W., Howell, S. B., & Mennickent, R. E. 2001, *ApJ*, 563, 351
 Mason, K. O., Reichert, G. A., Bowyer, S., & Thorstensen, J. R. 1982, *PASP*, 94, 521
 Matsumoto, K., Mennickent, R. E., & Kato, T. 2000, *A&A*, 363, 1029
 McLaughlin, D. B. 1945, *AJ*, 51, 136
 Meinunger, L. 1984a, *IBVS*, 2483

- Meinunger, L. 1984b, *Mitteil. Veränderl. Sterne*, 10, 56
- Mennickent, R. E., & Diaz, M. 1996, *A&A*, 309, 147
- Mukai, K., et al. 1990, *MNRAS*, 245, 385
- Mukai, K., Zietsman, E., & Still, M. 2009, *ApJ*, 707, 652
- Munari, U., & Zwitter, T. 1998, *A&AS*, 128, 277
- Nakata, C., Kuin, P., Kato, T., & Ohshima, T. 2013a, *Astron. Telegram*, 5253
- Nakata, C., et al. 2013b, *PASJ*, 65, 117
- Nogami, D., & Kato, T. 1995, *IBVS*, 4227, 1
- Nogami, D., Kato, T., Baba, H., Matsumoto, K., Arimoto, J., Tanabe, K., & Ishikawa, K. 1997, *ApJ*, 490, 840
- Nogami, D., Kato, T., & Hirata, R. 1996, *PASJ*, 48, 607
- Nogami, D., Masuda, S., & Kato, T. 1997, *PASP*, 109, 1114
- Nogami, D., et al. 2003, *A&A*, 404, 1067
- Noguchi, T., Maehara, H., & Kondo, M. 1980, *Tokyo Astron. Obs. Annals, Sec. Ser.*, 18, 55
- Noguchi, T., Yutani, M., & Maehara, H. 1982, *PASJ*, 34, 407
- O'Donoghue, D., Chen, A., Marang, F., Mittaz, J. P. D., Winkler, H., & Warner, B. 1991, *MNRAS*, 250, 363
- Ohshima, T., et al. 2012, *PASJ*, 64, L3
- Ohshima, T., et al. 2014, *PASJ*, in press (arXiv/1402.5747)
- Oizumi, S., et al. 2007, *PASJ*, 59, 643
- Olech, A., Mularczyk, K., Kędzierski, P., Złoczewski, K., Wiśniewski, M., & Szaruga, K. 2006, *A&A*, 452, 933
- Olech, A., Wisniewski, M., Złoczewski, K., Cook, L. M., Mularczyk, K., & Kedzierski, P. 2008, *Acta Astron.*, 58, 131
- Olech, A., Złoczewski, K., Mularczyk, K., Kedzierski, P., Wisniewski, M., & Stachowski, G. 2004, *Acta Astron.*, 54, 57
- Osaki, Y. 1989, *PASJ*, 41, 1005
- Osaki, Y. 1996, *PASP*, 108, 39
- Osaki, Y., & Kato, T. 2013a, *PASJ*, 65, 50
- Osaki, Y., & Kato, T. 2013b, *PASJ*, 65, 95
- Osaki, Y., & Kato, T. 2014, *PASJ*, 66, 15
- Osaki, Y., & Meyer, F. 2002, *A&A*, 383, 574
- Osaki, Y., & Meyer, F. 2003, *A&A*, 401, 325
- Osaki, Y., Shimizu, S., & Tsugawa, M. 1997, *PASJ*, 49, L19
- Otulakowska-Hypka, M., Olech, A., de Miguel, E., Rutkowski, A., Koff, R., & Bąkowska, K. 2013, *MNRAS*, 429, 868
- Patterson, J. 1979, *AJ*, 84, 804
- Patterson, J., Augusteijn, T., Harvey, D. A., Skillman, D. R., Abbott, T. M. C., & Thorstensen, J. 1996, *PASP*, 108, 748
- Patterson, J., et al. 2005, *PASP*, 117, 1204
- Patterson, J., Kemp, J., Saad, J., Skillman, D. R., Harvey, D., Fried, R., Thorstensen, J. R., & Ashley, R. 1997, *PASP*, 109, 468
- Patterson, J., et al. 1998, *PASP*, 110, 1290
- Patterson, J., McGraw, J. T., Coleman, L., & Africano, J. L. 1981, *ApJ*, 248, 1067
- Patterson, J., et al. 2002, *PASP*, 114, 721
- Patterson, J., Richman, H., Kemp, J., & Mukai, K. 1998, *PASP*, 110, 403
- Patterson, J., Thomas, G., Skillman, D. R., & Diaz, M. 1993, *ApJS*, 86, 235
- Patterson, J., et al. 2003, *PASP*, 115, 1308
- Pavlenko, E. P., et al. 2010, *Astron. Rep.*, 54, 6
- Petit, M. 1956, *Journal des Observateurs*, 39, 37
- Philip, A. G. D. 1971, *IAU Circ.*, 2308, 1
- Pojmański, G. 2002, *Acta Astron.*, 52, 397
- Prager, R., & Shapley, H. 1941, *Annals of the Astron. Obs. of Harvard Coll.* 111, 1
- Pretorius, M. L., Warner, B., & Woudt, P. A. 2006, *MNRAS*, 368, 361
- Ramsay, G., Barclay, T., Steeghs, D., Wheatley, P. J., Hakala, P., Kotko, I., & Rosen, S. 2012, *MNRAS*, 419, 2836
- Richter, G. A. 1969, *Mitteil. Veränderl. Sterne*, 5, 69
- Richter, G. A. 1986, *Astron. Nachr.*, 307, 221
- Richter, G. A. 1989, *Astron. Nachr.*, 310, 143
- Robertson, J. W., Honeycutt, R. K., & Turner, G. W. 1995, *PASP*, 107, 443
- Rodríguez-Gil, P., Gänsicke, B. T., Hagen, H.-J., Marsh, T. R., Harlaftis, E. T., Kitsionas, S., & Engels, D. 2005, *A&A*, 431, 269
- Rosino, L. 1961, *IAU Circ.*, 1782
- Rufanov, A., et al. 2013, *Astron. Telegram*, 5587
- Samsonov, D. A., Pavlenko, E. P., Andreev, M. V., Sklyanov, A., & Zubareva, A. M. 2010, *Odessa Astron. Publ.*, 23, 98
- Sanduleak, N. 1976, *IBVS*, 1218
- Satyvoldiev, V. 1972, *Astron. Tsirk.*, 711, 7
- Satyvoldiev, V. 1982, *Perem. Zvezdy, Prilozh.*, 4, 127
- Schoembs, R., & Vogt, N. 1981, *A&A*, 97, 185
- Semeniuk, I., Nalezty, M., Gembara, P., & Kwast, T. 1997, *Acta Astron.*, 47, 299
- Shafter, A. W., Coelho, E. A., & Reed, J. K. 2007, *PASP*, 119, 388
- Shafter, A. W., & Hessman, F. V. 1988, *AJ*, 95, 178
- Shappee, B. J., et al. 2013, *ApJ*, submitted (arXiv/1310.2241)
- Shappee, B. J., et al. 2014, *Astron. Telegram*, 5775
- Shears, J., Lloyd, C., Boyd, D., Brady, S., Miller, I., & Pickard, R. 2009, *J. Br. Astron. Assoc.*, 119, 31
- Shears, J., Wils, P., Bolt, G., Hamsch, F.-J., Krajci, T., Miller, I., Sabo, R., & Staels, B. 2011a, *J. Br. Astron. Assoc.*, 121, 155
- Shears, J. H., Gaensicke, B. T., Brady, S., Dubovsky, P., Miller, I., & Staels, B. 2011b, *New Astron.*, 16, 311
- Shumkov, V., et al. 2013, *Astron. Telegram*, 4814
- Shurpakov, S., et al. 2013, *Astron. Telegram*, 5526
- Skvarc, J., & Palcic, R. 2006, *Cent. Bur. Electron. Telegrams*, 701, 1
- Smak, J. 1985, *Acta Astron.*, 35, 357
- Smak, J. 2010, *Acta Astron.*, 60, 357
- Smith, A. J., Haswell, C. A., & Hynes, R. I. 2006, *MNRAS*, 369, 1537
- Solheim, J.-E. 2010, *PASP*, 122, 1133
- Splittgerber, E. 1971, *IBVS*, 578, 2
- Stellingwerf, R. F. 1978, *ApJ*, 224, 953
- Szkody, P. 1987, *ApJS*, 63, 685
- Szkody, P., & Feinswog, L. 1988, *ApJ*, 334, 422
- Szkody, P., Howell, S. B., Mateo, M., & Kreidl, T. J. 1989, *PASP*, 101, 899
- Szkody, P., & Mattei, J. A. 1984, *PASP*, 96, 988
- Tappert, C., & Bianchini, A. 2003, *A&A*, 401, 1101
- Thorstensen, J. R. 1999, *IBVS*, 4749
- Thorstensen, J. R., Patterson, J. O., Shambrook, A., & Thomas, G. 1996, *PASP*, 108, 73
- Thorstensen, J. R., Wade, R. A., & Oke, J. B. 1986, *ApJ*, 309, 721
- Tibshirani, R. 1996, *J. R. Statistical Soc. Ser. B*, 58, 267
- Tsevevich, V. P. 1969, *Astron. Tsirk.*, 529, 7
- Tsevevich, V. P., & Dragomiretskaia, B. A. 1973, *Zvezdy tipa RW Voznichego: fotograficheskie nablyudeniya bleska (Naukova dumka: Kiev)*
- Udalski, A. 1990, *IBVS*, 3425
- Udalski, A. 1990, *AJ*, 100, 226
- Uemura, M., et al. 2008, *IBVS*, 5815, 1
- Uemura, M., Kato, T., Ohshima, T., & Maehara, H. 2012, *PASJ*, 64, 92

- Uemura, M., et al. 2005, *A&A*, 432, 261
Vladimirov, V., et al. 2013, *Astron. Telegram*, 5481
Vogt, N. 1974, *A&A*, 36, 369
Vogt, N. 1980, *A&A*, 88, 66
Vogt, N. 1983, *A&A*, 118, 95
Vogt, N., & Bateson, F. M. 1982, *A&AS*, 48, 383
von Gessner, H., & Meinunger, I. 1974, *Veröff. Sternw. Sonneberg*, 6, 249
Walker, W. S. G., Marino, B. F., & Freeth, G. 1976, *IBVS*, 1185
Warner, B. 1995, *Cataclysmic Variable Stars* (Cambridge: Cambridge University Press)
Wegner, G., & McMahan, R. K. 1988, *AJ*, 96, 1933
Whitehurst, R. 1988, *MNRAS*, 232, 35
Wolf, M., & Wolf, G. 1906, *Astron. Nachr.*, 170, 361
Wood, M. A., & Burke, C. J. 2007, *ApJ*, 661, 1042
Wood, M. A., Winget, D. E., Nather, R. E., Hessman, F. V., Liebert, J., Kurtz, D. W., Wesemael, F., & Wegner, G. 1987, *ApJ*, 313, 757
Woudt, P. A., & Warner, B. 2001, *MNRAS*, 328, 159
Woudt, P. A., Warner, B., & Pretorius, M. L. 2004, *MNRAS*, 351, 1015
Wu, J.-H., Chen, Y., He, X.-T., Zhang, X.-Z., & Voges, W. 2001, *Chinese J. of Astron. and Astrophys.*, 1, 57
Zemko, P., Kato, T., & Shugarov, S. 2013, *PASJ*, 65, 54
Zhukov, G. V., Solov'ev, V. Y., & Solovjev, V. Y. 1972, *Astron. Tsirk.*, 729, 8
Zwicky, F. 1965, *IAU Circ.*, 1902
Zwitter, T., & Munari, U. 1995, *A&AS*, 114, 575